ULTRAFAST BROADBAND MIDINFRARED ABSORPTION SPECTROSCOPY ON SHOCKED ENERGETIC MATERIALS

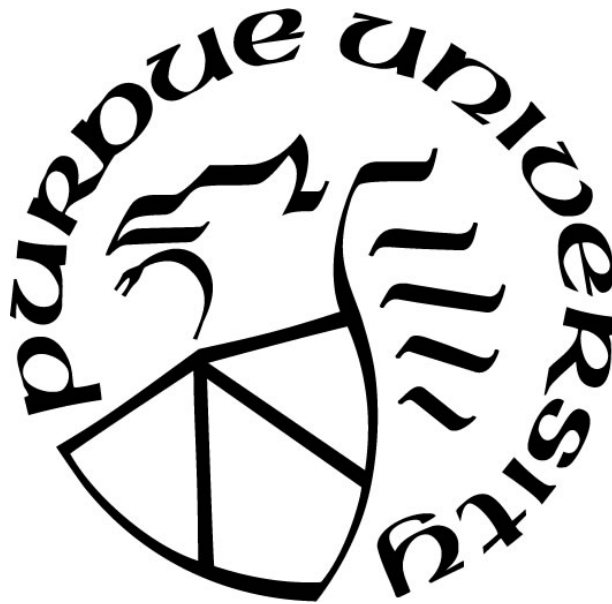by

Michael Stephan Powell

A Dissertation

Submitted to the Faculty of Purdue University

In Partial Fulfillment of the Requirements for the degree of

Doctor of Philosophy

School of Mechanical Engineering

West Lafayette, Indiana

May 2020

THE PURDUE UNIVERSITY GRADUATE SCHOOL
STATEMENT OF COMMITTEE APPROVAL

Dr. Steven F. Son, Chair

School of Mechanical Engineering

Dr. Alejandro H. Strachan

School of Materials Engineering

Dr. Christopher S. Goldenstein

School of Mechanical Engineering

Dr. Robert P. Lucht

School of Mechanical Engineering

Dr. Shawn D. McGrane

Shock and Detonation Physics, Los Alamos National Laboratory

Approved by:

Dr. Nicole Key

Head of the Mechanical Engineering Graduate Program

To Shawn and Dave who have been looking for insight into the chemistry of shock compressed energetics, here is your answer. Also to Neva, the magnificent lady who has always supported me during my endeavors.

ACKNOWLEDGMENTS

I would like to thank Dr. Son for giving me the opportunity to attend graduate school as well as the opportunity to perform my research at Los Alamos National Laboratory.

Dr. Strachan has my gratitude for supporting the research I have performed at Los Alamos as well as leading the MURI project.

Shawn McGrane and Dave Moore have my eternal gratitude for their time, mentorship, and patience for dealing with all of my questions and odd thought experiments during my time at Los Alamos. This work would not have been possible without their dedication, mentorship, and stewardship to the laser shock experiment(s) over the years.

I would like to thank Michael Sakano for his modeling work in ReaxFF during the course of the MURI project and providing comparisons to the experiments.

A special thanks to the molecular dynamics team comprised of Marc Cawkwell, Romain Perriot, and Enrique Martinez for the work on the DR project and tackling the comparisons to experiments.

I would like to thank several LANL staff for their advice, help, commentary, escorting, and colloquium series featuring breakfast burritos: Pam Bowlan, Katie Brown, Cindy Bolme, Kyle Ramos, Suzanne Sheehe, and Margo Greenfield.

I would like to thank Adam Golder, Adam Pacheco, and Claudine Armenta for all of their expertise and help with machining and microscopy.

Lastly, a special dedication is reserved to my wonderful fianceé, soon to be wife, Neva Ambrose who has always been there for me through the entirety of my Master and Doctoral degrees.

TABLE OF CONTENTS

LIST OF TABLES

LIST OF FIGURES

there is an almost opposite behavior between the two bonds. Reactions show some delay at medium pressure and are almost prompt at extreme pressure. 95

Figure 48 Comparison of the shocked transmission behavior for TNT at 16, 33, and 40 GPa. At 16 GPa no changes were observed. At 33 GPa, the NO_2 stretches broadened by ~50 cm^{-1}, and an absorption feature grew in the hydrogenic stretch region. Partial recovery was observed at 250 ps delay. At 40 GPa a broad absorption feature was observed over most of the spectral range. There was less absorption at >2700 cm^{-1} compared to 33 GPa. At 40 GPa, the ν_a-NO_2 transmission decreased from 40% to 25%, a decrease that is not duplicated at the ν_s-NO_2 mode. This could be due to strong scattering of the shocked sample. Sample thickness variations were also present as

ABSTRACT

Balancing increased safety against detonation performance is paramount for new explosive energetic materials in the development process. Often these two requirements are in opposition to each other. Sensitivity tests to external stimuli are used to determine how safe an energetic material is to phenomena such as impact, heat, or friction. Meanwhile, detonation performance is assessed by the maximum pressure and shock velocity induced from chemical reactions. Tailoring the performance while maintaining safety of the explosive would be possible with knowledge of the chemical reactions that functional groups provide during detonation. Current knowledge of the chemical reactions that occur during detonation is limited. Several mechanisms have been suggested for first step reactions throughout the detonation process for energetic molecules; however, no single chemical pathway has been irrefutably substantiated by experiments. Alternatively, models can provide insight into the types of reactions that may transpire, but lack direct experimental comparisons. If experiments and models could be compared at the equivalent time and length scales, then measurements could guide the physics and chemistry assumptions present in models. Experiments presented in this document bridge that gap by using an ultrafast laser system to generate shocks in samples and spectroscopically probe vibrational and electronic absorption changes that occur during shock compression. A review of how to turn a benchtop chirped pulse amplifier into a shock physics and chemistry laboratory is first presented. Applications of the spectroscopic techniques developed were then applied to trinitrotoluene (TNT) and pentaerythritol tetranitrate (PETN) during shock compression. Mid-infrared absorption results for shock compressed TNT and PETN were compared to current suggestions on chemical pathways and inconsistencies were present for both materials. It is suggested that a carbon-carbon bond breaking mechanism is present for PETN, and a hydrogenic stretch like hydroxyl or amide bond formation mechanism is suggested for TNT based on the MIR absorption measurements. Recommendations for future experimental thrusts are also provided. The results provided in this document could be directly compared to simulations to refine the assumptions present in models.

1. INTRODUCTION

1.1 Motivation

The chemistry that occurs during detonation of high explosives (HE) is poorly understood. Various theories exist on the chemical mechanisms that happen during detonation; however, there is a lack of direct experimental evidence to confirm these claims.[1-8] First step mechanisms for relatively simple HE systems like the molecule nitromethane (CH_3NO_2) are still debated between four primary reactions: CN-bond scission,[9, 10] nitrite rotation,[11, 12] aci-ion formation,[13, 14] or more complicated bimolecular reactions.[15-18] This is first step chemistry, and is neglecting the numerous chemical branching pathways that could be taken between reactants and products. Larger molecules, like pentaerythritol tetranitrate (PETN), introduce more complexity to these mechanisms from the presence of additional degrees of freedom for bond breaking events.[19-33] Shown in Fig. 1 is a comparison of several mechanisms for both of these molecules. To understand detonation chemistry, the pressure and temperature states that are present during detonation need to be attained. Emulation of detonation states, high pressure and temperature applied sonically or faster, can be achieved using shock waves. Various methods and facilities exist that are capable of generating shocks in materials.[2, 6, 21-23, 25, 28, 34-94] Typically, wave mechanics were measured when using many of these methods often inferring chemistry from these measurements.[2, 11, 41, 52, 55, 94-96] Experiments which attempted to directly measure chemistry were convoluted and results were difficult to interpret.[18, 23, 25, 27, 76, 84, 87, 88, 97]
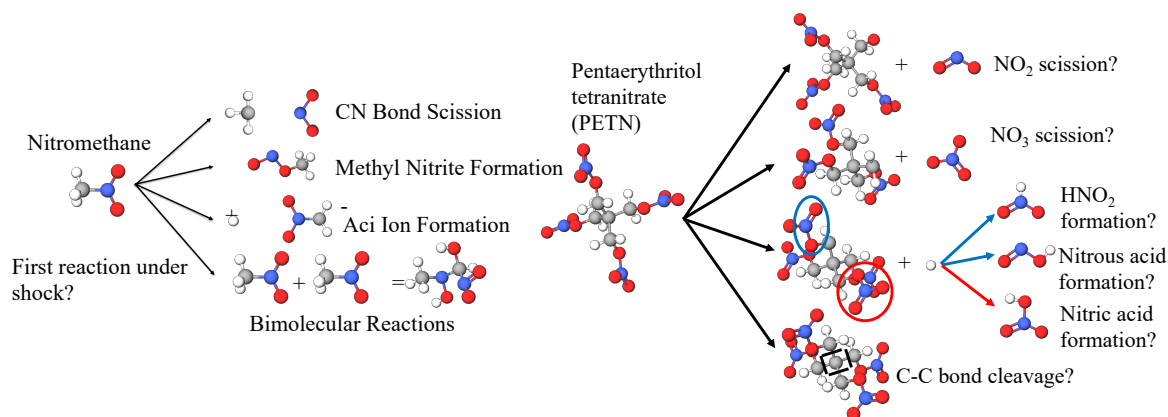
Figure 1 Possible chemical pathways that have been suggested for nitromethane (left) and pentaerythritol tetranitrate (PETN) when subjected to shock loading. These are the first steps to these molecules breaking up, neglecting the next steps between reactants and products.

Complimentary to experiments are physics- and chemistry-based models that are capable of predicting what reactions may occur during detonation for energetic materials. Predicting HE performance and safety would reduce the tremendous cost and time to synthesize, test, and qualify new energetic materials for use. Quantum molecular dynamics (QMD) and accelerated chemistry (AC) models have been shown to provide insight into chemical reactions and pathways when simulating energetic materials to extreme pressure and temperature conditions, like those present during detonation.[7, 15, 16, 24, 32, 33, 98-107] A caveat to this is that QMD and AC models are traditionally $O(N^3)$ necessitating the use of a small number of atoms, typically nanometer (nm) scale, to complete chemical predictions for practicality. This length scale requires sub-picosecond (ps) temporal resolution to model shocks at these length scales. Traditional methods of generating shocks in materials are usually at time and length scales 10^6 times greater, typically millimeter/microsecond (mm/μs), than capabilities present in predictions. Simulations are thus required to make assumptions in order to compare predictions to measurements. Ideally if an experiment could make measurements at nm length scales, with sub-ps temporal resolution, at shock pressures to induce reactions (GPa), and with chemical specificity then experiments could directly provide chemistry and physics measurements as a guide to models and the assumptions present. These requirements are impractical, if not impossible, to achieve with many traditional methods of generating shocks; however, are relatively simple to achieve using benchtop ultrafast laser systems.[108] The objective of the experiments presented in this document was to measure and understand the chemistry that occurs during shock compression of energetic materials at nearly identical time and length scales to modeling efforts in order to build models capable of predicting HE performance and safety.

1.2   Overview

A broad review of how to turn an ultrafast laser system into a benchtop shock physics laboratory will be presented in Chapter 2. Inclusive to this Chapter will be how laser energy is converted into mechanical work, interferometry techniques used to interpret wave mechanics, methods of spectroscopic investigation, and synchronization of ultrafast sources to shock physics and chemistry measurements. Chapter 3 will present an initial application of the techniques to measure the shock chemistry of trinitrotoluene (TNT). After refining techniques from Chapter 3 through procurement of an enhanced laser system, measurements were then performed on PETN

with results shown in Chapter 4. Results from shock compression of PETN suggested two distinct intermediates were formed with contradicting evidence to several previous publications. Since results from Chapter 3 were not conclusive, TNT was revisited using the new shock physics apparatus and results are shown in Chapter 5. Preliminary results shown in Chapter 5 suggest different behavior than several previous publications. Conclusions from experiments and suggestions on future experimental work with this apparatus are suggested in Chapter 6.

1.3   References

1.   An, Q.; Zybin, S. V.; Goddard III, W. A.; Jaramillo-Botero, A.; Blanco, M.; Luo, S.-N., Elucidation of the dynamics for hot-spot initiation at nonuniform interfaces of highly shocked materials. *Physical Review B* **2011,** *84* (22), 220101.

2.   Dick, R., Shock compression data for liquids. III. Substituted methane compounds, ethylene glycol, glycerol, and ammonia. *The Journal of Chemical Physics* **1981,** *74* (7), 4053-4061.

3.   Dlott, D. D.; Fayer, M. D., Shocked molecular solids: vibrational up pumping, defect hot spot formation, and the onset of chemistry. *The Journal of chemical physics* **1990,** *92* (6), 3798-3812.

4.   Gilman, J. J., Chemical reactions at detonation fronts in solids. *Philosophical Magazine B* **1995,** *71* (6), 1057-1068.

5.   Kuklja, M. M.; Aduev, B.; Aluker, E. D.; Krasheninin, V.; Krechetov, A.; Mitrofanov, A. Y., Role of electronic excitations in explosive decomposition of solids. *Journal of Applied Physics* **2001,** *89* (7), 4156-4166.

6.   Rice, M.; McQueen, R., JM Walsh in Solid State Physics, F. Seitz and D. Turnbull, Eds. Academic Press, New York: 1958.

7.   Tarver, C. M.; Chidester, S. K.; Nichols, A. L., Critical conditions for impact-and shock-induced hot spots in solid explosives. *The Journal of Physical Chemistry* **1996,** *100* (14), 5794-5799.

8.   Campbell, A.; Davis, W.; Ramsay, J.; Travis, J., Shock initiation of solid explosives. *The Physics of Fluids* **1961,** *4* (4), 511-521.

9.   Constantinou, C., The study of decomposition reactions through the exchange of thermal energy. *International Journal of Chemical Kinetics* **1994,** *26* (12), 1151-1166.

10. Constantinou, C.; Mukundan, T.; Chaudhri, M., Sensitization of nitrocompounds by amines. *Philosophical Transactions of the Royal Society of London. Series A: Physical and Engineering Sciences* **1992,** *339* (1654), 403-417.

11. Hardesty, D., An investigation of the shock initiation of liquid nitromethane. *Combustion and flame* **1976,** *27*, 229-251.

12. Shaw, R., Shock initiation of liquid nitromethane and methyl nitrite. *Combustion and Flame* **1973,** *21* (1), 127-130.

13. Engelke, R.; Earl, W. L.; Rohlfing, C. M., Microscopic evidence that the nitromethane aci ion is a rate controlling species in the detonation of liquid nitromethane. *The Journal of chemical physics* **1986,** *84* (1), 142-146.

14. Engelke, R.; Schiferl, D.; Storm, C.; Earl, W. L., Production of the nitromethane aci ion by static high pressure. *The Journal of Physical Chemistry* **1988,** *92* (23), 6815-6819.

15. Bardo, R. In *Calculated Reaction Pathways for Nitromethane and Their Role in the Shock Initiation Process*, Proceedings of the Eighth Symposium (Int.) on Detonation," Office of Naval Research, Washington, DC, to be published, 1985.

16. Bardo, R. D., Theoretical calculations of rate-determining steps for ignition of shocked, condensed nitromethane. *International Journal of Quantum Chemistry* **1986,** *30* (S20), 455-469.

17. Cook, M.; Fellows, J.; Haskins, P., Probing detonation physics and chemistry using molecular dynamics and quantum chemistry techniques. *MRS Online Proceedings Library Archive* **1995,** *418*.

18. Winey, J.; Gupta, Y., Shock-induced chemical changes in neat nitromethane: use of time-resolved Raman spectroscopy. *The Journal of Physical Chemistry B* **1997,** *101* (50), 10733-10743.

19. Budzien, J.; Thompson, A. P.; Zybin, S. V., Reactive Molecular Dynamics Simulations of Shock Through a Single Crystal of Pentaerythritol Tetranitrate. *The Journal of Physical Chemistry B* **2009,** *113* (40), 13142-13151.

20. Davis, L. L.; Brower, K. R., Reactions of organic compounds in explosive-driven shock waves. *The Journal of Physical Chemistry* **1996,** *100* (48), 18775-18783.

21. Dick, J., Anomalous shock initiation of detonation in pentaerythritol tetranitrate crystals. *Journal of applied physics* **1997,** *81* (2), 601-612.

22. Dick, J.; Mulford, R.; Spencer, W.; Pettit, D.; Garcia, E.; Shaw, D., Shock response of pentaerythritol tetranitrate single crystals. *Journal of applied physics* **1991,** *70* (7), 3572-3587.

23. Dreger, Z. A.; Gruzdkov, Y. A.; Gupta, Y. M.; Dick, J. J., Shock wave induced decomposition chemistry of pentaerythritol tetranitrate single crystals: time-resolved emission spectroscopy. *The Journal of Physical Chemistry B* **2002,** *106* (2), 247-256.

24. Gruzdkov, Y. A.; Dreger, Z. A.; Gupta, Y. M., Experimental and theoretical study of pentaerythritol tetranitrate conformers. *The Journal of Physical Chemistry A* **2004,** *108* (29), 6216-6221.

25. Gruzdkov, Y. A.; Gupta, Y. M., Shock wave initiation of pentaerythritol tetranitrate single crystals: Mechanism of anisotropic sensitivity. *The Journal of Physical Chemistry A* **2000,** *104* (47), 11169-11176.

26. Gruzdkov, Y. A.; Gupta, Y. M., Vibrational properties and structure of pentaerythritol tetranitrate. *The Journal of Physical Chemistry A* **2001,** *105* (25), 6197-6202.

27. Gruzdkov, Y. A.; Gupta, Y. M.; Dick, J. J., Time-resolved absorption spectroscopy in shocked PETN single crystals. *AIP Conference Proceedings* **2000,** *505* (1), 929-932.

28. Hemmi, N.; Dreger, Z.; Gruzdkov, Y.; Winey, J.; Gupta, Y., Raman spectra of shock compressed pentaerythritol tetranitrate single crystals: anisotropic response. *The Journal of Physical Chemistry B* **2006,** *110* (42), 20948-20953.

29. Landerville, A. C.; Oleynik, I. I.; White, C. T., Reactive Molecular Dynamics of Hypervelocity Collisions of PETN Molecules. *The Journal of Physical Chemistry A* **2009,** *113* (44), 12094-12104.

30. Naud, D. L.; Brower, K. R., Pressure effects on the thermal decomposition of nitramines, nitrosamines, and nitrate esters. *The Journal of Organic Chemistry* **1992,** *57* (12), 3303-3308.

31. Ng, W.; Field, J.; Hauser, H., Thermal, fracture, and laser-induced decomposition of pentaerythritol tetranitrate. *Journal of applied physics* **1986,** *59* (12), 3945-3952.

32. Shan, T.-R.; Wixom, R. R.; Mattsson, A. E.; Thompson, A. P., Atomistic Simulation of Orientation Dependence in Shock-Induced Initiation of Pentaerythritol Tetranitrate. *The Journal of Physical Chemistry B* **2013,** *117* (3), 928-936.

33. Zhurova, E. A.; Stash, A. I.; Tsirelson, V. G.; Zhurov, V. V.; Bartashevich, E. V.; Potemkin, V. A.; Pinkerton, A. A., Atoms-in-molecules study of intra-and intermolecular bonding in the pentaerythritol tetranitrate crystal. *Journal of the American Chemical Society* **2006,** *128* (45), 14728-14734.

34. Deal, W., Measurement of Chapman-Jouguet pressure for explosives. *The Journal of Chemical Physics* **1957,** *27* (3), 796-800.

35. Dlott, D.; Shaw, W.; Curtis, A.; Banishev, A. In *Laser-driven flyer plates for shock compression spectroscopy*, APS Shock Compression of Condensed Matter Meeting Abstracts, 2013.

36. Dlott, D. D., Ultrafast spectroscopy of shock waves in molecular materials. *Annual review of physical chemistry* **1999,** *50* (1), 251-278.

37. Dlott, D. D., Nanoshocks in molecular materials. *Accounts of Chemical Research* **2000,** *33* (1), 37.

38. Dlott, D. D.; Hambir, S.; Franken, J., The New Wave in Shock Waves. *The Journal of Physical Chemistry B* **1998,** *102* (12), 2121-2130.

39. Eidmann, K.; Meyer-ter-Vehn, J.; Schlegel, T.; Huller, S., Hydrodynamic simulation of subpicosecond laser interaction with solid-density matter. *Physical Review E (Statistical Physics, Plasmas, Fluids, and Related Interdisciplinary Topics)* **2000,** *62* (1), 1202.

40. Evans, R.; Badger, A. D.; Fallies, F.; Mahdieh, M.; Hall, T. A.; Audebert, P.; Geindre, J. P.; Gauthier, J. C.; Mysyrowicz, A.; Grillon, G.; Antonetti, A., Time- and space-resolved optical probing of femtosecond-laser-driven shock waves in aluminum. *Physical Review Letters* **1996,** *77* (16), 3359.

41. Fowles, G.; Duvall, G.; Asay, J.; Bellamy, P.; Feistmann, F.; Grady, D.; Michaels, T.; Mitchell, R., Gas gun for impact studies. *Review of Scientific Instruments* **1970,** *41* (7), 984-996.

42. Frank, A. M.; Trott, W. M. In *Stop-motion microphotography of laser-driven plates*, Ultrahigh-and High-Speed Photography, Videography, and Photonics' 94, International Society for Optics and Photonics: 1994; pp 196-206.

43. Funk, D.; Moore, D.; McGrane, S.; Gahagan, K.; Reho, J.; Buelow, S.; Nicholson, J.; Fisher, G.; Rabie, R., Ultrafast studies of shock waves using interferometric methods and transient infrared absorption spectroscopy. *Thin Solid Films* **2004,** *453*, 542-549.

44.	Funk, D. J.; Moore, D. S.; Gahagan, K. T.; Buelow, S. J.; Reho, J. H.; Fisher, G. L.; Rabie, R. L., Ultrafast measurement of the optical properties of aluminum during shock-wave breakout. *Physical Review B (Condensed Matter and Materials Physics)* **2001,** *64* (11), 115114.

45.	Funk, D. J.; Moore, D. S.; McGrane, S. D.; Reho, J. H.; Rabie, R. L., Ultra-fast spatial interferometry: a tool for characterizing material phase and hydrodynamic motion in laser-excited metals. *Applied Physics a-Materials Science & Processing* **2005,** *81* (2), 295-302.

46.	Funk, D. J.; Moore, D. S.; Reho, J. H.; Gahagan, K. T.; McGrane, S. D.; Rabie, R. L., Ultrafast measurement of the optical properties of shocked nickel and laser heated gold. In *Shock Compression of Condensed Matter-2001, Pts 1 and 2, Proceedings*, Furnish, M. D.; Thadhani, N. N.; Horie, Y., Eds. 2002; Vol. 620, pp 1227-1230.

47.	Gehr, R.; Bucholtz, S.; Rupp, T.; Robbins, D.; Stahl, D.; Sheffield, S. In *Line ORVIS Particle Velocity Measurements on the Laser-Driven Miniflyer Apparatus*, AIP Conference Proceedings, American Institute of Physics: 2004; pp 1163-1166.

48.	Glass, I.; Chan, S.; Brode, H., Strong planar shock waves generated by explosively-driven spherical implosions. *AIAA Journal* **1974,** *12* (3), 367-374.

49.	Grady, D. E.; Murri, W. J.; De Carli, P. S., Hugoniot sound velocities and phase transformations in two silicates. *Journal of Geophysical Research* **1975,** *80* (35), 4857-4861.

50.	Graham, R., Measurement of wave profiles in shock-loaded solids. In *High-Pressure Science and Technology*, Springer: 1979; pp 1886-1901.

51.	Greenaway, M.; Proud, W.; Field, J.; Goveas, S., A laser-accelerated flyer system. *International journal of impact engineering* **2003,** *29* (1-10), 317-321.

52.	Gustavsen, R.; Sheffield, S.; Alcon, R., Progress in measuring detonation wave profiles in PBX9501. In *11th International Detonation Symposium*, Snowmass, CO, 1998; pp 821-827.

53.	Gustavsen, R. L.; Sheffield, S. A.; Alcon, R. R. In *Detonation wave profiles in HMX based explosives*, AIP Conference Proceedings, American Institute of Physics: 1998; p 739.

54.	Hill, J.; Moore, D.; Schmidt, S.; Storm, C., Infrared, Raman, and coherent anti-Stokes Raman spectroscopy of the hydrogen/deuterium isotopomers of nitromethane. *The Journal of Physical Chemistry* **1991,** *95* (8), 3037-3044.

55.	Jones, A. H.; Isbell, W.; Maiden, C., Measurement of the very-high-pressure properties of materials using a light-gas gun. *Journal of Applied Physics* **1966,** *37* (9), 3493-3499.

56. Lee, I.-Y. S.; Hare, D. E.; Hill, J. R.; Franken, J.; Suzuki, H.; Dlott, D. D.; Baer, B. J.; Chronister, E. L., Ultrafast spectroscopy of the first nanosecond. *AIP Conference Proceedings* **1996,** *370* (1), 905-908.

57. Lindl, J. D.; Amendt, P.; Berger, R. L.; Glendinning, S. G.; Glenzer, S. H.; Haan, S. W.; Kauffman, R. L.; Landen, O. L.; Suter, L. J., The physics basis for ignition using indirect-drive targets on the National Ignition Facility. *Physics of Plasmas* **2004,** *11* (2), 339-491.

58. McGrane, S.; Bowlan, P.; Powell, M.; Brown, K.; Bolme, C., Broadband mid-infrared measurements for shock-induced chemistry. *AIP Conference Proceedings* **2018,** *1979* (1), 130004.

59. McGrane, S.; Moore, D.; Funk, D., Shock induced reaction observed via ultrafast infrared absorption in poly (vinyl nitrate) films. *The Journal of Physical Chemistry A* **2004,** *108* (43), 9342-9347.

60. McGrane, S.; Moore, D.; Funk, D. In *Measurement of shocked thin polymer film Hugoniot properties with ultrafast dynamic ellipsometry*, AIP Conference Proceedings, AIP: 2004; pp 1181-1186.

61. McGrane, S.; Moore, D. S.; Whitley, V. H.; Bolme, C. A.; Eakins, D. E. In *Molecular shock response of Explosives: Electronic absorption spectroscopy*, AIP Conference Proceedings, AIP: 2009; pp 1301-1304.

62. McGrane, S. D.; Bolme, C. A.; Whitley, V. H.; Moore, D. S., Ultrafast Dynamic Ellipsometry And Spectroscopy Of Laser Shocked Materials. In *International Symposium on High Power Laser Ablation 2010*, Phipps, C. R., Ed. 2010; Vol. 1278, pp 392-400.

63. McGrane, S. D.; Brown, K. E.; Bolme, C. A.; Moore, D. S., Interaction between measurement time and observed Hugoniot cusp due to chemical reactions. *AIP Conference Proceedings* **2017,** *1793* (1), 030033.

64. Mcgrane, S. D.; Dang, N. C.; Whitley, V. H.; Bolome, C. A.; Moore, D. *Transient absorption spectroscopy of laser shocked explosives*; Los Alamos National Lab.(LANL), Los Alamos, NM (United States): 2010.

65. McGrane, S. D.; Moore, D. S.; Funk, D. J., Ultrafast spectroscopy and interferometry of laser shocked thin films: practical considerations. In *High-Power Laser Ablation V, Pts 1 and 2*, Phipps, C. R., Ed. 2004; Vol. 5448, pp 165-170.

66.	McGrane, S. D.; Moore, D. S.; Funk, D. J., Measurement of shocked thin polymer film Hugoniot properties with ultrafast dynamic ellipsometry. In *Shock Compression of Condensed Matter - 2003, Pts 1 and 2, Proceedings*, Furnish, M. D.; Gupta, Y. M.; Forbes, J. W., Eds. 2004; Vol. 706, pp 1181-1186.

67.	McGrane, S. D.; Moore, D. S.; Funk, D. J.; Rabie, R. L., Spectrally modified chirped pulse generation of sustained shock waves. *Applied Physics Letters* **2002,** *80* (21), 3919.

68.	McGrane, S. D.; Moore, D. S.; Whitley, V. H.; Bolme, C. A.; Eakins, D. E., Molecular Shock Response Of Explosives: Electronic Absorption Spectroscopy. In *Shock Compression of Condensed Matter - 2009, Pts 1 and 2*, Elert, M. L.; Buttler, W. T.; Furnish, M. D.; Anderson, W. W.; Proud, W. G., Eds. 2009; Vol. 1195, pp 1301-1304.

69.	McQueen, R.; Marsh, S., Equation of state for nineteen metallic elements from shock-wave measurements to two megabars. *Journal of Applied Physics* **1960,** *31* (7), 1253-1269.

70.	McQueen, R.; Marsh, S.; Taylor, J.; Fritz, J.; Carter, W., The equation of state of solids from shock wave studies. *High velocity impact phenomena* **1970,** *293*, 293-417.

71.	Moore, D., Influence of hot bands on vibrational spectra of shock compressed materials. *The Journal of Physical Chemistry A* **2001,** *105* (19), 4660-4663.

72.	Moore, D.; Funk, D. J.; Gahagan, K.; Reho, J.; Fisher, G.; McGrane, S.; Rabie, R. In *Sub-picosecond Laser-Driven Shocks in Metals and Energetic Materials*, AIP Conference Proceedings, American Institute of Physics: 2002; pp 1333-1338.

73.	Moore, D.; Gahagan, K.; Reho, J.; Funk, D. J.; Buelow, S.; Rabie, R.; Lippert, T., Ultrafast nonlinear optical method for generation of planar shocks. *Applied Physics Letters* **2001,** *78* (1), 40-42.

74.	Moore, D.; McGrane, S.; Funk, D., Infrared complex refractive index measurements and simulated reflection mode infrared absorption spectroscopy of shock-compressed polymer thin films. *Applied spectroscopy* **2004,** *58* (5), 491-498.

75.	Moore, D.; McGrane, S.; Funk, D. In *Ultrafast spectroscopic investigation of shock compressed energetic polymer films*, AIP Conference Proceedings, AIP: 2004; pp 1285-1288.

76.	Moore, D.; Schmidt, S.; Shaner, J.; Shampine, D.; Holt, W., Coherent anti-Stokes Raman scattering in benzene and nitromethane shock-compressed to 11 GPa. In *Shock Waves in Condensed Matter*, Springer: 1986; pp 207-211.

77. Moore, D. S.; Gahagan, K. T.; Lippert, T.; Funk, D. J.; Buelow, S.; Rabie, R. In *Ultrafast nonlinear optical method for generation of flat-top shocks*, High-Power Laser Ablation III, Santa Fe, NM, International Society for Optics and Photonics: Santa Fe, NM, 2000; pp 490-495.

78. Moore, D. S.; McGrane, S. D.; Funk, D. J., Ultrafast infrared absorption and dynamic ellipsometry of shock-compressed energetic materials. *Abstracts of Papers of the American Chemical Society* **2004,** *227*, U316.

79. Moore, D. S.; McGrane, S. D.; Funk, D. J., Ultrashort laser shock dynamics. In *ShockWave Science and Technology Reference Library*, Springer: 2007; pp 47-104.

80. Paisley, D. *Laser-driven miniature flyer plates for shock initiation of secondary explosives*; Los Alamos National Lab., NM (USA): 1989.

81. Paisley, D.; Warnes, R.; Kopp, R., Laser-driven flat plate impacts to 100 GPa with sub-nanosecond pulse duration and resolution for material property studies. In *Shock Compression of Condensed Matter–1991*, Elsevier: 1992; pp 825-828.

82. Paisley, D. L.; Luo, S.-N.; Greenfield, S. R.; Koskelo, A. C., Laser-launched flyer plate and confined laser ablation for shock wave loading: Validation and applications. *Review of Scientific Instruments* **2008,** *79* (2), 023902.

83. Paisley, D. L.; Warnes, R. H.; Stahl, D. B. In *Experimental techniques for subnanosecond resolution of laser-launched plates and impact studies*, Ultrahigh-and High-Speed Photography, Videography, and Photonics' 94, International Society for Optics and Photonics: 1994; pp 167-172.

84. Pangilinan, G.; Gupta, Y., Time-resolved Raman measurements in nitromethane shocked to 140 kbar. *The Journal of Physical Chemistry* **1994,** *98* (17), 4522-4529.

85. Rice, M.; McQueen, R. G.; Walsh, J., Compression of solids by strong shock waves. In *Solid State Physics*, Elsevier: 1958; Vol. 6, pp 1-63.

86. Sandy Lee, I.; Hare, D. E.; Hill, J. R.; Franken, J.; Suzuki, H.; Dlott, D. D.; Baer, B. J.; Chronister, E. L. In *Ultrafast spectroscopy of the first nanosecond*, AIP Conference Proceedings, American Institute of Physics: 1996; pp 905-908.

87. Schmidt, S.; Moore, D.; Shaner, J.; Shampine, D.; Holt, W., Coherent anti-Stokes Raman scattering in benzene and nitromethane shock-compressed to 10 GPa. *Physica B+ C* **1986,** *139*, 587-589.

88. Schmidt, S. C.; Moore, D. S., Vibrational spectroscopy of high-temperature, dense molecular fluids by coherent anti-Stokes Raman scattering. *Accounts of chemical research* **1992,** *25* (9), 427-432.

89. Schmitt, M. J.; Kopp, R. A.; Moore, D. S.; McGrane, S. D. In *Analysis of Laser-Driven Shocks in Confined and Unconfined Geometries*, AIP Conference Proceedings, American Institute of Physics: 2004; pp 1409-1412.

90. Schulze, P. A.; Dang, N. C.; Bolme, C. A.; Brown, K. E.; McGrane, S. D.; Moore, D. S., Shock Hugoniot Equations of State for Binary Ideal (Toluene/Fluorobenzene) and Nonideal (Ethanol/Water) Liquid Mixtures. *Journal of Physical Chemistry A* **2013,** *117* (29), 6158-6163.

91. Schulze, P. A.; Ivanov, T. W.; Bolme, C. A.; Brown, K. E.; McGrane, S. D.; Moore, D. S., Shock Hugoniot equations of state for binary water-alcohol liquid mixtures. *Journal of Applied Physics* **2014,** *115* (2), 023512.

92. Shaw, W.; Curtis, A.; Banishev, A.; Dlott, D. In *Laser-driven flyer plates for shock compression spectroscopy*, Journal of Physics: Conference Series, IOP Publishing: 2014; p 142011.

93. Watson, S.; Field, J. E., Integrity of thin, laser-driven flyer plates. *Journal of Applied Physics* **2000,** *88* (7), 3859-3864.

94. Walsh, J. M.; Christian, R. H., Equation of state of metals from shock wave measurements. *Physical review* **1955,** *97* (6), 1544.

95. Boade, R., Compression of porous copper by shock waves. *Journal of Applied Physics* **1968,** *39* (12), 5693-5702.

96. Gustavsen, R. L.; Sheffield, S. A.; Alcon, R. R.; Forbes, J. W.; Tarver, C. M.; Garcia, F., Embedded Electromagnetic Gauge Measurements and Modeling of Shock Initiation in the TATB Based Explosives LX-17 and PBX 9502. *AIP Conference Proceedings* **2002,** *620* (1), 1019-1022.

97. Dodson, B. W.; Graham, R. A., Shock-induced organic chemistry. *AIP Conference Proceedings* **1982,** *78* (1), 42-51.

98. Tarver, C. M., Multiple roles of highly vibrationally excited molecules in the reaction zones of detonation waves. *The Journal of Physical Chemistry A* **1997,** *101* (27), 4845-4851.

99. Tarver, C. M.; Breithaupt, R. D.; Kury, J. W., Detonation waves in pentaerythritol tetranitrate. *Journal of applied physics* **1997,** *81* (11), 7193-7202.

100. Wu, C. J.; Manaa, M. R.; Fried, L. E., Tight binding molecular dynamic simulation of PETN decomposition at an extreme condition. *MRS Online Proceedings Library Archive* **2006,** *987*.

101. Wu, C. J.; Ree, F. H.; Yoo, C. S., A quantum mechanical molecular dynamics study of binary collisions of pentaerythritol tetranitrate (PETN): Its correlation to shock sensitivity. *Propellants, Explosives, Pyrotechnics: An International Journal Dealing with Scientific and Technological Aspects of Energetic Materials* **2004,** *29* (5), 296-303.

102. Mintmire, J. W.; Robertson, D. H.; White, C. T., Molecular-dynamics simulations of void collapse in shocked model-molecular solids. *Physical Review B (Condensed Matter)* **1994,** *49* (21), 14859.

103. Owens, F., Relationship between impact induced reactivity of trinitroaromatic molecules and their molecular structure. *Journal of Molecular Structure: Theochem* **1985,** *22* (1-5), 213-220.

104. Quenneville, J.; Germann, T. C., A quantum chemistry study of Diels–Alder dimerizations in benzene and anthracene. *The Journal of Chemical Physics* **2009,** *131* (2), 024313.

105. Rom, N.; Hirshberg, B.; Zeiri, Y.; Furman, D.; Zybin, S. V.; Goddard III, W. A.; Kosloff, R., First-principles-based reaction kinetics for decomposition of hot, dense liquid TNT from ReaxFF multiscale reactive dynamics simulations. *The Journal of Physical Chemistry C* **2013,** *117* (41), 21043-21054.

106. Cohen, R.; Zeiri, Y.; Wurzberg, E.; Kosloff, R., Mechanism of thermal unimolecular decomposition of TNT (2, 4, 6-trinitrotoluene): a DFT study. *The Journal of Physical Chemistry A* **2007,** *111* (43), 11074-11083.

107. Kunz, A. B., AnAb Initio Investigation of Crystalline PETN. *MRS Online Proceedings Library Archive* **1995,** *418*.

108. Powell, M. S.; Bowlan, P. R.; Son, S. F.; Bolme, C. A.; Brown, K. E.; Moore, D. S.; McGrane, S. D., A benchtop shock physics laboratory: Ultrafast laser driven shock spectroscopy and interferometry methods. *Review of Scientific Instruments* **2019,** *90* (6), 063001.

2. A BENCHTOP SHOCK PHYSICS LABORATORY: ULTRAFAST LASER DRIVEN SHOCK SPECTROSCOPY AND INTERFEROMETRY METHODS

2.1 Introduction

There are many methods of generating and characterizing material properties under shock loading conditions. Explosively driven plate impact experiments dominated early studies with time of arrival pins, rotating mirror cameras, and piezoelectric gauges being common diagnostics.[1-11] Gas guns that adiabatically accelerate flyer plates to high velocities for sustained constant pressure impacts coupled to interferometric velocimetry, embedded gauge, and spectroscopic methods have also been a staple of shock physics.[12-25] Gas gun and explosively-driven plate impact experiments are typically on the mm length and μs time scales. Laser driven flyer plate (100's of μm length and ns time scales)[26-38] and frustrated laser ablation (μm length and 100's of ps time scales) shock drive methods scaled these experiments down to the tabletop scale and allowed easy integration of complex optical diagnostics.[39-49] Facility scale direct drive lasers have also been utilized to generate very high pressure phenomena in fusion research and high energy density physics.[50, 51] As successful as these efforts have been, experimentally accessing the temporal and spatial scales commensurate with molecular dynamic models is a critical need for verification and validation of their predictions. This article reports the further development and practical integration of simultaneous spectroscopy techniques and interferometry designed to examine shock physics at the ps time and μm length scales,[39, 40, 43, 44, 52-72] with the corresponding reduction of energy required[63], and making high experimental repetition rate possible (100's of shots per day)[73, 74] compared to larger, conventional plate impact studies.

Advantages to using a single ultrafast laser to generate the shock and probe the dynamics are the 1) ps temporal resolution, 2) ease of generating new wavelengths for spectroscopic diagnostics, and 3) small laser energy (mJ) and sample sizes (100x100x1 μm) required. A disadvantage is that the duration of the sustained pressure is limited by the shock drive pulse, which is typically 80-350 ps for chirped pulse amplified (CPA) Ti:sapphire lasers, but can be extended to >1 ns.[49] Samples must be appropriately sized to allow measurement of the dynamics within this time range. Consequently, however, phenomena that happen too fast to be resolved using larger scale experiments (longer time scales) can be studied with these methods, such as

shock induced chemistry at high pressures[40, 56, 57, 65] and elastic-plastic deformation in metal films at very high strain rates.[44, 61, 75, 76] Experiments using the ultrafast laser shock apparatus at Los Alamos National Laboratory (LANL) have shown that features like the reactive cusp on the Hugoniot can be thought of as a time dependent property,[56, 57] and also demonstrated that the shock state reached with ultrafast laser driven shocks can be the same shock state observed at orders of magnitude longer time and larger spatial scales as observed in Hugoniot measurements of nonreactive liquids.[40, 53, 55] These techniques have allowed for the measurement of several thousand Hugoniot points for liquid mixtures, a number of experiments that exceeds the capabilities of traditional shock compression methods.[43, 60] These experiments are not limited to liquids and can be applied to organic, dielectric, and metallic solids as well.[44, 49, 54, 58, 61, 76-79] These shock generation and characterization techniques offer any ultrafast laser laboratory access to a broad range of interesting shock physics and chemistry problems, and the goal of this paper is to provide a level of detail on experimental methods and integration sufficient to propagate these techniques to laboratories that have not historically performed shock experiments. Presented in this paper are extensive details on methods of generating laser shocks, sample preparation, ultrafast dynamic ellipsometry (UDE) measurements and simultaneous fits for shock parameters, implementation of visible white light supercontinuum absorption measurements, generation and integration of broadband mid-infrared measurements into the shock experiment, and timing of all probing beams at the sample. This work was featured in American Institute of Physics, Review of Scientific Instruments, Volume 90, Issue 6. Permission to reprint this work has been granted by AIP Publishing under the license number 4781500396061.

2.2   Shock generation

The basis for the frustrated laser ablation shock generation technique using ultrafast lasers was the extraction of a fraction of the amplified chirped pulse before compression and the clipping of its temporally leading edge by clipping the long wavelength end of its spectrum to produce a sharp risetime of <5 ps. A beamsplitter was placed after the amplifier and before the compressor in order to extract a fraction of the chirped pulse. Depending on the needs of the experiment, the spectral clip can be performed 1) in the stretcher before amplification, as shown in Fig. 1A, 2) in an additional stretcher post amplification, or 3) by placing a short wavelength passing filter in the extracted stretched output and optimizing the desired spectrum via rotation of the filter. Option 1)

has the benefit of maintaining the full energy in the output beam, although the compressed pulses will not be as short due to the narrower spectrum and amplification in the regenerative amplifier tends to reduce the intensity risetime. Option 2) has significant additional costs as well as energy loss of ~50%. Despite this large energy loss, this technique is favorable when the stretched pulse is desired to be longer than the chirped pulse duration coming from the CPA (often the case for 1 kHz systems). Lastly, option 3) is exceptionally simple to implement at some loss of energy in the drive laser. Depending on the requirements for each experiment, one of these three methods have been used before.[42, 53, 67, 80, 81] The spectral shape, temporal duration, and rise time of the spectral profile was nominally the same for all three techniques with different 10 Hz and 1 kHz CPA systems;[42, 53, 67, 80, 81] however, the laser energy available to drive shocks was different for each technique and system. For most of the measurements presented in this paper, a 10 Hz Ti:sapphire laser system was used with ~8 mJ of uncompressed pulse energy after filtering, ~8 mJ of compressed pulse energy, ~120 fs pulse width after compression, and ~12 nm of bandwidth FWHM centered at 785 nm. An 842 nm short pass filter was rotated to clip the spectral leading edge so that a sufficiently steep rise time (<5 ps) was obtained. Such a rise time plus sufficient remaining pulse energy to support the shock wave was achieved when the filter was rotated to leave ~1/2-2/3 of the spectral bandwidth. An example of this can be seen in Fig. 2B. For shock generation methods, bandwidth is less important compared to the desired temporal duration of the shock measurement, but is important for spectroscopic techniques as shown below. No observable differences in the quality of the generated shocks were found using any of these methods to produce the spectral clip.

Figure 2A) One method of spectrally clipping the chirped beam from a chirped pulse amplifier was to place a beamblock in the red edge of the spectrum at the Fourier plane where the colors are dispersed and focused. After amplification, a beamsplitter extracted most of the energy into the chirped pulse that drove the shock and the ultrafast dynamic ellipsometry probes. B) The shaped shock drive was focused onto the sapphire/aluminum interface, while the probes reflected off the Al drive layer after transmission through the sample. The time dependent intensity of the chirped pulse is shown on the right with ~300 ps FWHM of shock duration. Typical focusing to 50-150 μm spot size allowed hundreds of shots on a 25.4 mm diameter substrate (bottom right). A) reprinted from S. D. McGrane, C. A. Bolme, V. H. Whitley and D. S. Moore, in International Symposium on High Power Laser Ablation 2010, edited by C. R. Phipps (2010), Vol. 1278, pp. 392-400., with the permission of AIP Publishing, and B) reprinted from S. D. McGrane, D. S. Moore, V. H. Whitley, C. A. Bolme and D. E. Eakins, in Shock Compression of Condensed Matter - 2009, Pts 1 and 2, edited by M. L. Elert, W. T. Buttler, M. D. Furnish, W. W. Anderson and W. G. Proud (2009), Vol. 1195, pp. 1301-1304., with the permission of AIP Publishing.

Figure 2B illustrates the geometry for a typical experiment. The chirped pulse shock drive was loosely focused to a spot size of 50-150 μm diameter at full width at half maximum (FWHM) at 0.2-8 mJ in shock drive energy. Since the drive is spatially Gaussian, the spatial extent of spectroscopic measurements must be smaller than the FWHM of the shock (see discussion below). A 2 μm thick aluminum film vapor deposited on a 0.5 mm sapphire substrate acted as a transducer, turning the laser energy into a mechanical shock while protecting the sample from direct laser excitation. The plasma expansion at the interface between the sapphire and the aluminum launched a shock wave through the aluminum and into the sample. The shock dynamics and shock induced electronic and vibrational spectral changes in the sample were probed in reflection geometry. Liquid samples, unlike solid thin film samples, required a window. Both the shock drive and chirped pulse interferometric probes had the same temporally dependent intensity (i.e. chirp), an

example is shown on the upper right of Fig. 2B. The sample was translated to a pristine location between shots using motor-controlled stages. The various interferometric and spectroscopic diagnostics shown in Fig. 2B were used to characterize the shock wave. Examples of material dynamics are detailed in the following sections.

Unlike gas gun and laser driven flyer plate experiments which generate relatively flat pressure waves, the spatial profile of the generated shock wave is nearly Gaussian in shape depending on the fluence of the shock drive laser beam.[82, 83] Fig. 3 shows the spatial profile of the shock drive into nitromethane at 5 mJ in energy producing a ~25 GPa shock wave. Spatially, the pressure was relatively constant at the near-flat top portion of the shock drive, but decayed outside of that region yielding a range of pressures that the sample experienced under shock loading. This shock drive profile has the benefit of measuring, with great care, multiple pressures in a single shot increasing data throughput of the experiment.[55] Unfortunately, the corollary to this is that the spectroscopic beams would probe a range of pressures unless the spectroscopic measurements were focused to be spatially narrower than the near-flat top portion of the beam. This latter approach was taken for most of the measurements presented. Alternatively, a diffractive optic or flat top beam shaper can be used to generate a flat top profile in the shock drive beam.[84-86] This approach negates any pressure convolution at the expense of experimental complication, as the flat top beam must be imaged at high demagnification with the sample at the focal plane. The use of a flat top beam shaper will be revisited in Chapter 4.
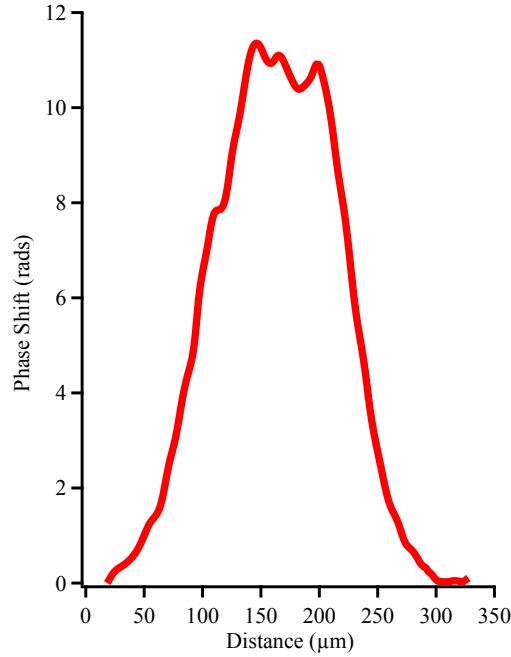
Figure 3 Spatial profile of the shock generation beam for nitromethane shocked to ~25 GPa at 5 mJ at the center of the shock. Phase shift measurements from ultrafast dynamic ellipsometry measurements are related to pressure.

2.3   XFROG chirp characterization of the shock drive pulse

The chirp or time dependent frequency of the shock drive pulse was characterized by cross correlation frequency resolved optical gating, or XFROG.[87-94] A collimated femtosecond pulse (the gate pulse) and the chirped laser pulse from the same Ti:sapphire laser pulse were crossed at a small angle (10°) in a beta-barium borate (BBO) crystal cut for frequency doubling (United Crystals, theta= 29.2°, phi=90°, thickness 0.1 mm, aperture diameter 5 mm). The time delay of one pulse was scanned with respect to the other and the spectrum of the sum frequency pulse was measured relative to the delay in a spectrometer. To better resolve the chirp and to increase time and spectral resolution from the XFROG trace, the spectral bandwidth of the gate pulse was reduced, either by placing a slit in the compressor, or using a narrow bandpass filter. This process increased the temporal duration of the gate pulse to ~1 ps, which was significantly smaller than the temporal duration of the chirped pulse. Without the spectral filter, the XFROG spectrum at each time delay would be too broad to accurately determine the chirped pulse frequency. The chirp of the shock-drive pulse was extracted from the XFROG trace, such as that shown in Fig. 4, where post measurement analysis software applied a threshold and width to the measured sum frequency

spectrum at each time delay to extract the peak wavelength versus time (the chirp). The chirp was fit to a second order polynomial for use in the analysis below.
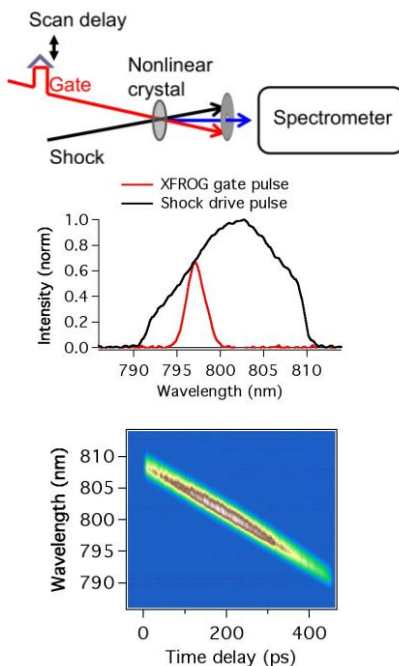
Figure 4 Cross correlation frequency resolved optical gating (XFROG) was used to measure the time dependent wavelength. The delay between a femtosecond spectrally narrowed gate pulse and the chirped pulse was scanned. The resulting sum frequency spectra were corrected for the energy of the gate pulse to produce the time dependent spectrum shown at the bottom.

2.4 Integration of shock drive pulses with multiple target diagnostics

A suite of diagnostic techniques has been developed to characterize the shock and material dynamics and chemistry: interferometry using ultrafast dynamic ellipsometry (UDE), visible white light (VIS) transient absorption spectroscopy, and mid-infrared (MIR) transient absorption spectroscopy. [39-41, 43, 44, 52-60, 64, 78, 95-101] UDE allowed the determination of shock and particle velocities and shocked refractive indices. VIS transient absorption spectroscopy was used to probe generation of absorbing products and intermediates due to reaction. MIR transient absorption spectroscopy probed vibrations corresponding to molecular functional groups to look for more detailed chemical changes. A broad overview of the overall experimental apparatus is shown in Fig. 5, although data will be shown from other similar arrangements (10 Hz and 1 kHz systems).
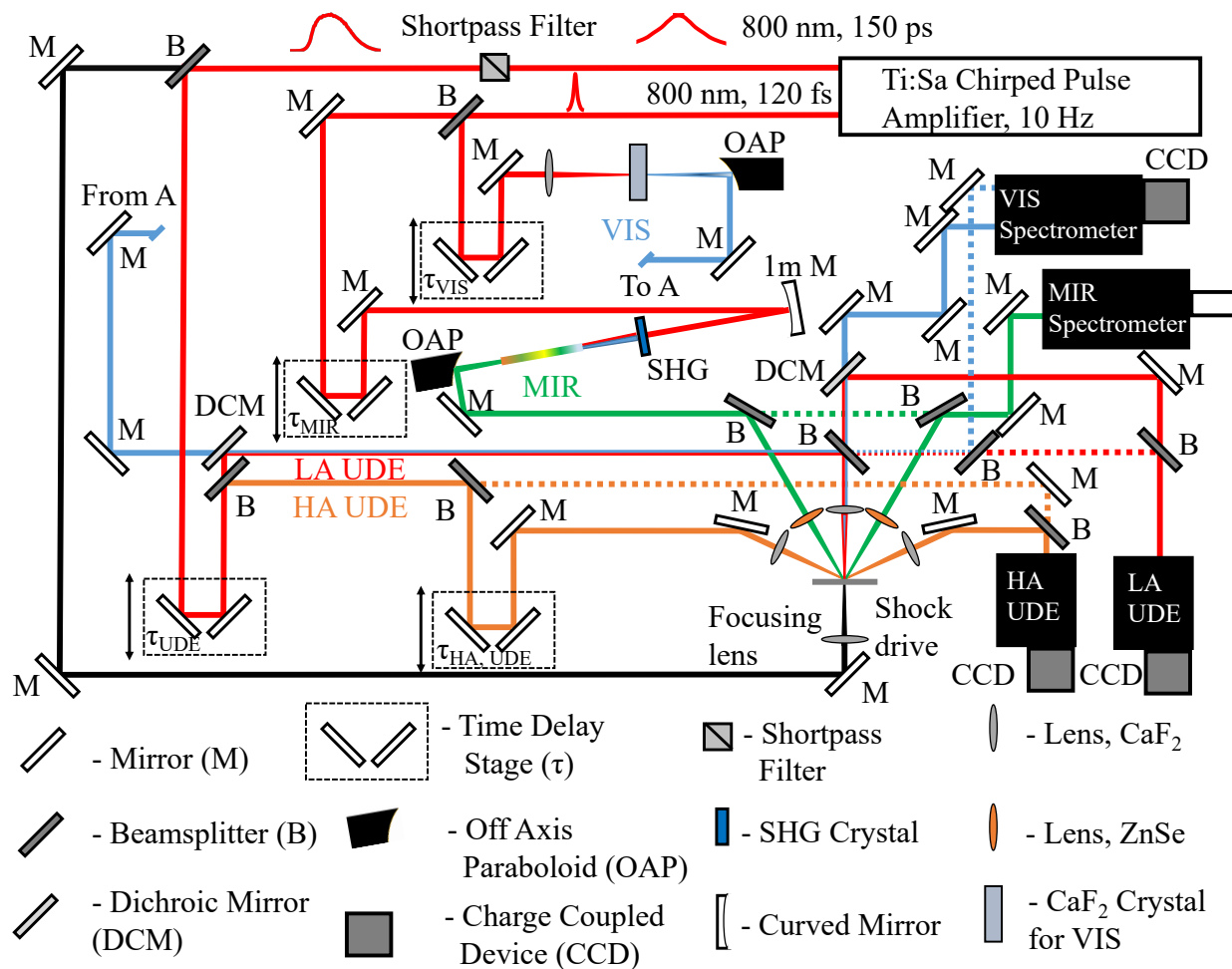
Figure 5 A single pulse out of the chirped pulse amplifier is split to pump five processes: shock generation (black), high angle (HA) UDE (orange), low angle (LA) UDE (red), VIS (blue), and MIR (green). Reference pulses are shown as dashed lines. Temporally, the reference pulses for the UDE have delay lines to ensure temporal overlap with the sample side for interference fringes, which are not pictured. Angles and distances are not to scale, but representative of actual pathways.

In addition to the diagnostics shown in Fig. 5, the sample was also continuously monitored using charge-coupled device (CCD) cameras to view the image going into the UDE spectrometer slits (HA and LA UDE) by placing a ~1% reflective beamsplitter in the beam path to utilize a small portion of the incoming light into the spectrometer. In each path, the cameras were placed at the same distance from the beamsplitter as was the slit. Fig. 6 shows an image before shocking the sample, and after, where the damaged hole in the Al, a bubble, and solid particles dispersed in the liquid can be seen, in this case for the low angle UDE. The field of view was ~ 0.5 mm x 0.5 mm. These cameras were helpful to ensure that the pre-shock sample location was of adequate quality

for data acquisition and had not been contaminated from nearby shots, that the UDE diagnostic beams were well centered and temporally overlapped with their reference which caused the interference fringes as seen in Fig. 6, and that the shock drive remained centered on the diagnostics as the sample was translated.
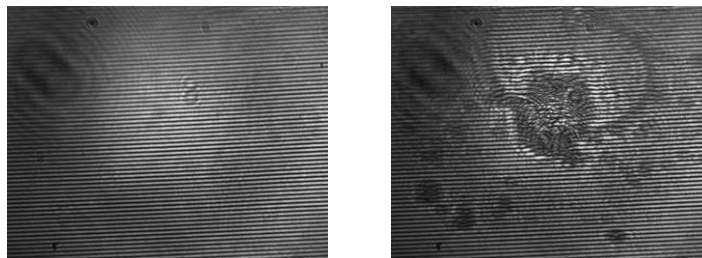
Figure 6 The beam entering the spectrometer was split to image the sample, showing the aliased fringes in the preshot (left) and the damage hole, gas bubble, and solid products formed post shot (right). The fringes in the image are caused by the interference between the reference and sample beams from Fig. 5.

2.5 Sample preparation

The thickness of the Al film and the sample need to be commensurate with the duration of the shock. In these experiments the typical shock velocities were <8 km/s, and shock duration was limited by the laser to ~350 ps. At 8 km/s, a 2 μm thick film will be traversed in 250 ps, but the shock or release wave from the Al/sample interface will have to travel back through the aluminum film, interact with the plasma/Al interface, and traverse the film again before it will affect the shocked material. This reshock or release will occur at times longer than the 350 ps observation window. The 2 μm aluminum coating was vapor deposited onto a 500 μm sapphire substrate (Esco Optics G110020) at 5 μTorr base pressure with a deposition rate of ~50 nm/s (Denton Explorer 14 High Vacuum Evaporator). Samples were allowed to cool prior to breaking vacuum in the deposition chamber to avoid columnar growth of the aluminum oxide layer. Opaque samples were typically produced when samples were not properly cooled. The sapphire substrates offer a high impedance that produced a stronger shock in the Al than substrates like glass or plastic. Similarly, various other metals could be used as the transducer layer: gold, nickel, tantalum, etc.[42, 80, 81] Aluminum was chosen for its close impedance match to most organic and dielectric materials.[102] Gold has been shown to ballistically accelerate electrons ahead of the shock propagation.[80, 103, 104] Substrates were treated with ultraviolet radiation and ozone (UVO cleaner 42-220) for ~5 minutes

to remove any organic adsorbates and volatile substances present on the substrates before aluminum deposition.

Liquid samples with a thickness of 6 µm (International Crystal Laboratories 6 µm gasket) for UDE and ~1-4 µm (no gasket) for VIS and MIR were prepared by dropping 50 µL or 20 µL (Eppendorf Research Pipette 1000 or 10), respectively, onto an Al coated sapphire substrate and then confined by a 2 mm thick 25.4 mm diameter potassium bromide (KBr) window (Edmund Optics #68-807). KBr windows were used as wavelengths from the near UV to mid-infrared were transmitted. VIS and interferometry measurements have been performed with optically transmissive windows: calcium fluoride, magnesium fluoride, or silica glass. For interferometry measurements, samples needed to be optically clear to measure the reflector (aluminum shock transducer) surface motion and the reflector needed to have near optical quality surface roughness. Thinner samples were required for MIR transient absorption spectroscopy as samples thicker than 4 µm resulted in saturation of the strong vibrational absorptions of the unshocked material. Solid samples were spin cast (MTI Corporation VTC-200P) onto the aluminum coated sapphire substrates and were typically limited to 2 µm in thickness by varying solution concentrations and spin casting conditions (rotation rate and time). Additionally, solid samples should be close to crystal density if wave dispersion and multiple shock interactions are to be avoided. Solid film thicknesses were measured using white light interferometry (Filmetrics F3).

2.6   Ultrafast Dynamic Ellipsometry (UDE)

The chirped pulse was passed through a time delay line to control the arrival time of the shock drive and interferometry beams with respect to the fs (spectroscopy) pulses. A small portion of the beam was taken (~2% energy – several tens of µJ) for UDE. An additional delay line was placed in the UDE path to control the timing between the shock drive beam and the UDE beam. UDE has been described in previous publications.[39, 52-55, 57] Here the method is summarized, and additional experimental details are provided.

A telescope was used to introduce a slow divergence to the beam and a 50:50 beam splitter formed two beams, one for high angle (HA, 62°) and one for 0° low angle (LA) interference. Previously angles of ~26° (LA) and ~70° (HA) at s- and p-polarizations were used.[39, 40, 43, 44, 52-58, 60] Concentrating first on the LA path, a further division using a 50-50 beam splitter produced sample and reference beams in a Mach-Zehnder interferometer configuration. A 90 mm focal

length (fl) triplet lens in the sample beam was placed approximately one focal length from the sample to illuminate a 500 μm diameter spot (coming to a focus after reflection from the sample) centered at the shock location. The UDE beam diameter was wider than the shock drive, in order to capture the entire shock diameter and additional unshocked area for background correction. The sample was imaged onto the entrance slit of the spectrometer using the same 90 mm fl triplet and a 750 mm fl singlet lens to give a magnification of 8.3x. Figure 7 shows the details of the LA UDE beam path. A second 750 mm fl lens was used in the reference beam to match the divergence of the sample beam. A neutral density filter was used to match the energies of the reference and sample beams which maximized the interference fringe contrast. The reference and samples beams were temporally overlapped at the slit via a time delay stage in the reference beam path.
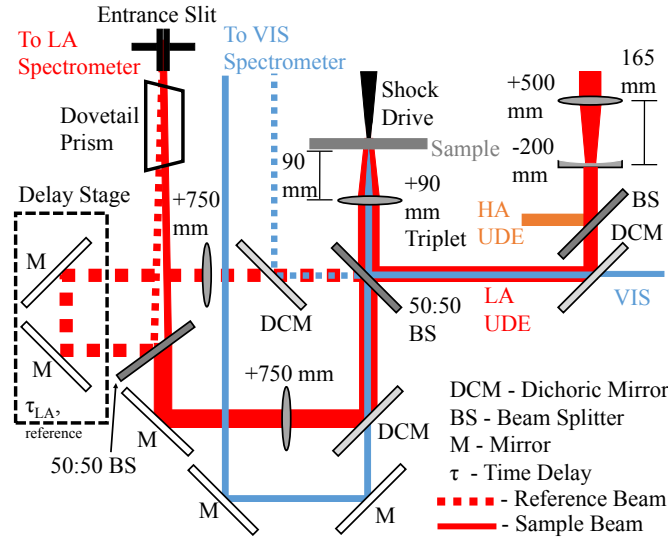
Figure 7 The LA UDE and VIS beam paths at 0° incidence. Prior to the first beam splitter (right, top), the UDE beam was passed through a positive 500 mm then a negative 200 mm lens to make a slowly divergent beam. A dichroic mirror reflected the UDE beam and passed the VIS beam. A 50:50 beam splitter was used to split both beams into sample and reference beams. A time delay stage was placed in the reference beam path to temporally overlap the reference and sample beams. A dovetail prism is positioned in the beam prior to the entrance slit. The HA UDE path was similar in design with the exception of no concentric beams and separate illumination and imaging lenses.

Reference and sample beams were crossed at a small angle at the entrance slit of a homemade spectrometer to produce interference fringes. The decision to use a homemade spectrometer considered the modularity of components (CCD array, lenses, and grating), and significantly decreased cost compared to commercial spectrometers. Nevertheless, a commercial spectrometer with a flat image plane could be used. Before the spectrometer slit, the image was rotated by 90°

using a Dove prism inserted at 45 degrees. Rotating the image was found to enable more accurate determination of the central portion of the shock for beams that were incident at the sample at high angle (60-70°). The LA image was also rotated so that the LA and HA imaged the same location and orientation on the sample. The CCD array (Thorlabs 8051M-USB) was binned by two pixels in both horizontal and vertical directions and a region of interest of 700 x 900 bins was used to increase recording speed during data collection. Spatial interference fringe frequency was measured to be ~0.7 fringes/μm. Images were collected at 0.5 Hz. The temporal duration of the UDE beams was the same as the shock drive beam (~300 ps FWHM). With the LA UDE beam at 0° there was no polarization dependence, which provided only a single measurement of the phase data; previous LA UDE measurements at ~26° added a Wollaston prism in the spectrometer just prior to the camera to separate the beam into s- and p-polarizations allowing two measurements (see discussion on HA UDE below). The switch to the zero degree path was to spatially accommodate more spectroscopic measurements at the sample.

The HA UDE was performed in a similar way to LA UDE, but the linear polarization of the sample incident beam was rotated to an angle of ~45° using a λ/2 achromatic waveplate prior to interacting with the sample. A 100 mm fl lens illuminated the sample with a ca. 500 μm tall elliptical spot. The reflected beam was collected via a 50 mm fl lens and imaged onto the spectrometer entrance slit by a 500 mm focal length lens with a magnification of 10x. The HA UDE reference beam was sent through a similar set of optics to match the size, polarization, energy, and magnification of the sample beam. A detailed schematic can be seen in Fig. 8. S- and p-polarizations images were separated using a Wollaston prism just prior to the CCD. A mask was placed on the Wollaston prism to fully separate the two images, and the camera to prism distance was optimized for this as well. Half waveplates for both the sample and the reference beams were rotated such that the s- and p-polarization images were matched as closely as possible in energy. The region of interest used by the HA UDE camera was 1500 x 1200 bins to accommodate both polarizations on the same image. Spatial dispersion was ~1.205 μm/bin, and the spatial fringe frequency was ~0.25 fringes/μm for HA UDE.
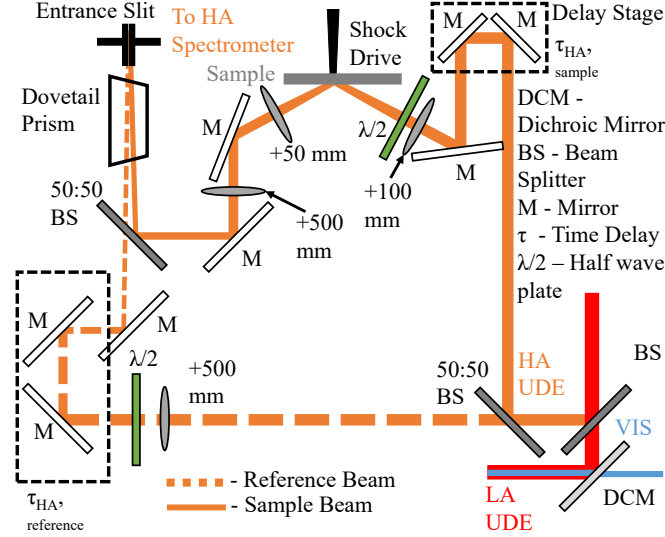
Figure 8 Detailed HA UDE pathway. HA UDE was performed at 62°. A time delay was added to the sample beam path for the HA to overlap the HA probe beam with the LA probe beam.

2.6.1 UDE data analysis

UDE data analysis required calibration of the spectrometer first for wavelength and then for time. Spectral dispersion on the temporal axis for the camera was measured to be 39 bins/nm and 49 bins/nm for the LA and HA UDE, respectively (1 bin = 2 x 2 pixels). The chirp was measured by XFROG (Section III) to be ~0.041 nm/ps, which resulted in temporal dispersion of ~0.62 ps/bin and ~0.50 ps/bin for LA and HA UDE, respectively. The temporal resolution was limited to 3-5 ps because of the assumed linear mapping between wavelength and time. The spectrometers were calibrated using atomic emission lines from spectral lamps of krypton and argon (Newport 6031 and 6030). A linear wavelength calibration fit was calculated for each spatial position along the slit. The very slight curvature of the atomic emission lines present in the image on the CCD was corrected using these calibrations when data images were interpolated onto an evenly spaced time grid, which also used the XFROG wavelength to time calibration.

Fourier analysis was used to determine the space and time dependent phase and reflectivity changes caused by the shock, as detailed in references. Four images were recorded for each shot: preshock and shock images for HA and LA UDE. Each lineout in the spatial dimension was multiplied by a tapered cosine function (flat top over central 60% and falling smoothly to zero as a cosine at the edges) prior to inverse Fourier transformation to avoid edge artifacts. The resulting image was split into amplitude (reflectivity) and phase. Phase data ranged from $-\pi$ to π and were

unwrapped to give total phase shifts. Shock images were divided by or subtracted from the preshock image for amplitude or phase calculations, respectively. Planar background tilt was removed using three user-selected reference points away from the shock region. A final user-selected point for offset could then be prescribed, which was only necessary if there was a small constant phase at the center of the shock region due to a prepulse arriving ns before the main shock drive pulse. The contrast between the prepulse and the shock drive pulse should be <0.1% and larger energies may require better contrast. Maximal prepulse phase offset values were <0.2 radians, meaning the aluminum surface was estimated to move approximately <13 nm at long times (>10 ns) from prepulse excitation. Typical prepulse phase shift are much less than this, and often unobservable. Raw LA UDE images and the analyzed phase and reflectivity image data for shocked liquid phenylacetylene are shown in Fig. 9 (these data were obtained when the LA UDE used 30° beam incidence). The oscillations are due to thin film interference between the reflection from the aluminum interface moving at the particle velocity, u_p and the partial reflection of the UDE probe light off the shock front moving at the shock velocity, u_s. Temporal lineouts for phase change were spatially averaged over two to five pixels and were centered at either a user selected line or at the peak position (obtained from a Gaussian fit to the phase data). These lineouts were then fit to models of the shock dynamics to determine material response to the shock as shown below.
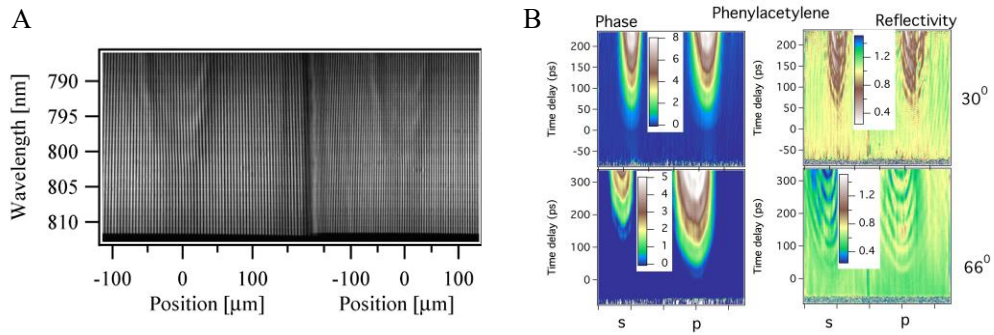
Figure 9 Low angle UDE raw images during shock with calibrated wavelength and spatial axes B) Phase and reflectivity maps after Fourier analysis for s- and p- polarizations and 30º and 66 º angles for shocked phenylacetylene.

2.6.2 Determining shock parameters from fitting UDE data

Coupling thin film interference to a constant shock propagation model allowed the UDE data to be fit to determine shock velocity (u_s), particle velocity of the Al/sample interface (u_p), and shocked refractive index (n_s). A detailed analysis has been provided by Brown et. al. and Bolme et. al., but is shown again here for completeness.[39, 53, 56] Description of the light propagation through the shocked and unshocked materials follows the same treatment as for multilayer films.[105] A transfer matrix for the interface between two films can be written as:

$$M_m = \begin{bmatrix} \cos(\phi_m) & \dfrac{i \sin(\phi_m)}{\gamma_m} \\ i\gamma_m \sin(\phi_m) & \cos(\phi_m) \end{bmatrix} \tag{1}$$

where the subscript m is the index for a given layer in the multilayer media, ϕ_m, given by

$$\phi_m = \frac{2\pi}{\lambda} n_m d_m \cos(\theta_m) \tag{2}$$

is the phase difference between the entrance and exit of a film at interface between layer m and m-1, λ is the wavelength of the incident beam in vacuum, n_m is the refractive index, d_m is the thickness, and

$$\gamma_m = n_m \cos(\theta_m) \tag{3}$$

is the s-polarization refractive index change upon transit into layer m. Eqn. 3 holds for s-polarization, while for p-polarization eqn. 4 is used. Refractive index change for the p-polarization takes the form,

$$\gamma_m = \frac{n_m}{\cos(\theta_m)} \tag{4}$$

where θ_m is the refracted angle, which can be determined from Snell's law,

$$\theta_m = arc\sin\left(\frac{n_{m-1}}{n_m}\sin(\theta_{m-1})\right). \tag{5}$$

42

A transfer matrix was implemented to account for the interaction of light with multiple layers of the film in the order in which the light encounters the layers. The transfer matrix going through n films takes the form,

$$M = M_1 M_2 M_3 \ldots M_n \tag{6}$$

with M_1 being the first material to interact with the light (outer most layer), and M_n being the final reflective medium in this article. The reflection is due to the large imaginary component of the refractive index of the metal film, although any layer can have a complex refractive index. Two types of experimental configurations were considered for this specific apparatus: solid and liquid films. Liquid films necessitated the use of a thick or wedged window which must be accounted for in the above transfer matrix. Since there was not a resolved coherent reflection from the window/air interface, M_1 was taken to be the window instead of the air, and the angle of incidence inside the window was used. Note that, therefore, the high angle for a liquid sample was thus lower than the high angle for a solid sample because the incidence angle inside the window is less than the angle in air. For liquid films a matrix order from outermost to the reflective layer was typically: window (calcium fluoride (CaF_2) or potassium bromide (KBr)), unshocked liquid, shocked liquid, 5 nm of aluminum oxide, and 2 μm of aluminum drive layer. The oxide layer was observed in static ellipsometry measurements, so was included for completeness.

Shocked and unshocked layer thicknesses changed during the experiment with shocked material thickness growing and unshocked thickness decreasing with time. Assuming a steady shock velocity, the unshocked material thickness was calculated by,

$$d_u = d_0 - d_s \tag{7}$$

where d_0 is the original film thickness and d_s is the distance traveled by the shock. The shock pressure was assumed constant, thus velocity, for simplicity.[39, 53, 56] The shocked layer film thickness was calculated by,

$$d_s = (u_s - u_p)t \tag{8}$$

where u_p is the particle velocity, u_s is the shock velocity, and t is time.

Previous studies by Gahagan et. al.[81] demonstrated that the free surface position of a shocked metal layer could be modeled well using,

$$d_{\text{fs}} = \int \frac{1}{2}\left[1 + tanh\left(\frac{t - t_0}{\tau}\right)\right] u_{\text{fs}} dt \qquad (9)$$

where t_0 is the time to maximum acceleration of the flyer, τ is the rise constant of the flyer, and t is the time of interest.[81] The rise time in a shocked aluminum layer was determined to be 5.5 ps. Depending on the shock conditions and aluminum film thickness, the separation of the elastic and plastic wave may also have to be taken into account.[44, 77] Data illustrating the elastic and plastic waves are shown for 2 μm thick aluminum films on sapphire in Fig. 10, but the required laser energies will vary with laser spot size and substrate material. Typical experiments were operated at sufficiently high pressures to overdrive the elastic-plastic transition. The elastic-plastic separation and risetimes could also be implemented in the model using multiple risetimes of the form given by Eqn. 9 in the simulations.
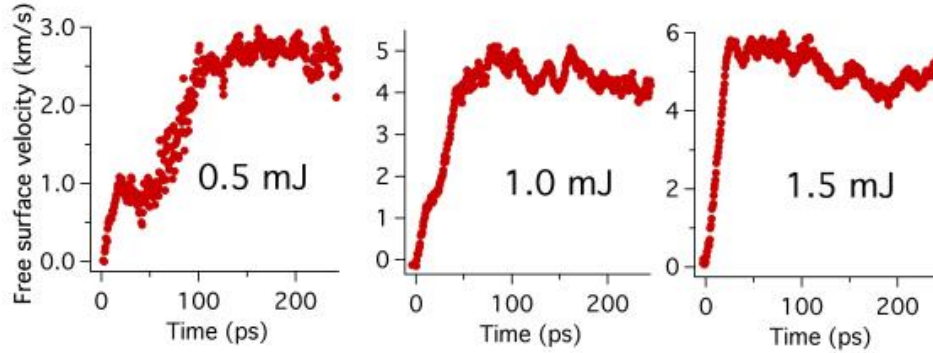
Figure 10 Free surface velocities for 2 μm thick Al films at 3 different drive energies. The initial rise is due to the elastic wave, with the plastic wave following, but not resolved at the higher energy.

The difference between the simulated data and measured data was then minimized in a multiparameter fitting procedure. Phase values were calculated using the time dependent thicknesses at each polarization and angle by combining the thin film transfer matrix and the shock dynamics equations above. The Levenberg-Marquardt (LM) parameter optimization method used was found to be sensitive to initial parameter guesses. In order to have an automated set of good initial starting points for the minimization, a second order central difference derivative was used

to calculate the derivative of the phase data, which was then smoothed with a Savitsky-Golay filter with 21 side points (~13 ps). This phase derivative data was analyzed by using Armstrong's method for fitting the offset, oscillation frequency, and oscillation amplitude to determine initial parameters for u_s, u_p, n_s.[47] The derivative data were also appended to the phase data using a scaling factor set to make the derivative similar in magnitude to the peak values of the phase data, in order to force the LM minimization algorithm to fit the oscillatory behavior in the phase data. The phase and derivative data from all polarizations and angles were appended to form a single data set and fit simultaneously for u_s, u_p, n_s. Unless there was large loss of reflectivity at 800 nm due to the shock, the reflectivity data were typically not fit and the imaginary part of the shocked refractive index was fixed at zero. Although the Armstrong fitting method was used to get initial variables for the LM program to fit the UDE data, the measurements differ slightly in that UDE utilizes a Mach-Zehnder (spatial) interferometer design compared to a spectral interferometer design that measures the change in phase over a fixed time delay with both beams reflecting off of the sample.[47]

An example of how well this model can fit the data is shown in Fig. 11 for acrylonitrile shocked to 14 GPa. Note that only the center lineout of the spatially resolved data is shown. More careful analysis can allow many Hugoniot measurements in a single shot by using multiple spatial lineouts and provided the total shock front travel is significantly smaller than the diameter of the shock.[55] Alternatively stated, the transverse velocity should be <2% of the axial velocity to claim near uniaxial conditions.[55]
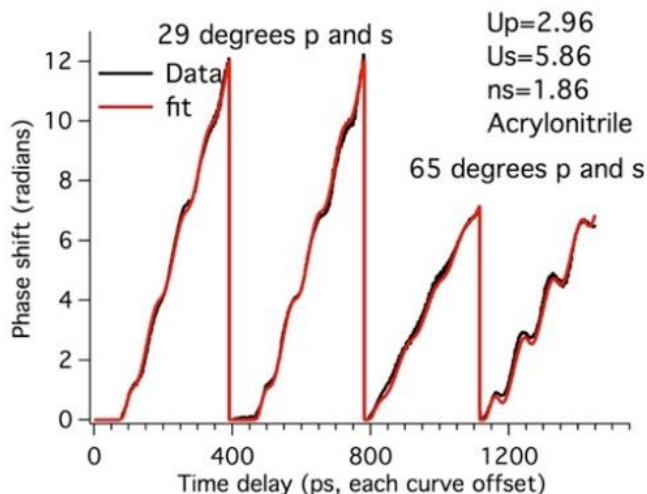
Figure 11 UDE along with fit determining u_p, u_s, and $n_{shocked}$ for acrylonitrile shocked to 14 GPa final pressure. Reprinted (adapted) with permission from N. C. Dang, C. A. Bolme, D. S. Moore and S. D. McGrane, Journal of Physical Chemistry A 116 (42), 10301-10309 (2012). Copyright (2012) American Chemical Society.

Reactive materials can be measured using the analysis above; however, the results from this model are only strictly valid when the shock velocity is constant. When the time scale of the reactive wave is slower than the time scale of the UDE experiment, the material is considered unreactive and the measured shock and particle velocities will follow the unreacted Hugoniot.[40, 43, 55, 60, 99] Figure 12 shows that acylonitrile Hugoniot points measured in 300 ps time scale UDE experiments follow the unreacted universal liquid Hugoniot to substantially higher shock velocities than the same material measured at time scales longer than 10s of ns.[99] The UDE data at u_p> 2.5 km/s in Fig. 12 demonstrate results where acrylonitrile partially completed a volume decreasing reaction within the <0.3 ns measurement, which results in deviation of the measured points from the unreacted universal liquid Hugoniot and toward the product curve, which is seen in >10 ns experiments at u_p>1.8 km/s. Similarly, when the time scale of the reactive wave is significantly faster than the probing time, the time dependent phase data can be fit to determine the product Hugioniot.[40, 56, 57] Reaction time scales that are fast enough to result in changing wave speeds during the experiment (10s of ps) violate the assumption of constant velocity. An example of this phenomenon can be seen in Fig. 13, for the case of nitromethane (NM) shocked to ~28 GPa, as determined by the final fit. In this case, there was a time dependent phase shift that occurred due

to reaction in the middle of the data acquisition. The decrease in oscillation amplitude and increase in oscillation frequency that begins around 200 ps suggest a time dependent change in the physics or chemistry that was not captured by the simple model used to fit the data. Fitting the UDE data with a sliding window is one method that could be used for time dependent wave dynamics. Alternatively, a full simulation considering the time dependent reaction history could be implemented. In practice, there is a narrow range of shock pressures where the reaction will be resolved during the 300 ps observation time.
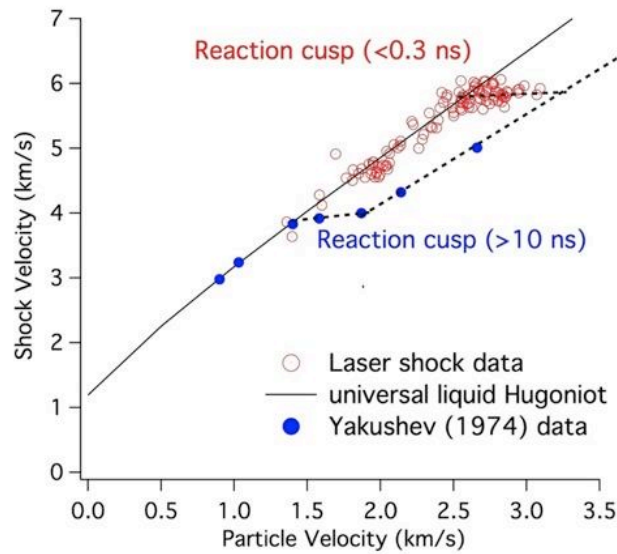
Figure 12 Data produced with laser driven shock measurements occurring in <0.3 ns follow the unreactive universal liquid Hugoniot to higher velocities than seen in measurements occurring at times longer than 10 ns. Reprinted (adapted) with permission from S. D. McGrane, K. E. Brown, C. A. Bolme and D. S. Moore, AIP Conference Proceedings 1793, 030033 (030036 pp.)-030033 (030036 pp.) (2017). Copyright (2017) American Institute of Physics.
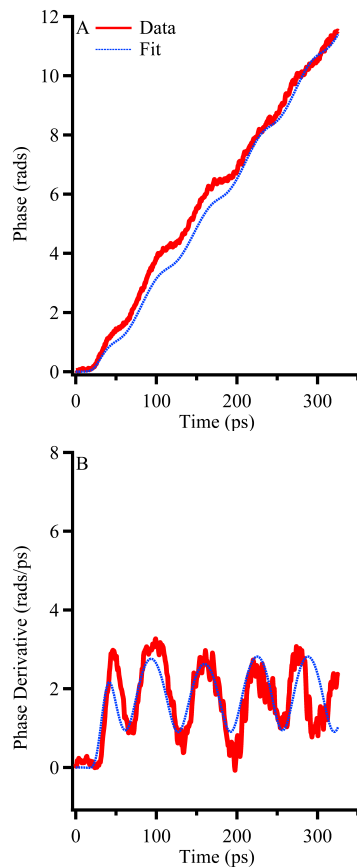
Figure 13 Comparison of the phase for (A) and phase derivative (B) for LA UDE for reacting nitromethane. A change in the oscillatory behavior appears in the data trace for the phase data and a frequency shift to higher frequency can be seen in phase derivative data. A shift to higher periodicity indicates the shock wave is accelerating. Specifically, u_s-u_p is increasing in this figure.

2.7 Visible (VIS) transient absorption spectroscopy

A small portion of the 800 nm compressed (fs) pulse from the Ti:sapphire laser was spatially isolated using an iris and focused with a 101.6 mm fl lens into a calcium fluoride window to generate visible white light (i.e., VIS, 425-750 nm), allowing transient absorption spectroscopy, which probes changes in the electronic spectra of shocked material[40, 56-58] or broad absorptions due to chemical reaction products or intermediates. Damage to the calcium fluoride crystal would appear after prolonged excitation (hours under optimal conditions at 10 Hz) requiring the crystal to be translated to a new location. A 101.6 mm fl 90° off-axis parabolic (OAP) mirror collimated the VIS beam. The temporal duration of the VIS pulse was calculated to be <1 ps using the Sellmeier equation and estimation of the thicknesses for optics traversed between the VIS generation and the sample. Since our typical time step was 25-50 ps, any inaccuracies that could

48

be caused by the temporal duration of the VIS beam were ignored. Following the OAP, an aperture of 15 mm diameter was used to control the size of the VIS beam. The VIS beam was then transmitted through the dichroic mirror used to point the LA UDE beam to the sample. The beamsplitter used by LA UDE also split the VIS beam into a sample and reference beams, as seen in Fig. 7. The dichroic mirror limited the spectral range at both the blue and red edges of the VIS pulse, whereas a broader spectrum could be obtained if the VIS and UDE did not share the same beam path. The VIS beam was viewed on the same cameras used to align the LA UDE beam, and its focus at the sample was translated onto a hole left after a shock to achieve spatial overlap. An 90 mm fl achromatic triplet lens was used to focus the VIS beam to <75 μm FWHM at the sample, as well as to collimate the reflected beam before it was sent to the spectrometer. Notch filters at 441.6, 532.0, 568.2, and 632.8 nm (Kaiser Holographic) placed in the VIS beam were used to calibrate the spectrometer.

The VIS spectrometer was a homemade grating spectrometer. CCD camera pixels were binned 2x2, and the CCD array was synchronized to the laser with a 1 ms electronic gate, with a region of interest of 150 x 1648 bins. Wavelengths in the range of 425-750 nm could be detected at the CCD at a dispersion of ~0.15 nm/bin. Since the incoming beams were collimated laser sources, the spectrometer did not use a slit, and the entire signal beam was used. Previously, a traditional spectrometer with a focusing lens, slit, and collimating lens was used; however, the sample and reference spectra that transmitted through the slit had to be carefully matched. The reference pulse was offset spatially from the sample beam by introducing a small vertical angle. Lenses were placed in the reference path to match the divergence of the reference beam to the sample beam. Similarly, a beam splitter was placed in the sample path to match the spectrum of the sample side to the reference side. Figure 14 shows an example of the preshock and shock images. Each spectrum (sample and reference) was spatially integrated (horizontal direction in Fig. 14).
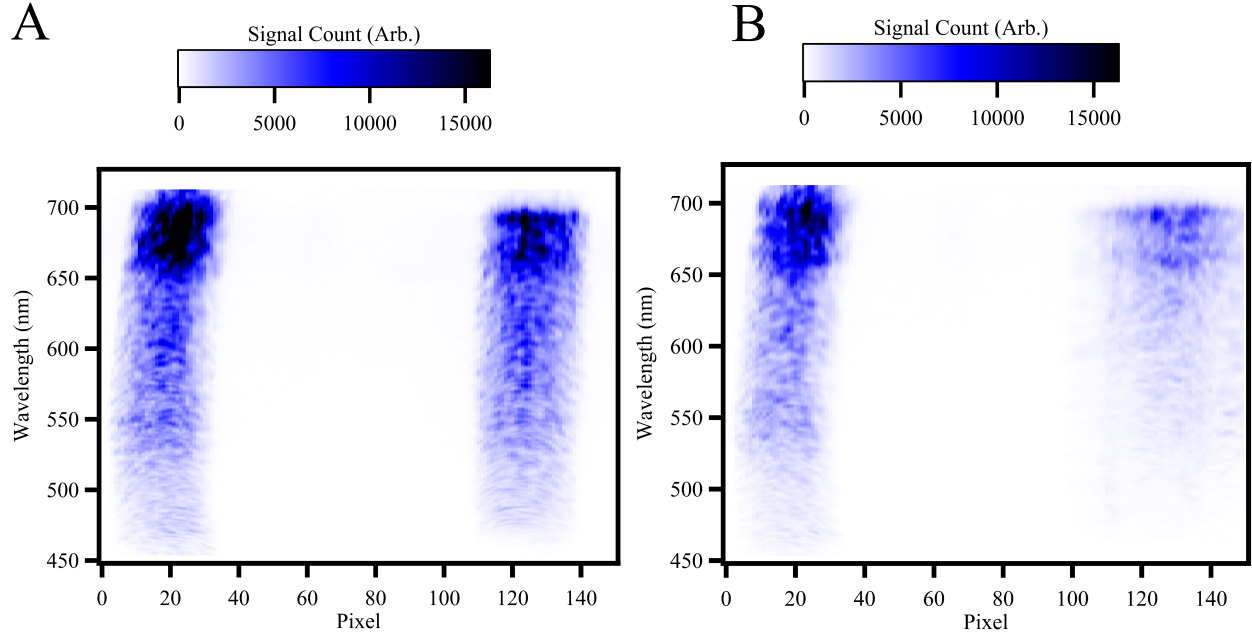
Figure 14 A, image of static spectrum of reference (left side) and sample (right side). B, image during shock loading for nitromethane at 25 GPa. Significant intensity changes can be seen comparing the preshock image to the shock image.

Normalization of the sample beam by the reference removed pulse to pulse spectral fluctuations. The shocked spectrum was then normalized by the preshocked spectrum to determine changes from shock compression. The change in absorbance (ΔA) in the shocked material was defined by:

$$\Delta A = -log\left(\frac{\left(\frac{T_{Sample}}{T_{Reference}}\right)_{Shocked}}{\left(\frac{T_{Sample}}{T_{Reference}}\right)_{Preshock}}\right) \tag{10}$$

where T is transmission spectra of the sample/reference shocked frame, or preshocked frame.[40, 56, 57] Absorbance changes due to electronic structure, chemical reaction, or material deformation had to be distinguished from the shock induced reflectivity decrease of the aluminum drive layer. To accomplish this, a nonreactive film, in this case diethylenetriamine (DETA), was shocked and the absorbance compared to the material of interest. Figure 15 shows the VIS transient absorption spectra of the nonreactive material DETA contrasted with that of nitromethane (NM) as well as NM with DETA. The DETA sensitized the NM causing faster reactions and more absorption. Pure

DETA shows the loss of reflectivity due to shock induced roughening of the aluminum. An aluminum free surface expanding into air would have an even larger loss of reflectivity as shown in Fig. 16.
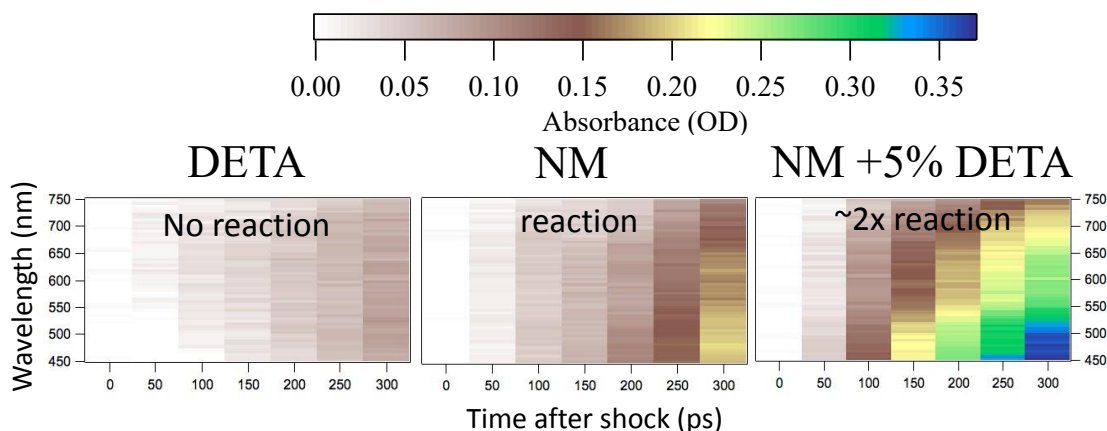
Figure 15 VIS data illustrating the effect of the roughening of the Al reflective layer in DETA, where there is no reaction. This contrasts with the increased absorption seen in shocked nitromethane, and nitromethane sensitized with 5% DETA, which have reaction products that absorb in the visible range. All images at $u_p > 2.5$ km/s. Reprinted (adapted) with permission from K. E. Brown, S. D. McGrane, C. A. Bolme and D. S. Moore, Journal of Physical Chemistry A 118 (14), 2559-2567 (2014). Copyright (2014) American Chemical Society.
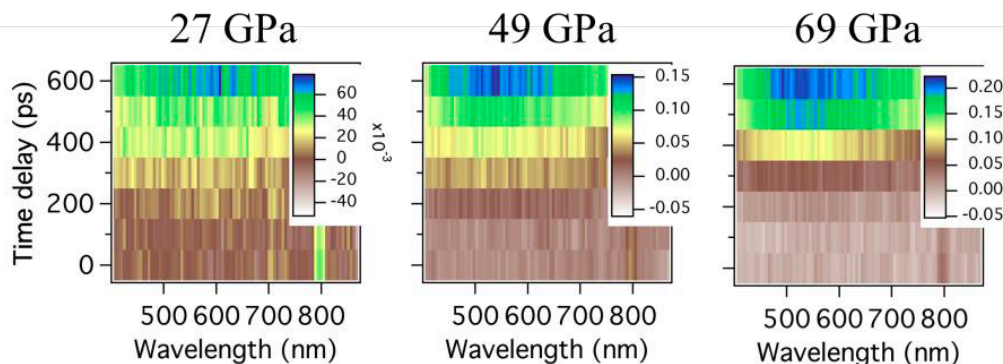
Figure 16 VIS absorption data for an aluminum free surface shocked at various pressures. VIS absorptions are stronger for aluminum expanding into air than when driving a shock into a material.

2.8   Mid-infrared (MIR) transient absorption spectroscopy

Broadband mid-infrared (MIR) wavelengths of 4-15 μm were generated using a technique similar to Nomura et. al.[106-109] The filamentation region was ~4 cm in length and broadened the spectra of the 400 and 800 nm beams through self-focusing and self-phase modulation, as shown

in Fig. 17. Note that the long wavelength MIR edge was limited by the HgCdTe detector used in the measurement, while the short wavelength edge was limited by the spectral bandwidth of the ~110 fs pulses. Typically, a calcite delay crystal was used to delay the 800 nm beam relative to the 400 nm beam to achieve temporal overlap, and a dual waveplate was used to match the polarizations of the two beams. Removal of the calcite delay crystal and the dual waveplate still yielded broadband MIR wavelengths, but with a polarization that was not linear, as measured with wire grid polarizers. Different rotations of the optics, pulse compression, and focusing affected intensity, spectrum, and stability while producing multiple μJ of MIR over a range of conditions.
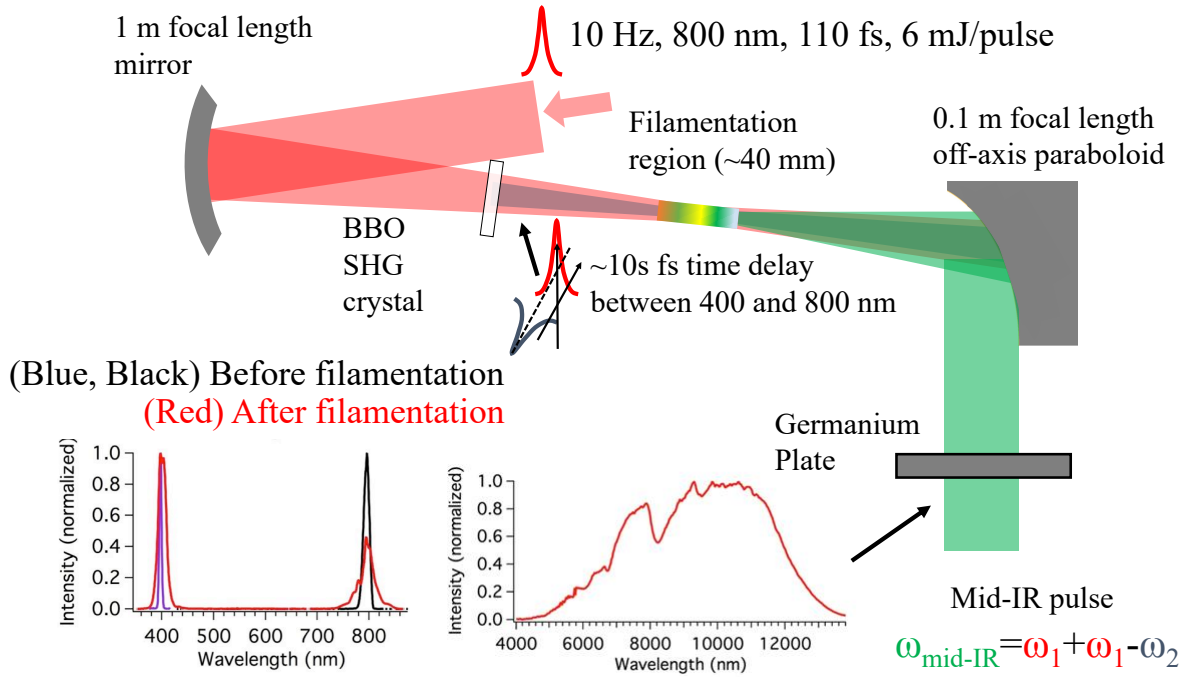
Figure 17) Four wave mixing of 400 nm and 800 nm in an air filament were used to create broadband mid-infrared. Due to the thickness of the BBO a small delay was introduced between the 400 nm and 800 nm beams. Self-phase modulation broadened the 400 nm and 800 nm beams after the filamentation region. An antireflection coated germanium plate was used as a long pass filter to only pass the MIR beam.

A toroidal spatial profile of the MIR beam was produced from the filamentation process. A 152.4 mm fl 90° OAP collimated the MIR beam. The 800 nm at the center damaged the OAP, but the damage spot was contained within the MIR toroid. A spatial filter composed of two zinc selenide (ZnSe) lenses (100 and 75 mm fl before and after the pinhole respectively) and a 400 μm pinhole (slightly off the focus for more precise spatial filter control) was used after the OAP to

allow tight focusing of the MIR beam onto the center of the shock, as shown in Fig 18. Chromatic aberrations and spot size at the sample were minimized using a 75 mm fl ZnSe/ZnS achromatic doublet lens. The spot size of the spatially filtered beam at the sample was 75 μm FWHM. A single side anti-reflective coated germanium window was used as a beamsplitter to produce reference and sample beams.
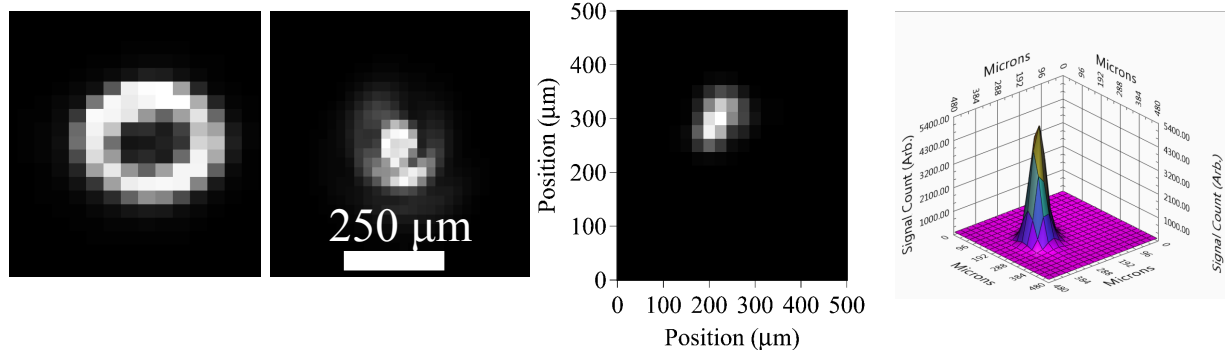
Figure 18 From left to right, image of the MIR beam after collimation from the filamentation process, the focus of the toroidal beam, the spatially filtered beam focused at the sample, and the three dimensional view of the focused beam at the sample. The FWHM of the beam at the sample was ~75 μm.

The reference and sample MIR beams, spatially offset, entered a spectrometer that consisted of a prism, lens, and microbolometer array. A right angle 25.4 mm ZnSe prism (ISP Optics ZC-RP-25) dispersed the MIR. An incidence angle of 68° was used on one of the 25.4 mm sides of the prism to disperse the beam almost exactly perpendicular to the incoming beam path with low reflection losses near Brewster's angle. The MIR spectra were focused with a positive meniscus 38 mm diameter, 63 mm fl ZnSe lens onto the microbolometer array (FLIR A35), as shown in Fig. 19. The reference beam was offset vertically from the sample beam through the spectrometer and used to normalize laser fluctuations. System response (spectral throughput for sample and reference) was also considered for the normalization of the spectra. The normalized transmission spectra (T) were calculated using

$$T = \frac{\dfrac{S_{\text{sample}}}{S_{\text{system, sample}}}}{\dfrac{S_{\text{reference}}}{S_{\text{system, reference}}}} \tag{11}$$

where S refers to the signal measured by the microbolometer for the sample beam and reference beam during an experiment (shock and preshock), or a time averaged spectral response for both the sample and reference (laser energy fluctuations) beam prior to an experiment (S_{system} response was measured using an Al mirror). Transmission difference (ΔT) is the difference between the normalized transmission spectra for shocked and preshocked spectra. Fig. 20. demonstrates how eqn. 11 normalized spectra for the case of NM.
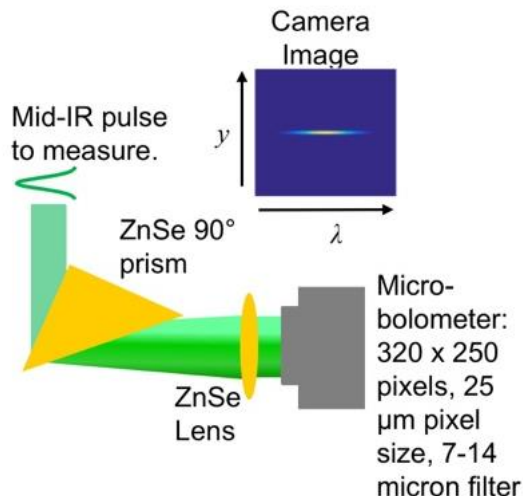
Figure 19 MIR spectrometer. The collimated MIR beams dispersed by a prism were focused on a thermal imaging camera. Adapted from Probing Ultrafast Shock-Induced Chemistry In Liquids Using Broad-Band Mid-Infrared Absorption Spectroscopy with permission from P. Bowlan, M. Powell, R. Perriot, E. Martinez, E. Kober, M. Cawkwell, and S. McGrane, which has been submitted for publication in Journal of Chemical Physics.
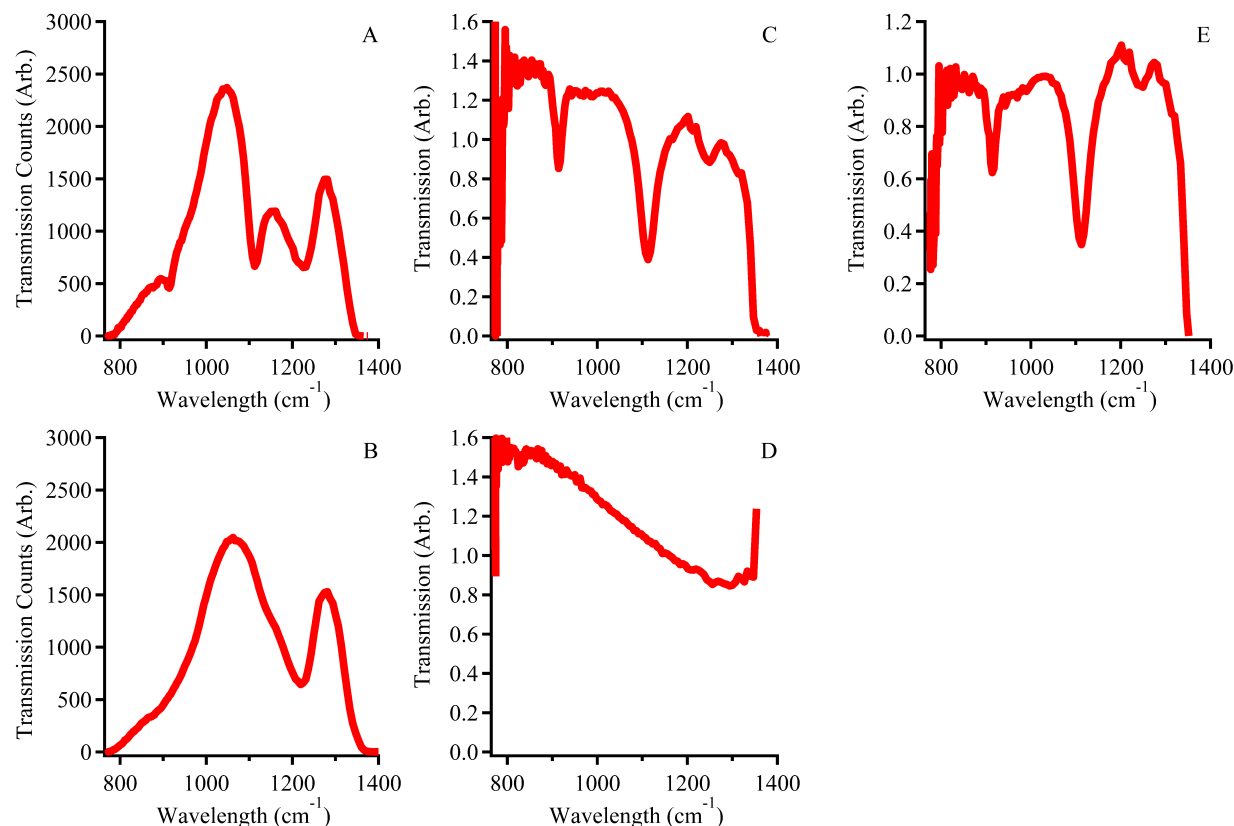
Figure 20 MIR spectral analysis. Normalization process for the reported transmission spectra for nitromethane. The raw transmission data (A) was first normalized by an averaged system response (B) producing a transmission spectrum (C). Following the system response, C was normalized for energy fluctuations in the laser by the normalized reference spectrum (D) leading to the transmission spectrum (E) from our MIR spectrometer. Similar to the sample spectrum the reference spectrum was first normalized by an average background. In this example, a CN-stretch at 920 cm^{-1}, a CH3-rock at 1100 cm^{-1}, and the edge of an NO_2 stretch at 1350 cm^{-1} were observable in this spectral range.

Calibration of the spectrometer was completed by comparing the transmission spectrum to the spectrum recorded by a commercial FTIR spectrometer (Fisher Nicolet iS5) for a MIR absorbing material. A spectral resolution of <30 cm^{-1} on average was achieved in the spectrometer using the chosen lens and prism combination. The dispersed wavelengths measured by our spectrometer follow a cubic order with less resolution at greater frequencies. Detection of the MIR beam was limited in this implementation to the spectral range of 750-1350 cm^{-1} by the coating on the microbolometer detector array and the optics used in the experiment. A comparison of the FTIR spectrum and our MIR spectrometer for polystyrene is shown in Fig. 21.
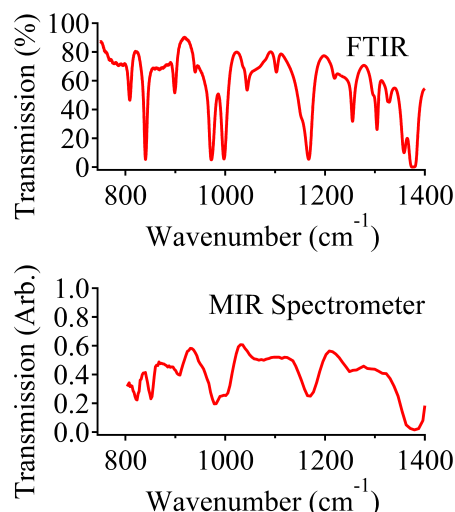
Figure 21 Comparison of the the MIR spectrum of polystyrene as measured by an FTIR compared to a 10 shot average of our MIR spectrometer. The resolution, spectrum produced by the MIR generation process, and spectral detection method was improved in later chapters.

As an example, the MIR spectral changes in trinitrotoluene (TNT) shocked to ~30 GPa are shown in Fig. 22. TNT has three modes available in the accessible MIR spectrum: two CN stretches at 910 and 930 cm^{-1}, and a ring breathing mode at 1080 cm^{-1}.[110, 111] Fig. 22 illustrates the shift to higher frequencies and broadening due to the high pressure and temperature. Increased baseline absorption may also be indicating partial reaction. Differences in preshock spectra at each time delay are attributed to data being acquired at different locations across the film that vary slightly in thickness.
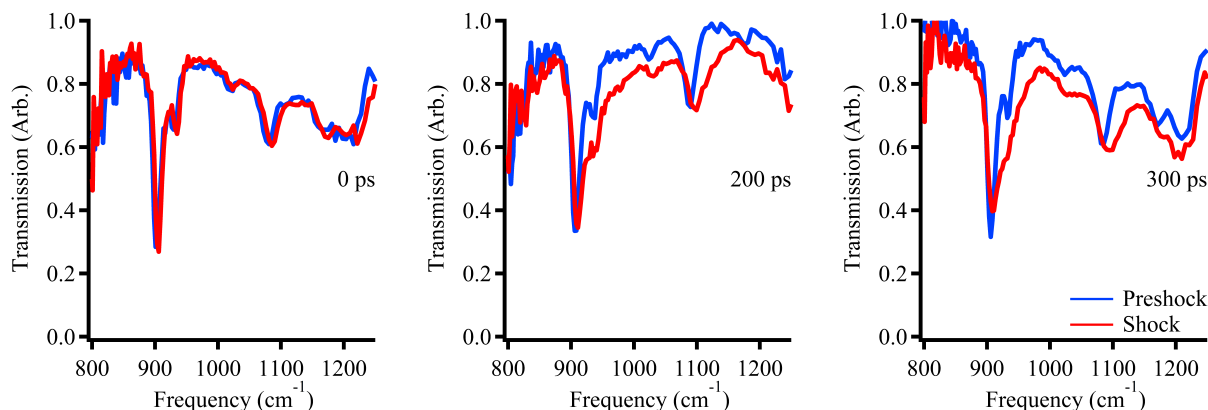
Figure 22 TNT MIR transmission spectra when shocked to ~30 GPa. Spectral peaks shift towards higher frequencies and broaden when shocked. The shifting and broadening increase as more material is shocked. A broad absorption feature also shows up over most of the spectral range. These spectral changes may be due to partial reaction of the TNT or strong scattering.

The mechanism behind the spectral broadening and shifting of the peaks in TNT in this MIR spectral range is still under investigation. Possible mechanisms include pressure induced frequency shifts, phonon lifetime broadening, vibrational hot bands, thin film interference effects, dephasing of the vibrations, or chemical reaction of the TNT when shocked to 30 GPa.[112-121] Efforts are in progress to better understand the underlying mechanisms that alter the MIR absorption spectra for shocked materials and will be published in the future. The MIR results presented in this paper are simply to demonstrate the technique and the application to probe materials under shocked conditions. As examples of the future utility of this technique, the MIR absorption spectra of shocked liquid samples have shown radically different behavior for reactive and unreactive materials.[64, 100]

2.9 Synchronization of diagnostics to the shock

Synchronization of the MIR beam to the shock drive, UDE, and VIS beams was performed using pump-probe reflectivity measurements of germanium placed at the sample location. The MIR reflectivity (probe) signal was monitored during a temporal scan of the chirped (pump) pulse. Temporal overlap between the MIR and the leading edge of the UDE spectrum was defined as the time when the probe beam signal changed from the baseline reflection signal by >3 standard deviations. It should be noted that germanium reflectivity initially decreased during temporal overlap, then increased at delays longer than shown in Fig. 23. MIR and VIS cross timing was achieved by visually monitoring the MIR reflectivity while adjusting a micrometer stage delaying the VIS pump. Achieving ps synchronicity of the MIR and VIS was straightforward as the temporal duration of both pulses were sub-ps.

The VIS was synchronized with the UDE by crossing the beams in BBO (United Crystal 10 x 10 x 6 mm, theta= 29.2º, phi=90º) and measuring the cross-correlation sum frequency generation signal. By spatially masking a small portion on one side of the UDE and the opposite side of the VIS, the beams could be crossed at the focus and the cross correlation signal spatially isolated and measured with an amplified photodiode (Thorlabs DET210), transmitted to an boxcar averager (Stanford Research Systems SR200) , and then to an analog math processor (Stanford Research Systems SR235) to further increase the signal to noise ratio. Fig. 23 illustrates that the cross-correlation VIS/UDE method demonstrated the same delay as the germanium reflectivity UDE/MIR method once the VIS and MIR pulses were synchronized.
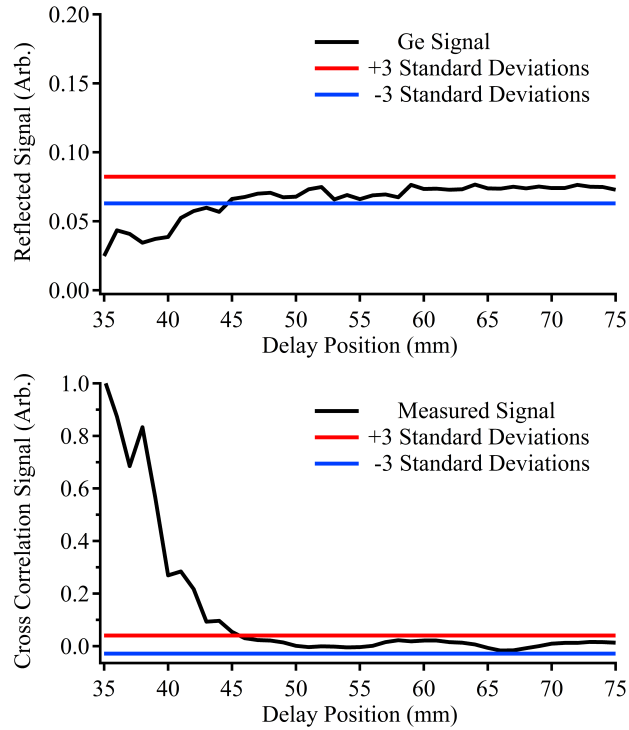
Figure 23 Top: MIR reflectivity using the LA UDE beam as the pump as a function of delay stage position. Bottom: cross correlation sum frequency generation between the LA UDE and VIS using BBO at the sample. Both signals change at 45 mm on the delay stage position, signaling the overlap of MIR with UDE and VIS with UDE. Cross-correlation measurements were notably slow compared to Ge reflectivity measurements requiring a few hours of data collection for cross correlation and ~15 minutes for Ge reflectivity.

The UDE to shock arrival time was then used to synchronize the MIR and VIS pulses to the shock. Fig. 24 illustrates how the sharp spectral edge of the UDE was signaled by the transition from noise to zero phase change, while the shock arrival was indicated by an increase in phase with time. This phase data was measured by LA UDE, and translated from pixels to wavelength to time using XFROG and the spectral calibrations described earlier.
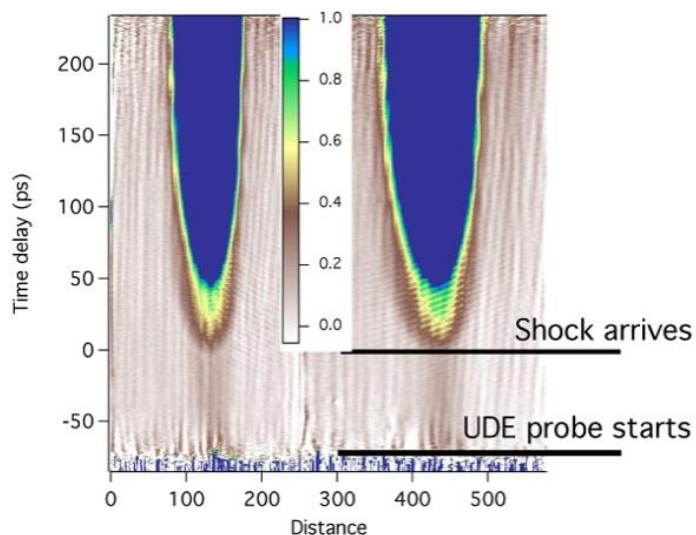
Figure 24 Low angle UDE data determines the UDE to shock temporal offset. A small amount of pre pulse can be seen in the time before the shock arrival.

2.10 Summary

Common chirped pulse amplified ultrafast lasers can be utilized as shock generation platforms that allow easy integration of multiple diverse interferometric and spectroscopic diagnostics. Several such diagnostics have been developed and implemented, including ultrafast dynamic ellipsometry, visible transient absorption spectroscopy, and mid-infrared transient absorption spectroscopy. This paper details the methods used to integrate all of these techniques together for ultrafast studies of shock dynamics. UDE was developed to measure the shocked material state by characterizing the shock velocity, particle velocity, and shocked refractive index in a single shot on various organic materials, energetic materials, and metals. VIS transient absorption spectroscopy during shock loading was integrated to measure absorption changes in the visible spectral region from electronic structure changes or strongly absorbing products and intermediates, which have been observed in several cases where chemical products are formed picoseconds behind the shock front. Broadband MIR transient absorption spectroscopy based on a two color filamentation supercontinuum source and low cost thermal imaging microbolometer camera allowed measurements of shock induced changes to vibrational spectra, especially as the result of shock-induced chemical reaction. All of the methods can be performed in a single shot shock experiment on micron scale samples using techniques that are accessible to small scale

ultrafast laser laboratories, and allow measurement of the very fast chemistry and material dynamics occurring in picoseconds following a compressive shock in a variety of materials.

2.11 References

1. Dick, R., Shock compression data for liquids. III. Substituted methane compounds, ethylene glycol, glycerol, and ammonia. *The Journal of Chemical Physics* **1981,** *74* (7), 4053.

2. Rice, M.; McQueen, R. G.; Walsh, J., Compression of solids by strong shock waves. In *Solid State Physics*, Elsevier: 1958; Vol. 6, pp 1-63.

3. Walsh, J. M.; Christian, R. H., Equation of State of Metals from Shock Wave Measurements. *Physical Review* **1955,** *97* (6), 1544-1556.

4. Glass, I.; Chan, S.; Brode, H., Strong planar shock waves generated by explosively-driven spherical implosions. *AIAA Journal* **1974,** *12* (3), 367-374.

5. McQueen, R.; Marsh, S.; Taylor, J.; Fritz, J.; Carter, W., The equation of state of solids from shock wave studies. *High Velocity Impact Phenomena* **1970,** *293*, 294-417.

6. McQueen, R.; Marsh, S., Equation of state for nineteen metallic elements from shock-wave measurements to two megabars. *Journal of Applied Physics* **1960,** *31* (7), 1253-1269.

7. Campbell, A.; Davis, W.; Ramsay, J.; Travis, J., Shock initiation of solid explosives. *The Physics of Fluids* **1961,** *4* (4), 511-521.

8. Deal, W., Measurement of Chapman-Jouguet pressure for explosives. *The Journal of Chemical Physics* **1957,** *27* (3), 796-800.

9. Grady, D. E.; Murri, W. J.; De Carli, P. S., Hugoniot sound velocities and phase transformations in two silicates. *Journal of Geophysical Research* **1975,** *80* (35), 4857-4861.

10. Graham, R., Measurement of wave profiles in shock-loaded solids. In *High-Pressure Science and Technology*, Springer: 1979; pp 1886-1901.

11. Boade, R., Compression of porous copper by shock waves. *Journal of Applied Physics* **1968,** *39* (12), 5693-5702.

12. Gruzdkov, Y. A.; Gupta, Y. M.; Dick, J. J., Time-resolved absorption spectroscopy in shocked PETN single crystals. *AIP Conference Proceedings* **2000,** *505* (1), 929-932.

13. Gustavsen, R. L.; Sheffield, S. A.; Alcon, R. R.; Forbes, J. W.; Tarver, C. M.; Garcia, F., Embedded Electromagnetic Gauge Measurements and Modeling of Shock Initiation in the TATB Based Explosives LX-17 and PBX 9502. *AIP Conference Proceedings* **2002,** *620* (1), 1019-1022.

14. Jones, A. H.; Isbell, W.; Maiden, C., Measurement of the very-high-pressure properties of materials using a light-gas gun. *Journal of Applied Physics* **1966,** *37* (9), 3493-3499.

15. Fowles, G.; Duvall, G.; Asay, J.; Bellamy, P.; Feistmann, F.; Grady, D.; Michaels, T.; Mitchell, R., Gas gun for impact studies. *Review of Scientific Instruments* **1970,** *41* (7), 984-996.

16. Hardesty, D., An investigation of the shock initiation of liquid nitromethane. *Combustion and Flame* **1976,** *27*, 229-251.

17. Schmidt, S.; Moore, D.; Shaner, J.; Shampine, D.; Holt, W., Coherent anti-stokes Raman scattering in benzene and nitromethane shock-compressed to 10 GPa. *Physica B+ C* **1986,** *139*, 587-589.

18. Moore, D.; Schmidt, S.; Shaner, J.; Shampine, D.; Holt, W., Coherent anti-Stokes Raman scattering in benzene and nitromethane shock-compressed to 11 GPa. In *Shock Waves in Condensed Matter*, Springer: 1986; pp 207-211.

19. Schmidt, S. C.; Moore, D. S., Vibrational spectroscopy of high-temperature, dense molecular fluids by coherent anti-Stokes Raman scattering. *Accounts of Chemical Research* **1992,** *25* (9), 427-432.

20. Winey, J.; Duvall, G.; Knudson, M.; Gupta, Y., Equation of state and temperature measurements for shocked nitromethane. *The Journal of Chemical Physics* **2000,** *113* (17), 7492-7501.

21. Pangilinan, G.; Gupta, Y., Time-resolved Raman measurements in nitromethane shocked to 140 kbar. *The Journal of Physical Chemistry* **1994,** *98* (17), 4522-4529.

22. Gustavsen, R. L.; Sheffield, S. A.; Alcon, R. R., Detonation wave profiles in HMX based explosives. *AIP Conference Proceedings* **1998,** *429* (1), 739-742.

23. Sheffield, S. A.; Engelke, R.; Alcon, R. R.; Gustavsen, R. L.; Robins, D.; Stahl, D. B.; Stacy, H. L.; Whitehead, M., Particle velocity measurements of the reaction zone in nitromethane. In *12th International Detonation Symposium*, San Diego, CA, 2002; pp 159-166.

24. Sheffield, S. A.; Gustavsen, R. L.; Alcon, R. R., Hugoniot and initiation measurements on TNAZ explosive. *AIP Conference Proceedings* **1996,** *370* (1), 879-882.

25. Gustavsen, R.; Sheffield, S.; Alcon, R., Progress in measuring detonation wave profiles in PBX9501. In *11th International Detonation Symposium*, Snowmass, CO, 1998; pp 821-827.

26. Brown, K. E.; Shaw, W. L.; Zheng, X.; Dlott, D. D., Simplified laser-driven flyer plates for shock compression science. *Review of Scientific Instruments* **2012,** *83* (10), 103901.

27. Frank, A. M.; Trott, W. M., Stop-motion microphotography of laser-driven plates. In *SPIE's 1994 International Symposium on Optics, Imaging, and Instrumentation*, SPIE: San Diego, CA, 1994; Vol. 2273, pp 196-206.

28. Gehr, R. J.; Bucholtz, S. M.; Rupp, T. D.; Robbins, D. L.; Stahl, D. B.; Sheffield, S. A., Line orvis particle velocity measurements on the laser-driven miniflyer apparatus. In *Shock Compression of Condensed Matter - 2003, Pts 1 and 2, Proceedings*, Furnish, M. D.; Gupta, Y. M.; Forbes, J. W., Eds. 2004; Vol. 706, pp 1163-1166.

29. Paisley, D., Laser-driven miniature flyer plates for shock initiation of secondary explosives. In *Shock Compression of Condensed Matter*, 1989.

30. Paisley, D.; Warnes, R.; Kopp, R., Laser-driven flat plate impacts to 100 GPa with sub-nanosecond pulse duration and resolution for material property studies. In *Shock Compression of Condensed Matter–1991*, Elsevier: 1992; pp 825-828.

31. Bassett, W. P.; Dlott, D. D., Shock initiation of explosives: Temperature spikes and growth spurts. *Applied Physics Letters* **2016,** *109* (9), 091903.

32. Hare, D. E.; Franken, J.; Dlott, D. D., A new method for studying picosecond dynamics of shocked solids: application to crystalline energetic materials. *Chemical Physics Letters* **1995,** *244* (3-4), 224-230.

33. Lee, I.-Y. S.; Hare, D. E.; Hill, J. R.; Franken, J.; Suzuki, H.; Dlott, D. D.; Baer, B. J.; Chronister, E. L., Ultrafast spectroscopy of the first nanosecond. *AIP Conference Proceedings* **1996,** *370* (1), 905-908.

34. Bassett, W. P.; Johnson, B. P.; Neelakantan, N. K.; Suslick, K. S.; Dlott, D. D., Shock initiation of explosives: High temperature hot spots explained. *Applied Physics Letters* **2017,** *111* (6), 061902.

35. Greenaway, M. W.; Proud, W. G.; Field, J. E.; Goveas, S. G., A laser-accelerated flyer system. *International Journal of Impact Engineering* **2003,** *29* (1), 317-321.

36. Paisley, D. L.; Luo, S.-N.; Greenfield, S. R.; Koskelo, A. C., Laser-launched flyer plate and confined laser ablation for shock wave loading: Validation and applications. *Review of Scientific Instruments* **2008,** *79* (2), 023902.

37. Swift, D. C.; Niemczura, J. G.; Paisley, D. L.; Johnson, R. P.; Luo, S.-N.; IV, T. E. T., Laser-launched flyer plates for shock physics experiments. *Review of Scientific Instruments* **2005,** *76* (9), 093907.

38. Watson, S.; Field, J. E., Integrity of thin, laser-driven flyer plates. *Journal of Applied Physics* **2000,** *88* (7), 3859-3864.

39. Bolme, C. A. Ultrafast dynamic ellipsometry of laser driven shock waves. Massachusetts Institute of Technology, 2008.

40. Dang, N. C.; Bolme, C. A.; Moore, D. S.; McGrane, S. D., Shock Induced Chemistry In Liquids Studied With Ultrafast Dynamic Ellipsometry And Visible Transient Absorption Spectroscopy. *Journal of Physical Chemistry A* **2012,** *116* (42), 10301-10309.

41. Schmitt, M. J.; Kopp, R. A.; Moore, D. S.; McGrane, S. D., Analysis of laser-driven shocks in confined and unconfined geometries. In *Shock Compression of Condensed Matter - 2003, Pts 1 and 2, Proceedings*, Furnish, M. D.; Gupta, Y. M.; Forbes, J. W., Eds. 2004; Vol. 706, pp 1409-1412.

42. Moore, D. S.; Funk, D. J.; Gahagan, K. T.; Reho, J. H.; Fisher, G. L.; McGrane, S. D.; Rabie, R. L., Sub-picosecond laser-driven shocks in metals and energetic materials. In *Shock Compression of Condensed Matter-2001, Pts 1 and 2, Proceedings*, Furnish, M. D.; Thadhani, N. N.; Horie, Y., Eds. 2002; Vol. 620, pp 1333-1338.

43. Schulze, P. A.; Ivanov, T. W.; Bolme, C. A.; Brown, K. E.; McGrane, S. D.; Moore, D. S., Shock Hugoniot equations of state for binary water-alcohol liquid mixtures. *Journal of Applied Physics* **2014,** *115* (2).

44. Whitley, V. H.; McGrane, S. D.; Eakins, D. E.; Bolme, C. A.; Moore, D. S.; Bingert, J. F., The elastic-plastic response of aluminum films to ultrafast laser-generated shocks. *Journal of Applied Physics* **2011,** *109* (1).

45. Armstrong, M. R.; Zaug, J. M.; Goldman, N.; Kuo, I.-F. W.; Crowhurst, J. C.; Howard, W. M.; Carter, J. A.; Kashgarian, M.; Chesser, J. M.; Barbee, T. W., Ultrafast shock initiation of exothermic chemistry in hydrogen peroxide. *The Journal of Physical Chemistry A* **2013,** *117* (49), 13051-13058.

46. Armstrong, M. R.; Zaug, J. M.; Grant, C. D.; Crowhurst, J. C.; Bastea, S., Ultrafast Shock Compression of an Oxygen-Balanced Mixture of Nitromethane and Hydrogen Peroxide. *The Journal of Physical Chemistry A* **2014,** *118* (32), 6148-6153.

47. Armstrong, M.; Crowhurst, J.; Bastea, S.; Zaug, J., Observation of off-Hugoniot shocked states with ultrafast time resolution. In *14th International Detonation Symposium*, Coeur d'Alene, ID, United States, 2010; pp 435-443.

48. Armstrong, M. R.; Crowhurst, J. C.; Bastea, S.; Zaug, J. M., Ultrafast observation of shocked states in a precompressed material. *Journal of Applied Physics* **2010,** *108* (2), 023511.

49. Zaug, J. M.; Austin, R. A.; Armstrong, M. R.; Crowhurst, J. C.; Goldman, N.; Ferranti, L.; Saw, C. K.; Swan, R. A.; Gross, R.; Fried, L. E., Ultrafast dynamic response of single-crystal β-HMX (octahydro-1, 3, 5, 7-tetranitro-1, 3, 5, 7-tetrazocine). *Journal of Applied Physics* **2018,** *123* (20), 205902.

50. Lindl, J. D.; Amendt, P.; Berger, R. L.; Glendinning, S. G.; Glenzer, S. H.; Haan, S. W.; Kauffman, R. L.; Landen, O. L.; Suter, L. J., The physics basis for ignition using indirect-drive targets on the National Ignition Facility. *Physics of Plasmas* **2004,** *11* (2), 339-491.

51. Batha, S. H.; Aragonez, R.; Archuleta, F.; Archuleta, T.; Benage, J.; Cobble, J.; Cowan, J.; Fatherley, V.; Flippo, K.; Gautier, D., TRIDENT high-energy-density facility experimental capabilities and diagnostics. *Review of Scientific Instruments* **2008,** *79* (10), 10F305.

52. Bolme, C.; Funk, D., Ultrafast dynamic ellipsometry measurements of early time laser ablation of titanium thin films. *Applied Physics A* **2008,** *92* (4), 761.

53. Bolme, C. A.; McGrane, S. D.; Moore, D. S.; Funk, D. J., Single shot measurements of laser driven shock waves using ultrafast dynamic ellipsometry. *Journal of Applied Physics* **2007,** *102* (3).

54. Bolme, C. A.; McGrane, S. D.; Moore, D. S.; Funk, D. J., Ultrafast dynamic ellipsometry of laser ablated silicon. In *High-Power Laser Ablation VII, Pts 1-2*, Phipps, C. R., Ed. 2008; Vol. 7005.

55. Bolme, C. A.; McGrane, S. D.; Moore, D. S.; Whitley, V. H.; Funk, D. J., Single shot Hugoniot of cyclohexane using a spatially resolved laser driven shock wave. *Applied Physics Letters* **2008,** *93* (19).

56. Brown, K. E.; Bolme, C. A.; McGrane, S. D.; Moore, D. S., Ultrafast shock-induced chemistry in carbon disulfide probed with dynamic ellipsometry and transient absorption spectroscopy. *J. Appl. Phys.* **2015,** *118* (8), 85903.

57. Brown, K. E.; McGrane, S. D.; Bolme, C. A.; Moore, D. S., Ultrafast Chemical Reactions in Shocked Nitromethane Probed with Dynamic Ellipsometry and Transient Absorption Spectroscopy. *Journal of Physical Chemistry A* **2014,** *118* (14), 2559-2567.

58. McGrane, S. D.; Bolme, C. A.; Whitley, V. H.; Moore, D. S., Ultrafast Dynamic Ellipsometry And Spectroscopy Of Laser Shocked Materials. In *International Symposium on High Power Laser Ablation 2010*, Phipps, C. R., Ed. 2010; Vol. 1278, pp 392-400.

59. McGrane, S. D.; Moore, D. S.; Whitley, V. H.; Bolme, C. A.; Eakins, D. E., Molecular Shock Response Of Explosives: Electronic Absorption Spectroscopy. In *Shock Compression of Condensed Matter - 2009, Pts 1 and 2*, Elert, M. L.; Buttler, W. T.; Furnish, M. D.; Anderson, W. W.; Proud, W. G., Eds. 2009; Vol. 1195, pp 1301-1304.

60. Schulze, P. A.; Dang, N. C.; Bolme, C. A.; Brown, K. E.; McGrane, S. D.; Moore, D. S., Shock Hugoniot Equations of State for Binary Ideal (Toluene/Fluorobenzene) and Nonideal (Ethanol/Water) Liquid Mixtures. *Journal of Physical Chemistry A* **2013,** *117* (29), 6158-6163.

61. Zuanetti, B.; McGrane, S. D.; Bolme, C. A.; Prakash, V., Measurement of elastic precursor decay in pre-heated aluminum films under ultra-fast laser generated shocks. *Journal of Applied Physics* **2018,** *123* (19), 195104.

62. Armstrong, M. R.; Crowhurst, J. C.; Zaug, J. M.; Radousky, H. B., Extreme dynamic compression with a low energy laser pulse. In *Shock Compression of Condensed Matter - 2015*, Chau, R.; Germann, T.; Oleynik, I.; Peiris, S.; Ravelo, R.; Sewell, T., Eds. 2017; Vol. 1793.

63. Armstrong, M. R.; Crowhurst, J. C.; Bastea, S.; Howard, W. M.; Zaug, J. M.; Goncharov, A. F., Prospects for achieving high dynamic compression with low energy. *Applied Physics Letters* **2012,** *101* (10), 101904.

64. McGrane, S.; Bowlan, P.; Powell, M.; Brown, K.; Bolme, C., Broadband mid-infrared measurements for shock-induced chemistry. *AIP Conference Proceedings* **2018,** *1979* (1), 130004.

65. McGrane, S. D.; Moore, D. S.; Funk, D. J., Shock induced reaction observed via ultrafast infrared absorption in poly(vinyl nitrate) films. *Journal of Physical Chemistry A* **2004,** *108* (43), 9342.

66. McGrane, S. D.; Moore, D. S.; Funk, D. J., Sub-picosecond shock interferometry of transparent thin films. *Journal of Applied Physics* **2003,** *93* (9), 5063.

67. McGrane, S. D.; Moore, D. S.; Funk, D. J.; Rabie, R. L., Spectrally modified chirped pulse generation of sustained shock waves. *Applied Physics Letters* **2002,** *80* (21), 3919.

68. Armstrong, M. R.; Grivickas, P. V.; Sawvel, A. M.; Lewicki, J. P.; Crowhurst, J. C.; Zaug, J. M.; Radousky, H. B.; Stavrou, E.; Alviso, C. T.; Hamilton, J.; Maxwell, R. S., Ultrafast shock compression of PDMS-based polymers. *Journal of Polymer Science Part B: Polymer Physics* **2018,** *56* (11), 827-832.

69. Armstrong, M. R.; Zaug, J. M.; Goldman, N.; Kuo, I. F. W.; Crowhurst, J. C.; Howard, W. M.; Carter, J. A.; Kashgarian, M.; Chesser, J. M.; Barbee, T. W.; Bastea, S., Ultrafast Shock Initiation of Exothermic Chemistry in Hydrogen Peroxide. *The Journal of Physical Chemistry A* **2013,** *117* (49), 13051-13058.

70. Carter, J. A.; Zaug, J. M.; Nelson, A. J.; Armstrong, M. R.; Manaa, M. R., Ultrafast Shock Compression and Shock-Induced Decomposition of 1,3,5-Triamino-2,4,6-trinitrobenzene Subjected to a Subnanosecond-Duration Shock: An Analysis of Decomposition Products. *The Journal of Physical Chemistry A* **2012,** *116* (20), 4851-4859.

71. Crowhurst, J. C.; Armstrong, M. R.; Gates, S. D.; Zaug, J. M.; Radousky, H. B.; Teslich, N. E., Yielding of tantalum at strain rates up to 109 s−1. *Applied Physics Letters* **2016,** *109* (9), 094102.

72. Park, S. D.; Armstrong, M. R.; Kohl, I. T.; Zaug, J. M.; Knepper, R.; Tappan, A. S.; Bastea, S.; Kay, J. J., Ultrafast Shock-Induced Reactions in Pentaerythritol Tetranitrate Thin Films. *The Journal of Physical Chemistry A* **2018,** *122* (41), 8101-8106.

73. Dlott, D. D., Nanoshocks in molecular materials. *Accounts of chemical research* **2000,** *33* (1), 37-45.

74. Dlott, D. D.; Hambir, S.; Franken, J., The New Wave in Shock Waves. *The Journal of Physical Chemistry B* **1998,** *102* (12), 2121-2130.

75. Ashitkov, S. I.; Agranat, M. B.; Kanel', G. I.; Komarov, P. S.; Fortov, V. E., Behavior of aluminum near an ultimate theoretical strength in experiments with femtosecond laser pulses. *JETP Letters* **2010,** *92* (8), 516-520.

76. Crowhurst, J. C.; Reed, B. W.; Armstrong, M. R.; Radousky, H. B.; Carter, J. A.; Swift, D. C.; Zaug, J. M.; Minich, R. W.; Teslich, N. E.; Kumar, M., The $\alpha \rightarrow \epsilon$ phase transition in iron at strain rates up to~ 109 s− 1. *Journal of Applied Physics* **2014,** *115* (11), 113506.

77. Crowhurst, J. C.; Armstrong, M. R.; Knight, K. B.; Zaug, J. M.; Behymer, E. M., Invariance of the Dissipative Action at Ultrahigh Strain Rates Above the Strong Shock Threshold. *Physical Review Letters* **2011,** *107* (14), 144302.

78. McGrane, S. D.; Moore, D. S.; Funk, D. J., Ultrafast spectroscopy and interferometry of laser shocked thin films: practical considerations. In *High-Power Laser Ablation V, Pts 1 and 2*, Phipps, C. R., Ed. 2004; Vol. 5448, pp 165-170.

79. McGrane, S. D.; Moore, D. S.; Funk, D. J., Measurement of shocked thin polymer film Hugoniot properties with ultrafast dynamic ellipsometry. In *Shock Compression of Condensed Matter - 2003, Pts 1 and 2, Proceedings*, Furnish, M. D.; Gupta, Y. M.; Forbes, J. W., Eds. 2004; Vol. 706, pp 1181-1186.

80. Funk, D. J.; Moore, D. S.; Reho, J. H.; Gahagan, K. T.; McGrane, S. D.; Rabie, R. L., Ultrafast measurement of the optical properties of shocked nickel and laser heated gold. In *Shock Compression of Condensed Matter-2001, Pts 1 and 2, Proceedings*, Furnish, M. D.; Thadhani, N. N.; Horie, Y., Eds. 2002; Vol. 620, pp 1227-1230.

81. Gahagan, K. T.; Moore, D. S.; Funk, D. J.; Rabie, R. L.; Buelow, S. J.; Nicholson, J. W., Measurement of shock wave rise times in metal thin films. *Physical Review Letters* **2000,** *85* (15), 3205.

82. Moore, D.; Gahagan, K.; Reho, J.; Funk, D. J.; Buelow, S.; Rabie, R.; Lippert, T., Ultrafast nonlinear optical method for generation of planar shocks. *Applied Physics Letters* **2001,** *78* (1), 40-42.

83. Moore, D. S.; Gahagan, K. T.; Lippert, T.; Funk, D. J.; Buelow, S.; Rabie, R. In *Ultrafast nonlinear optical method for generation of flat-top shocks*, High-Power Laser Ablation III, Santa Fe, NM, International Society for Optics and Photonics: Santa Fe, NM, 2000; pp 490-495.

84.   Curtis, A. D.; Banishev, A. A.; Shaw, W. L.; Dlott, D. D., Laser-driven flyer plates for shock compression science: Launch and target impact probed by photon Doppler velocimetry. *Review of Scientific Instruments* **2014,** *85* (4), 043908.

85.   Banishev, A. A.; Shaw, W. L.; Bassett, W. P.; Dlott, D. D., High-speed laser-launched flyer impacts studied with ultrafast photography and velocimetry. *Journal of Dynamic Behavior of Materials* **2016,** *2* (2), 194-206.

86.   Shaw, W.; Curtis, A.; Banishev, A.; Dlott, D. In *Laser-driven flyer plates for shock compression spectroscopy*, Journal of Physics: Conference Series, IOP Publishing: 2014; p 142011.

87.   Amat-Roldan, I.; Cormack, L. G.; Loza-Alvarez, P.; Artigas, D., Measurement of electric field by interferometric spectral trace observation. *Optics Letters* **2005,** *30* (9), 1063.

88.   Delong, K. W.; Trebino, R.; Kane, D. J., COMPARISON OF ULTRASHORT-PULSE FREQUENCY-RESOLVED-OPTICAL-GATING TRACES FOR 3 COMMON BEAM GEOMETRIES. *Journal of the Optical Society of America B-Optical Physics* **1994,** *11* (9), 1595.

89.   Fittinghoff, D. N.; Bowie, J. L.; Sweetser, J. N.; Jennings, R. T.; Krumbugel, M. A.; DeLong, K. W.; Trebino, R.; Walmsley, I. A., Measurement of the intensity and phase of ultraweak, ultrashort laser pulses. *Optics Letters* **1996,** *21* (12), 884.

90.   Gruetzmacher, J. A.; Scherer, N. F., Few-cycle mid-infrared pulse generation, characterization, and coherent propagation in optically dense media. *Review of Scientific Instruments* **2002,** *73* (6), 2227.

91.   Siders, C. W.; Siders, J. L. W.; Omenetto, F. G.; Taylor, A. J., Multipulse interferometric frequency-resolved optical gating. *IEEE Journal of Quantum Electronics* **1999,** *35* (4), 432.

92.   Stibenz, G.; Steinmeyer, G., Interferometric frequency-resolved optical gating. *Optics Express* **2005,** *13* (7), 2617.

93.   Trebino, R.; DeLong, K. W.; Fittinghoff, D. N.; Sweetser, J. N.; Krumbugel, M. A.; Richman, B. A.; Kane, D. J., Measuring ultrashort laser pulses in the time-frequency domain using frequency-resolved optical gating. *Review of Scientific Instruments* **1997,** *68* (9), 3277.

94.   Linden, S.; Giessen, H.; Kuhl, J., XFROG—a new method for amplitude and phase characterization of weak ultrashort pulses. *Physica Status Solidi (b)* **1998,** *206* (1), 119-124.

95.   Funk, D. J.; Moore, D. S.; Gahagan, K. T.; Buelow, S. J.; Reho, J. H.; Fisher, G. L.; Rabie, R. L., Ultrafast measurement of the optical properties of aluminum during shock-wave breakout. *Physical Review B (Condensed Matter and Materials Physics)* **2001,** *64* (11), 115114.

96.   Funk, D. J.; Moore, D. S.; McGrane, S. D.; Gahagan, K. T.; Reho, J. H.; Buelow, S. J.; Nicholson, J.;   Fisher, G. L.; Rabie, R. L., Ultrafast studies of shock waves using interferometric methods and transient infrared absorption spectroscopy. *Thin Solid Films* **2004,** *453/454*, 542.

97.   Funk, D. J.; Moore, D. S.; McGrane, S. D.; Reho, J. H.; Rabie, R. L., Ultra-fast spatial interferometry: a tool for characterizing material phase and hydrodynamic motion in laser-excited metals. *Applied Physics a-Materials Science & Processing* **2005,** *81* (2), 295-302.

98.   Moore, D. S.; McGrane, S. D.; Funk, D. J., Ultrafast spectroscopic investigation of shock compressed energetic polymer films. In *Shock Compression of Condensed Matter - 2003, Pts 1 and 2, Proceedings*, Furnish, M. D.; Gupta, Y. M.; Forbes, J. W., Eds. 2004; Vol. 706, pp 1285-1288.

99.   McGrane, S. D.; Brown, K. E.; Bolme, C. A.; Moore, D. S., Interaction between measurement time and observed Hugoniot cusp due to chemical reactions. *AIP Conference Proceedings* **2017,** *1793* (1), 030033.

100.   Bowlan, P.; Powell, M.; Perriot, R.; Martinez, E.; Cawkwell, M.; McGrane, S., Probing ultrafast shock-induced chemistry in liquids using broad-band mid-infrared absorption spectroscopy. *Journal of Chemical Physics* **2018 (In Preparation)**.

101.   Powell, M. S.; Bowlan, P. R.; Son, S. F.; McGrane, S. D., Ultrafast Mid-Infrared Spectroscopy on Shocked Thin Film Explosive Crystals. In *16th International Detonation Symposium*, Cambridge, MD, 2018 (In Submission).

102.   Marsh, S. P., *LASL Shock Hugoniot Data*. Univ of California Press: 1980; Vol. 5.

103.   Lagutchev, A. S.; Patterson, J. E.; Huang, W.; Dlott, D. D., Ultrafast Dynamics of Self-Assembled Monolayers under Shock Compression: Effects of Molecular and Substrate Structure. *The Journal of Physical Chemistry B* **2005,** *109* (11), 5033-5044.

104. Hohlfeld, J.; Wellershoff, S. S.; Güdde, J.; Conrad, U.; Jähnke, V.; Matthias, E., Electron and lattice dynamics following optical excitation of metals. *Chemical Physics* **2000,** *251* (1), 237-258.

105. Born, M.; Wolf, E., *Principles of Optics: Electromagnetic Theory of Propagation, Interference and Diffraction of Light*. Elsevier: 2013.

106. Fuji, T.; Nomura, Y., Generation of phase-stable sub-cycle mid-infrared pulses from filamentation in nitrogen. *Applied Sciences* **2013,** *3* (1), 122-138.

107. Fuji, T.; Shirai, H.; Nomura, Y., Ultrabroadband mid-infrared spectroscopy with four-wave difference frequency generation. *Journal of Optics* **2015,** *17* (9), 094004.

108. Nomura, Y.; Shirai, H.; Ishii, K.; Tsurumachi, N.; Voronin, A. A.; Zheltikov, A. M.; Fuji, T., Phase-stable sub-cycle mid-infrared conical emission from filamentation in gases. *Optics Express* **2012,** *20* (22), 24741-24747.

109. Nomura, Y.; Wang, Y.-T.; Kozai, T.; Shirai, H.; Yabushita, A.; Luo, C.-W.; Nakanishi, S.; Fuji, T., Single-shot detection of mid-infrared spectra by chirped-pulse upconversion with four-wave difference frequency generation in gases. *Optics Express* **2013,** *21* (15), 18249-18254.

110. Nash, C.; Nelson, T.; Stewart, J.; Carper, W., Molecular structure and vibrational analysis of 2, 4, 6-trinitrotoluene and 2, 4, 6-trinitrotoluene-a-d3. *Spectrochimica Acta Part A: Molecular Spectroscopy* **1989,** *45* (5), 585-588.

111. Prasad, R.; Prasad, R.; Bhar, G.; Thakur, S., Photoacoustic spectra and modes of vibration of TNT and RDX at CO2 laser wavelengths. *Spectrochimica Acta Part A: Molecular and Biomolecular Spectroscopy* **2002,** *58* (14), 3093-3102.

112. Dlott, D. D.; Fayer, M. D., Shocked molecular solids: vibrational up pumping, defect hot spot formation, and the onset of chemistry. *Journal of Chemical Physics* **1990,** *92* (6), 3798.

113. Cohen, R.; Zeiri, Y.; Wurzberg, E.; Kosloff, R., Mechanism of thermal unimolecular decomposition of TNT (2, 4, 6-trinitrotoluene): a DFT study. *The Journal of Physical Chemistry A* **2007,** *111* (43), 11074-11083.

114. Engelke, R.; Blais, N. C.; Sheffield, S. A.; Sander, R. K., Production of a chemically-bound dimer of 2, 4, 6-TNT by transient high pressure. *The Journal of Physical Chemistry A* **2001,** *105* (28), 6955-6964.

115. Quenneville, J.; Germann, T. C., A quantum chemistry study of Diels–Alder dimerizations in benzene and anthracene. *The Journal of Chemical Physics* **2009,** *131* (2), 024313.

116. Owens, F., Relationship between impact induced reactivity of trinitroaromatic molecules and their molecular structure. *Journal of Molecular Structure: Theochem* **1985,** *22* (1-5), 213-220.

117. Rom, N.; Hirshberg, B.; Zeiri, Y.; Furman, D.; Zybin, S. V.; Goddard III, W. A.; Kosloff, R., First-principles-based reaction kinetics for decomposition of hot, dense liquid TNT from ReaxFF multiscale reactive dynamics simulations. *The Journal of Physical Chemistry C* **2013,** *117* (41), 21043-21054.

118. Dodson, B. W.; Graham, R. A., Shock-induced organic chemistry. *AIP Conference Proceedings* **1982,** *78* (1), 42-51.

119. Owens, F.; Sharma, J., X-ray photoelectron spectroscopy and paramagnetic resonance evidence for shock-induced intramolecular bond breaking in some energetic solids. *Journal of Applied Physics* **1980,** *51* (3), 1494-1497.

120. Moore, D. S.; McGrane, S. D., Comparative infrared and Raman spectroscopy of energetic polymers. *Journal of Molecular Structure* **2003,** *661/662*, 561.

121. Moore, D., Influence of hot bands on vibrational spectra of shock compressed materials. *The Journal of Physical Chemistry A* **2001,** *105* (19), 4660-4663.

3. ULTRAFAST MID-INFRARED SPECTROSCOPY ON THIN FILMS OF TNT

3.1 Introduction

The chemistry during detonation of high explosives (HE) is not well understood even though detonable materials have been used for centuries. Various theories exist that predict reaction mechanisms; however, there are few direct experimental measurements of the chemical reactions prevalent during shocks.[1-6] Even such a ubiquitous HE as trinitrotoluene (TNT) has little definitive information regarding initiation chemistry with competing theories from experiments and models that suggest dimerization through Diels-Alder reactions, nitrite (NO_2) isomerization, and HONO elimination as possible mechanisms.[7-13]

The aim of this research is to gain insight into initiation chemistry of explosives namely, TNT, through ultrafast broadband mid-infrared (MIR) spectroscopy. TNT was chosen as it produced transparent and relatively uniform thin films when spin cast, a useful trait for the probing techniques available. Thin films of HE were shocked via laser drive through an aluminum transduction layer and probed by ultrafast dynamic ellipsometry (UDE), visible transient absorption spectroscopy (VIS), and MIR absorption spectroscopy. Through the combination of these techniques shock dynamics, electronic transitions, and functional groups can be probed on ps time scales. This work was presented at the 16th International Detonation Symposium (IDS), in Cambridge Maryland, July 2018, as well as featured in the conference proceedings for IDS.

3.2 Experimental

3.2.1 Thin film preparation

Samples were prepared in a similar method to that performed by McGrane et. al.[14, 15] TNT was dissolved into acetone at 10% by mass. This produced thin films of approximately two micron thickness. Film thickness of 1-2 µm was selected based on estimated shock velocities (about 7 µm/ns, or 2.3 µm/300 ps) and sustained shock duration from the shock drive laser (300 ps). Films of HE were spin cast onto 25.4 mm diameter sapphire substrates (Esco Optics, not oriented) coated with 1.5-2.5 µm of aluminum. Measurements of the HE film thickness was accomplished using

white light reflectivity (Filmetrics) with sample thickness being uniform to within a few percent across the entire substrate. Samples appeared to be polycrystalline when observed under a microscope. The sample was affixed to a translational stage in both vertical and horizontal directions to allow for 100s of shots to be performed on one substrate. See Fig. 25 for an example of the sample geometry used in experiments.
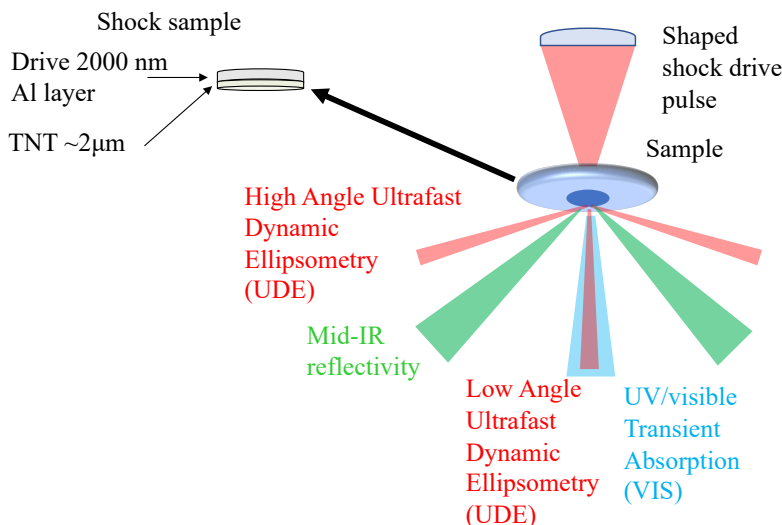
Figure 25 Sample geometry with probing beams shown. Films were spin cast onto 0.5 mm sapphire substrates coated with 2 μm of aluminum.

3.3   Laser techniques employed

Figure 5 has a detailed schematic of the laser techniques used for these experiments. The laser shock drive experiment has been described in great detail in several previous works.[16-21] Briefly, a flash lamp pumped 10 Hz Ti-Sapphire chirped pulse amplifier (TSA-25) was used to generate the five laser beams used in these experiments. Prior to compression of a pulse, a 60% beamsplitter was placed in the beam path to pick off part of the uncompressed pulse (300 ps in duration) to operate the shock drive and ultrafast dynamic ellipsometry technique. Spectrally, the leading edge of the uncompressed pulse was clipped with a shortpass filter to give a sharp rise time (~5 ps) for producing the shock at the substrate. The shock drive pulse was focused to 150 μm FWHM at the sample with tunable energies from 0.5-8 mJ. This allowed for a wide range of achievable shock pressures from 10-40 GPa. UDE was performed at 0° and 65° to probe for phase shifts which have been shown through fitting and optimization via thin film equations to yield shock refractive indices, shock, and particle velocities.[14, 19, 21] Notably, the 65° UDE data was not

analyzable due to localized surface roughness scattering the sample illumination source prior to data collection.

The rest of the pulse was compressed to ~120 fs and further split by an external 75% beam splitter to generate the beams for the two transient absorption spectroscopy techniques: mid-infrared (MIR) and visible (VIS). Generation of the VIS beam was completed by focusing part of the compressed pulse (a few microjoules) into 12 mm of CaF_2, generating wavelengths of 450-700 nm. A reference pulse was used to normalize shot to shot variation from the generation mechanism. Absorbance, which is defined by eqn. 10, was measured at 50 ps intervals to track changes in electronic absorptions, which may be important in initiation chemistry.[4, 5, 22] Interpretation of broadband VIS spectra is difficult with peaks and features not being chemically specific; however, minor changes in absorbance in VIS can suggest structural and chemical changes when combined with UDE.[17, 18] More detailed information on the VIS technique can be found in previous literature.[17-19, 23]

New to the experimental apparatus is the MIR generation technique. A four wave difference frequency generation via filamentation (FWDFGF) approach has been adapted from Nomura. et. al. to generate broadband MIR radiation.[24] In these experiments the optics necessary for MIR generation were simplified by removal of the delay crystal and dual waveplate using only a 1 m focal length silver mirror (Newport) and BBO (Eskma Optics 15 x 15 x 0.1). This led to a factor of about five increase in signal count from MIR generated by the filament when compared to generation that include the delay crystal and dual waveplate. Direct detection of the MIR radiation was preferential by using a microbolometer and MIR spectrometer. This approach to generate MIR was taken in opposition to using an optical parametric amplifier (OPA) to increase spectral range detectable in a single shot. Wavelengths of 5-20 micron were generated with this approach. Filamentation yields a toroidal spatial profile for the generated MIR radiation. It has been shown that the focus of a torus produces a spherical Bessel function, which is also its Fourier transform.[25] In order to minimize spot size at the sample we spatially filtered the MIR using a 150 µm pinhole at the focus of a 100 mm lens to remove the rings surrounding the peak, which yields approximately a Lorentzian beam profile. The beam was split prior to probing the sample with a germanium window with one side having an anti-reflective (AR) coating. This forms a reference pulse and sample pulse in order to normalize shot to shot variation. For this paper the reference

was neglected for data analysis as energy fluctuations were not observed to change strongly (>10% fluctuation). Shot to shot variations affected the spectral normalization of the pre-shot pulses.

The sample portion was focused by a 75 mm Zn-Se achromat lens to a spot size of 75 micrometers FWHM and then imaged and dispersed at the MIR spectrometer. The MIR spectrometer consisted of a 90° Zn-Se prism (ISP) using a 45^0 edge to disperse at a right angle into a 65 mm focal length ZnSe lens that focused the spectrum onto a microbolometer (FLIR AX5). Spectral range for the MIR was limited to from 750-1250 cm^{-1} due to the AR coating on the Zn-Se lenses used as well as the filter coated onto the microbolometer itself.

3.4   Results

VIS and MIR were recorded for thin films of TNT shocked with 5 mJ from the drive laser, which corresponds to ~30 GPa. This value was calculated by impedance matching from a measurement of the aluminum free surface velocity to the shock velocity curve using reported Hugoniots.[26] About 25 shots were averaged at each time delay. VIS data are presented in a similar manner to previous experiments.[17-19] Notably, a broad feature is observed with an increase in absorbance as time progresses for TNT using VIS. MIR results also suggest a large absorptive feature that increases with time; however, the peaks in the measured spectral range can be observed to be decreasing as the broad absorption features increase.

Figure 26 shows the VIS absorption results and Figs. 27-29 show the MIR absorption results for TNT. Both techniques show differences in absorptions beginning around 200 ps. The increase in absorbance at later times can be attributed to changes in the TNT film when combined with Fig. 27-29.
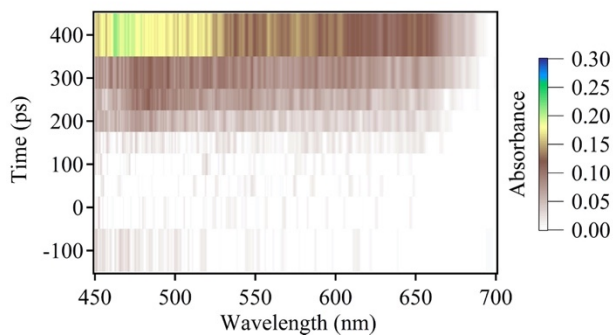
Figure 26 VIS results for TNT. Broadband absorption features increase as more material is shocked. Time steps were recorded at ~50 ps intervals except for -100 and 400 ps delay.

Shocked MIR spectra showed increased absorption features at later times, shown in Figs. 27-29, similar to VIS. Available to our spectral region are three modes for TNT with mode assignments from Nash et. al.[27] Two CN stretches were available with one at 935 cm⁻¹ and the other at 980 cm⁻¹. The ring breathing mode at 1075 cm⁻¹ is also available. The peaks decreased at about the same rate as the broadband features came in.
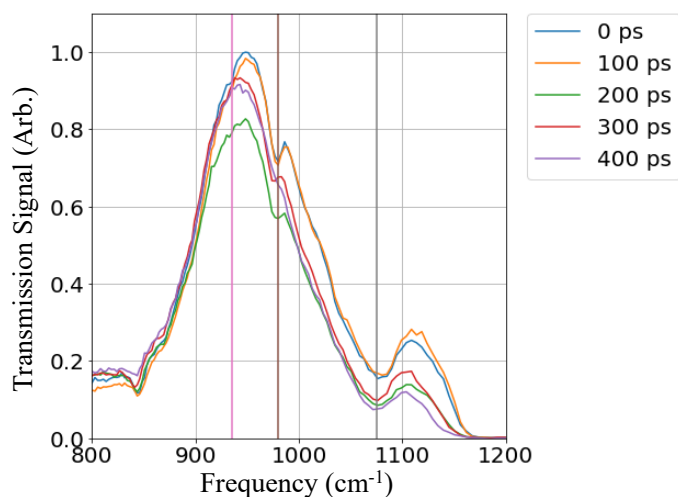
Figure 27 Transmission spectra of shocked TNT. The CN mode at 935 cm⁻¹ shows less changes than that at 980 cm⁻¹, while the ring breathing mode at 1075 cm⁻¹ shows significant changes as more material is shocked.
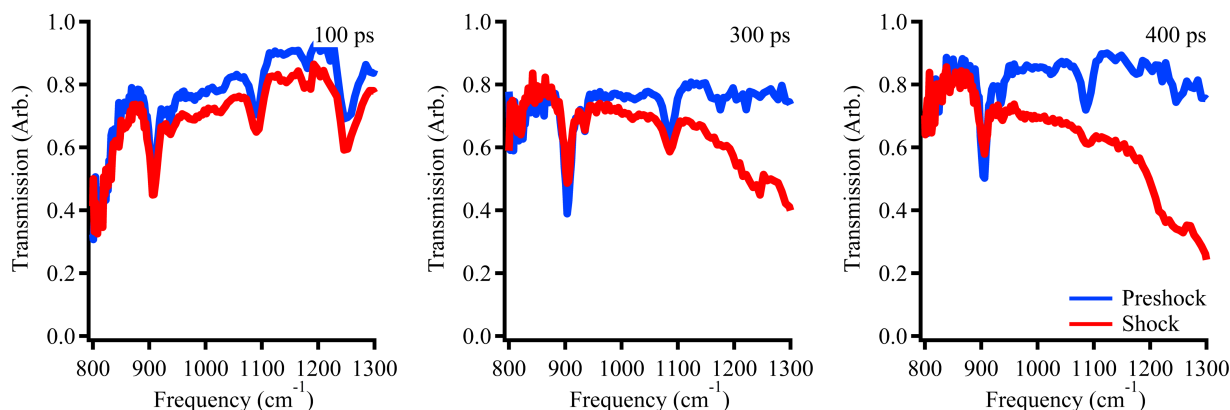
Figure 28 Normalized transmission spectra for three select time delays for MIR shocked to ~30 GPa. Preshock spectra are different at each time delay as shot to shot variability of the MIR was not accounted for in this series. Modes available decreased in peak absorption while a broad absorption feature grew as the shock consumed more material.
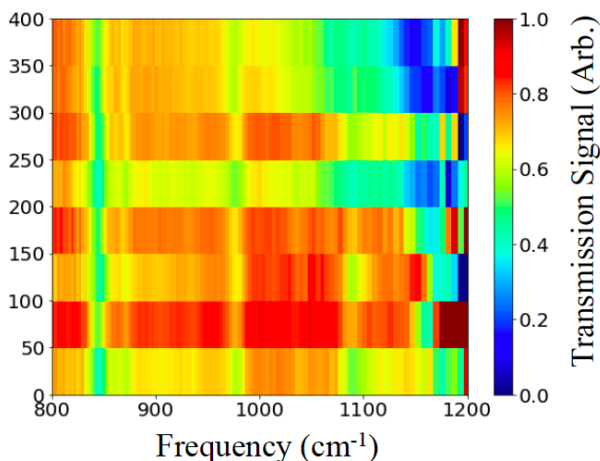
Figure 29 Color map of the normalized transmission spectra of Fig. 28, but with all time delays. The ring breathing mode (1075 cm^{-1}) strongly changes in transmission compared to the two CN modes. The changes begin at 200 ps at the same time when VIS changes start.

3.5 Conclusions

Several mechanisms exist that could be suggestive of why vibrational absorption changes occur during shock compression of the TNT film. Vibrational ladders, inhomogeneous broadening, vibrational hot bands, chemical reaction, or thin film interference effects are possible mechanisms that can contribute to vibrational absorption changes.[2, 17, 18, 28, 29] For MIR, the decrease in the peaks, and increase in broad absorptive features is suggestive of reactants being consumed. VIS results complement this as electronic absorptions increase continually during the shock duration

indicating electronically absorptive species are forming during the shock. Future experiments are necessary to determine what effect may be dominant for the thin films as well as probe for shock dynamics at times beyond the sustained shock to further characterize absorption changes during compression and after release. Shock compression effects on spectral changes also need to be measured and accounted for at pressures below the reaction threshold. Determination of these effects on the MIR spectra may help in determining the type of chemical changes in initiation chemistry for TNT. It should be noted the data presented in Chapter 3 was very preliminary and speculative. More definitive results on the shock chemistry of TNT will be presented in Chapter 5.

3.6   References

1.   An, Q.; Zybin, S. V.; Goddard III, W. A.; Jaramillo-Botero, A.; Blanco, M.; Luo, S.-N., Elucidation of the dynamics for hot-spot initiation at nonuniform interfaces of highly shocked materials. *Physical Review B* **2011,** *84* (22), 220101.

2.   Dlott, D. D.; Fayer, M. D., Shocked molecular solids: vibrational up pumping, defect hot spot formation, and the onset of chemistry. *The Journal of chemical physics* **1990,** *92* (6), 3798-3812.

3.   Gilman, J. J., Chemical reactions at detonation fronts in solids. *Philosophical Magazine B* **1995,** *71* (6), 1057-1068.

4.   Kuklja, M. M.; Aduev, B.; Aluker, E. D.; Krasheninin, V.; Krechetov, A.; Mitrofanov, A. Y., Role of electronic excitations in explosive decomposition of solids. *Journal of Applied Physics* **2001,** *89* (7), 4156-4166.

5.   Kunz, A. B.; Kuklja, M. M.; Botcher, T.; Russell, T., Initiation of chemistry in molecular solids by processes involving electronic excited states. *Thermochimica acta* **2002,** *384* (1-2), 279-284.

6.   Tarver, C. M.; Chidester, S. K.; Nichols, A. L., Critical conditions for impact-and shock-induced hot spots in solid explosives. *The Journal of Physical Chemistry* **1996,** *100* (14), 5794-5799.

7.   Cohen, R.; Zeiri, Y.; Wurzberg, E.; Kosloff, R., Mechanism of thermal unimolecular decomposition of TNT (2, 4, 6-trinitrotoluene): a DFT study. *The Journal of Physical Chemistry A* **2007,** *111* (43), 11074-11083.

8. Dodson, B. W.; Graham, R. A., Shock-induced organic chemistry. *AIP Conference Proceedings* **1982,** *78* (1), 42-51.

9. Engelke, R.; Blais, N. C.; Sheffield, S. A.; Sander, R. K., Production of a chemically-bound dimer of 2, 4, 6-TNT by transient high pressure. *The Journal of Physical Chemistry A* **2001,** *105* (28), 6955-6964.

10. Owens, F., Relationship between impact induced reactivity of trinitroaromatic molecules and their molecular structure. *Journal of Molecular Structure: Theochem* **1985,** *22* (1-5), 213-220.

11. Owens, F.; Sharma, J., X-ray photoelectron spectroscopy and paramagnetic resonance evidence for shock-induced intramolecular bond breaking in some energetic solids. *Journal of Applied Physics* **1980,** *51* (3), 1494-1497.

12. Quenneville, J.; Germann, T. C., A quantum chemistry study of Diels–Alder dimerizations in benzene and anthracene. *The Journal of Chemical Physics* **2009,** *131* (2), 024313.

13. Rom, N.; Hirshberg, B.; Zeiri, Y.; Furman, D.; Zybin, S. V.; Goddard III, W. A.; Kosloff, R., First-principles-based reaction kinetics for decomposition of hot, dense liquid TNT from ReaxFF multiscale reactive dynamics simulations. *The Journal of Physical Chemistry C* **2013,** *117* (41), 21043-21054.

14. McGrane, S.; Moore, D.; Funk, D., Shock induced reaction observed via ultrafast infrared absorption in poly (vinyl nitrate) films. *The Journal of Physical Chemistry A* **2004,** *108* (43), 9342-9347.

15. Moore, D.; McGrane, S.; Funk, D. In *Ultrafast spectroscopic investigation of shock compressed energetic polymer films*, AIP Conference Proceedings, AIP: 2004; pp 1285-1288.

16. Bolme, C. A.; McGrane, S. D.; Moore, D. S.; Funk, D. J., Single shot measurements of laser driven shock waves using ultrafast dynamic ellipsometry. *Journal of Applied Physics* **2007,** *102* (3).

17. Brown, K. E.; McGrane, S. D.; Bolme, C. A.; Moore, D. S., Ultrafast Chemical Reactions in Shocked Nitromethane Probed with Dynamic Ellipsometry and Transient Absorption Spectroscopy. *Journal of Physical Chemistry A* **2014,** *118* (14), 2559-2567.

18.   Dang, N. C.; Bolme, C. A.; Moore, D. S.; McGrane, S. D., Shock Induced Chemistry In Liquids Studied With Ultrafast Dynamic Ellipsometry And Visible Transient Absorption Spectroscopy. *Journal of Physical Chemistry A* **2012,** *116* (42), 10301-10309.

19.   Mcgrane, S. D.; Dang, N. C.; Whitley, V. H.; Bolome, C. A.; Moore, D. *Transient absorption spectroscopy of laser shocked explosives*; Los Alamos National Lab.(LANL), Los Alamos, NM (United States): 2010.

20.   McGrane, S. D.; Moore, D. S.; Whitley, V. H.; Bolme, C. A.; Eakins, D. E., Molecular Shock Response Of Explosives: Electronic Absorption Spectroscopy. In *Shock Compression of Condensed Matter - 2009, Pts 1 and 2*, Elert, M. L.; Buttler, W. T.; Furnish, M. D.; Anderson, W. W.; Proud, W. G., Eds. 2009; Vol. 1195, pp 1301-1304.

21.   Whitley, V.; McGrane, S.; Moore, D.; Eakins, D.; Bolme, C. In *Single shot ultrafast dynamic ellipsometry of laser-driven shocks in single crystal explosives and thin films of metals*, 16th Shock Compression of Condensed Matter Conference, Nashville, TN, APS: Nashville, TN, 2009.

22.   Kuklja, M., On the initiation of chemical reactions by electronic excitations in molecular solids. *Applied Physics A* **2003,** *76* (3), 359-366.

23.   McGrane, S.; Moore, D. S.; Whitley, V. H.; Bolme, C. A.; Eakins, D. E. In *Molecular shock response of Explosives: Electronic absorption spectroscopy*, AIP Conference Proceedings, AIP: 2009; pp 1301-1304.

24.   Nomura, Y.; Wang, Y.-T.; Kozai, T.; Shirai, H.; Yabushita, A.; Luo, C.-W.; Nakanishi, S.; Fuji, T., Single-shot detection of mid-infrared spectra by chirped-pulse upconversion with four-wave difference frequency generation in gases. *Optics Express* **2013,** *21* (15), 18249-18254.

25.   Yang, L.; Xie, X.; Wang, S.; Zhou, J., Minimized spot of annular radially polarized focusing beam. *Optics letters* **2013,** *38* (8), 1331-1333.

26.   McGrane, S.; Bowlan, P.; Powell, M.; Brown, K.; Bolme, C., Broadband mid-infrared measurements for shock-induced chemistry. *AIP Conference Proceedings* **2018,** *1979* (1), 130004.

27.   Nash, C.; Nelson, T.; Stewart, J.; Carper, W., Molecular structure and vibrational analysis of 2, 4, 6-trinitrotoluene and 2, 4, 6-trinitrotoluene-a-d3. *Spectrochimica Acta Part A: Molecular Spectroscopy* **1989,** *45* (5), 585-588.

28.   Moore, D., Influence of hot bands on vibrational spectra of shock compressed materials. *The Journal of Physical Chemistry A* **2001,** *105* (19), 4660-4663.

29.   Moore, D. S.; McGrane, S. D., Comparative infrared and Raman spectroscopy of energetic polymers. *Journal of Molecular Structure* **2003,** *661/662*, 561.

4. INSIGHT INTO THE CHEMISTRY OF PETN UNDER SHOCK COMPRESSION THROUGH ULTRAFAST BROADBAND MID-INFRARED ABSORPTION SPECTROSCOPY

4.1 Introduction

Large quantities of high explosives (HE) are used on an annual basis at the global scale. Applications vary from mining, pyrotechnics, defense, or more exotic applications like micro-electromechanical materials (MEMS).[1] The initial chemical reactions that occur immediately following a shock wave are not well understood, but are the extremely important first steps in the chemistry that allows HE to release energy. To build models capable of predicting HE performance, we need insight into the chemical pathways followed when the HE is subjected to conditions similar to detonation. HE near detonation temperatures and pressures can be studied with explosively or gas gun driven plate impact experiments.[2-31] Chemical reactions can be inferred from equation of state measurements.[2-10, 12-15] However, the interpretation of experimental measurements that only indirectly observe chemical reactions in situ is typically complicated.[16-23] Alternatively, engineering and physics models are capable of predicting HE performance; however, they rely on making assumptions to fill in critical information gaps, like equation of state and chemical pathways, that have not been measured experimentally. Simulations have been able to predict the chemical dynamics of HE,[32-37] but lack direct experimental evidence at relevant length and time scales to confirm the results.

An important and common HE in defense applications is pentaerythritol tetranitrate (PETN).[4, 10] PETN is commonly used in detonators and in detonating cord. Significant experimental efforts have been undertaken to determine the important intermediate molecules involved in PETN shock chemistry. Several mechanisms have been proposed, including NO_2 scission,[38-41] NO_3 scission,[40, 42, 43] HNO_3 formation,[44] HONO elimination,[44] C-C bond cleavage or CH_2ONO_2 formation,[40] conformational and phase changes,[16, 17, 45-51] or vibrational energy transfer and electronic structure changes.[52] Of particular interest are the results from Ng et al. which suggested NO_2 elimination was dominant at slow heating rates, NO_3 elimination was dominant at fast heating rates like those induced by a laser, and C-C bond cleavage was dominant during high energy fracture mechanisms similar to explosively driven impactors or gas guns.[40] A similar result was found by Tailleur et al. through nanosecond Raman spectroscopy.[52] Results from Dreger et al.

and Grudzkov et al. suggested NO_3 elimination and subsequent NO_2 formation as an important intermediate reaction in gas gun experiments.[38, 41, 43, 53] Modeling suggests similar chemical paths to the experimental list above: NO_2 scission,[33-35, 54, 55] NO_3 scission,[35, 37, 55] NO formation,[36] HONO elimination,[33] H-ion formation,[35] O-radical formation,[35] C-C bond cleavage or CH_2ONO_2 formation.[35] Determination of the dominant mechanism under shock conditions requires diagnostics with chemical specificity coupled to experiments with resolution commensurate to reactive chemical time and length scales. It has been shown that adding such spectroscopic diagnostics to shock experiments is achievable through the use of ultrafast lasers.[56]

In this study, the LANL laser shock apparatus was used to shock compress thin films of crystalline PETN on ultrafast time scales measured out to 250 ps with 25 ps time steps, while probing the sample for electronic and vibrational spectroscopic changes. Shock and particle velocities were obtained using ultrafast dynamic ellipsometry (UDE). Complementary to the UDE shock characterization were two spectroscopic probes: visible white light (VIS) and ultrafast broadband mid-infrared (MIR) absorption. These techniques were used to observe the shocked electronic and vibrational spectroscopic changes in PETN and thereby determine the chemical species present in shocked PETN and assess possible reaction pathways.

4.2   Experimental methods

The laser driven shock apparatus has multiple diagnostics available that have been detailed in various publications over several years.[56-77] A single pulse from a Ti:Sapphire chirped pulse amplifier (CPA) was used to simultaneously generate the shock, characterize the shock, and generate spectroscopic probe beams for electronic and vibrational absorption spectroscopy. An in-depth description of how each beam is generated and used can be found elsewhere.[56]

Recently, there have been several notable improvements to the shock generation and diagnostic portions of the experiment in this laboratory. First, the laser system was upgraded from a 25 mJ, 110 fs CPA system (Spectra Physics TSA 50 CPA) to a 13 mJ, 35 fs CPA (Coherent Legend Elite Duo HE+ USP-III). This change introduced temporally shorter chirped pulses (300 ps to 150 ps), but also spectrally broader beams (12 nm to 35 nm FWHM). The temporal duration of the chirped laser pulse is directly related to the supported shock duration.[56-60, 68, 71, 76] The broader spectrum of the compressed pulse primarily affected the MIR generation mechanism. There was no noticeable difference between the spectrum of the VIS radiation produced using the

new CPA and the VIS radiation generated using the previous system. Previous experiments were limited to generating and detecting MIR in the spectral range of 700-1400 cm-1.[56, 61, 66] Using the spectrally broader compressed pulses, implementing a calcite delay crystal and a dual waveplate,[78-80] and using an uncoated microbolometer array (INO Microcam-384i), generation and detection MIR radiation in two ranges was possible: 1150-3000 cm^{-1} (low frequency range) or 1450-3800 cm^{-1} (high frequency range). The spectrum could not be simultaneously optimized over the entire range from 1150 to 3800 cm^{-1}, so these two ranges were used to achieve the optimal signal to noise. The MIR spectrometer resolution was on average ~10 cm^{-1} per pixel in the low frequency range, and ~25 cm^{-1} per pixel in the high frequency region. In the low frequency region, NO_2 stretches, CH_2 bending modes, and the CO_2 region can be observed simultaneously. The high frequency region permitted probing of the anti-symmetric NO_2 stretch, CO_2 stretch, and the CH-, NH-, and OH-stretch regions (2800-3000, 3000-3200, 3200-3500 cm^{-1} respectively). The MIR absorption spectrum of the shocked PETN was measured simultaneously with the VIS absorption spectrum. Spectroscopic measurements for an experiment were measured for a time delayed series that consisted of 25 ps time steps from -50 to 250 ps with respect to the shock entrance into the sample. Although the shock was sustained for ~150 ps, time delays were measured to 250 ps to understand changes during shock release of the sample as the shock reaches the front surface of the PETN film sending a rarefaction wave back into the sample. Averaged for each time step were 25 shots, making 325 total shots for an experiment. Two experiments could be completed per 25.4 mm diameter substrate and two substrates were used for each pressure range totaling four experiments per pressure range. These data sets were then averaged to give an averaged response for each pressure range.

Additionally, a flat top spatial beam shaping optic (Newport GBS-AR16) was placed into the chirped pulse path and imaged at a magnification of 30:1 onto the sample by a 250 mm achromatic lens to a spot diameter of ~120 μm. The sample experienced a near uniform pressure across the spatial region sampled by the spectroscopic probes using the flat top beam shaper; thus, pressure convolution in our spectroscopic measurements was avoided.[56, 61] Shown in Fig. 30 is the comparisons between the gaussian beam shape and the flat top beam shape, as well as phase information (related to shock pressure). Achievable free surface velocities in the aluminum drive layer were in the range of 0.5 km/s to 6 km/s, which, when impedance matched to an extrapolated unreacted PETN Hugoniot, produced pressures ranging from ~3-55 GPa in PETN. The driver layer

particle velocities used in these experiments can be found in Table 1. UDE was used to characterize the shock state was measured immediately prior to the spectroscopy measurements on the same sample and substrate (see below in section 4.3.1).
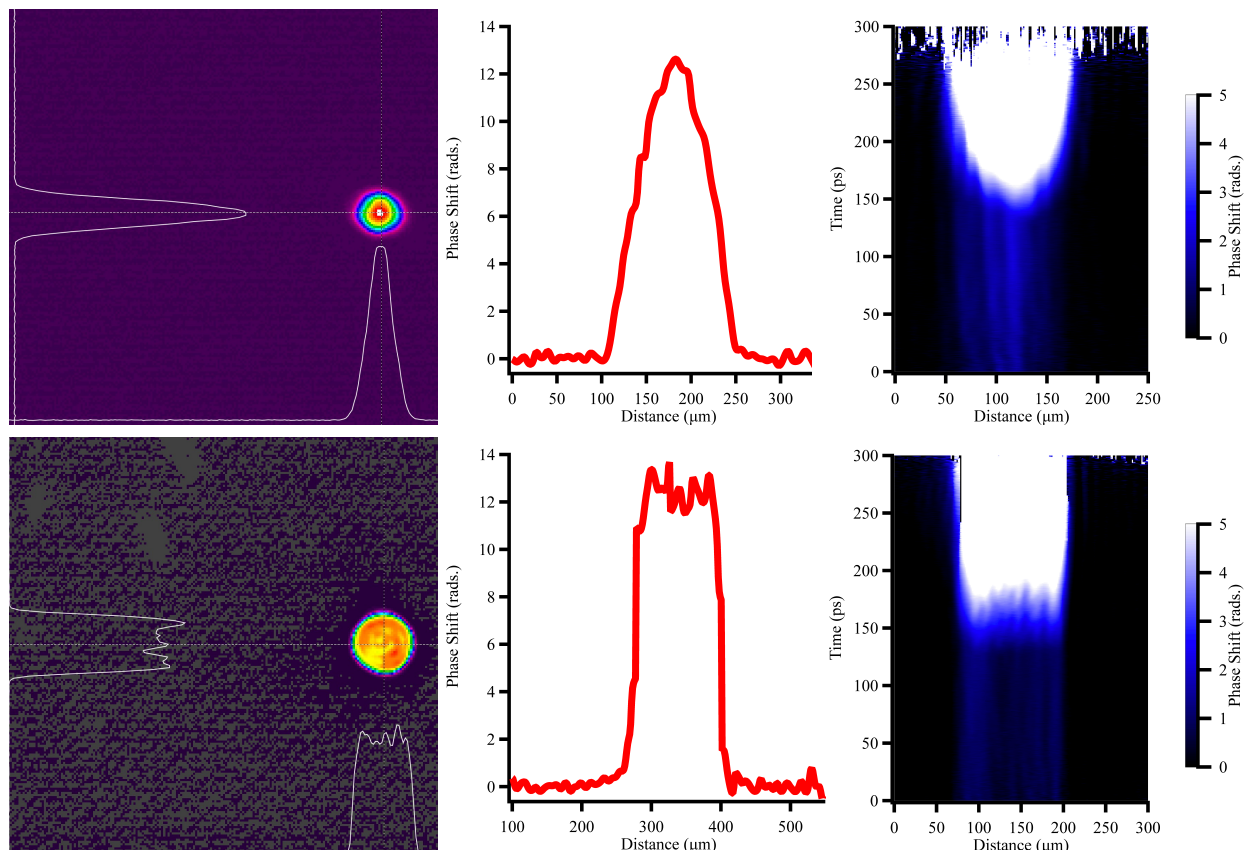
Figure 30 (Top) Gaussian profile of shock drive beam at sample with lineout (center) and phase (right) behavior. Phase shifts are directly related to pressure induced. (Bottom) Flat top profile of shock drive beam at the sample location with lineout (center) and phase behavior (right).

Samples consisted of three layers: 0.5 mm of sapphire, nominally 1 μm of vapor-deposited aluminum, and nominally 1 μm crystalline PETN. The starting PETN was recrystallized to remove contaminants present from PETN production. The PETN was then dissolved in acetone to create a solution of ~16% PETN in acetone by mass. The solution was spin cast onto a heated substrate in a small vented cup to crash out microcrystals of PETN. 150 μL of solution was deposited through the vented cup at the very start of spinning. The surface temperature of the substrate was measured to be 40 ºC by a thermal camera and a thermocouple. Important spin casting parameters were speed, acceleration, and spin duration which were 1500 rpm, 500 rpm/s, and 15 s, respectively. Thicker films could be achieved using more concentrated solution or changing spinning

parameters to be slower; however, light scattering from larger needle-like crystals impeded white light interference measurements leading to error-prone measurements of film thickness when samples were spun at slower rates. A small region of the PETN was removed from the substrate with a cotton swab and acetone to allow measurement of the free surface velocity of the aluminum drive layer, which was subsequently used for impedance matching the drive layer in order to complement the UDE measurements. Typical thicknesses of PETN were in the range of 0.8 μm to 1.3 μm as measured by a white light interferometer, assuming a refractive index of 1.55 for crystalline PETN. The PETN thin films were determined to be PETN without impurities by comparing the MIR spectra obtained using a commercial Fourier transform infrared spectrometer (FTIR) in reflection mode to recrystallized PETN in a KBr pellet, shown in Fig. 31.[4] The exact homolog content of the PETN used was indeterminant as FTIR spectra of PETN compared to its homologs are almost identical.[4, 81] Nevertheless, it is suggested that the PETN crystals that were spin-cast out of solution were PETN I, as PETN II and III are unstable at room temperature and pressure and revert to PETN I at those conditions.[48, 82]
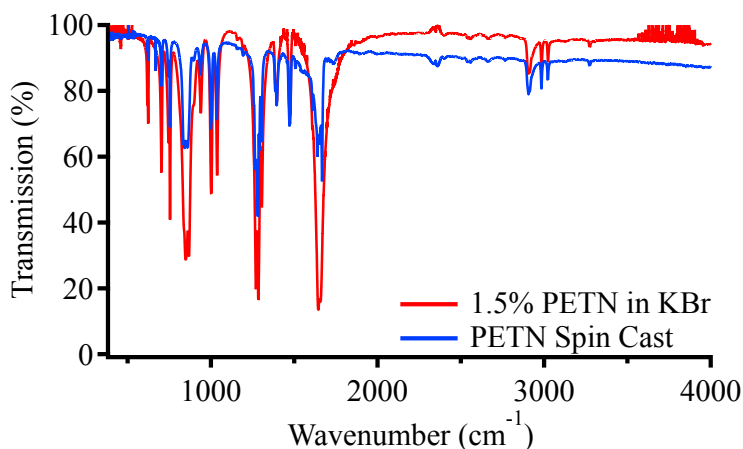
Figure 31 FTIR comparison of spin cast films and recrystallized PETN pressed in KBr.

High resolution white light confocal microscopy and FTIR microscopy were used to characterize the ambient PETN films for sample uniformity and crystal orientation and can be seen in Fig. 32. A mix of <25 to 100 μm crystals existed on a single substrate with two particular microstructures that appear needle-like (Fig. 32, top) or brick-like in shape (Fig. 32, bottom). Strong differences were present in the microstructure of these samples when observed via microscopy like that of Fig. 33. There were significant microstructural, and sub-micrometer-scale

features present on the substrates that were smaller than the shock diameter. These features were considered to be unresolved on the scale of our experiment as the shock generated was ~120 μm in diameter, which was the same diameter probed by the FTIR microscope. Further, changes in microstructure were averaged over with 25 sequential shots per time delay. Notably, there was no observable difference in crystal orientation or polymorphism of the PETN between substrates as noted by the FTIR microscope traces at various positions in Fig. 32. Changes in FTIR absorptions were mostly due to thickness variations across the sample and the corresponding thin film interference effects.
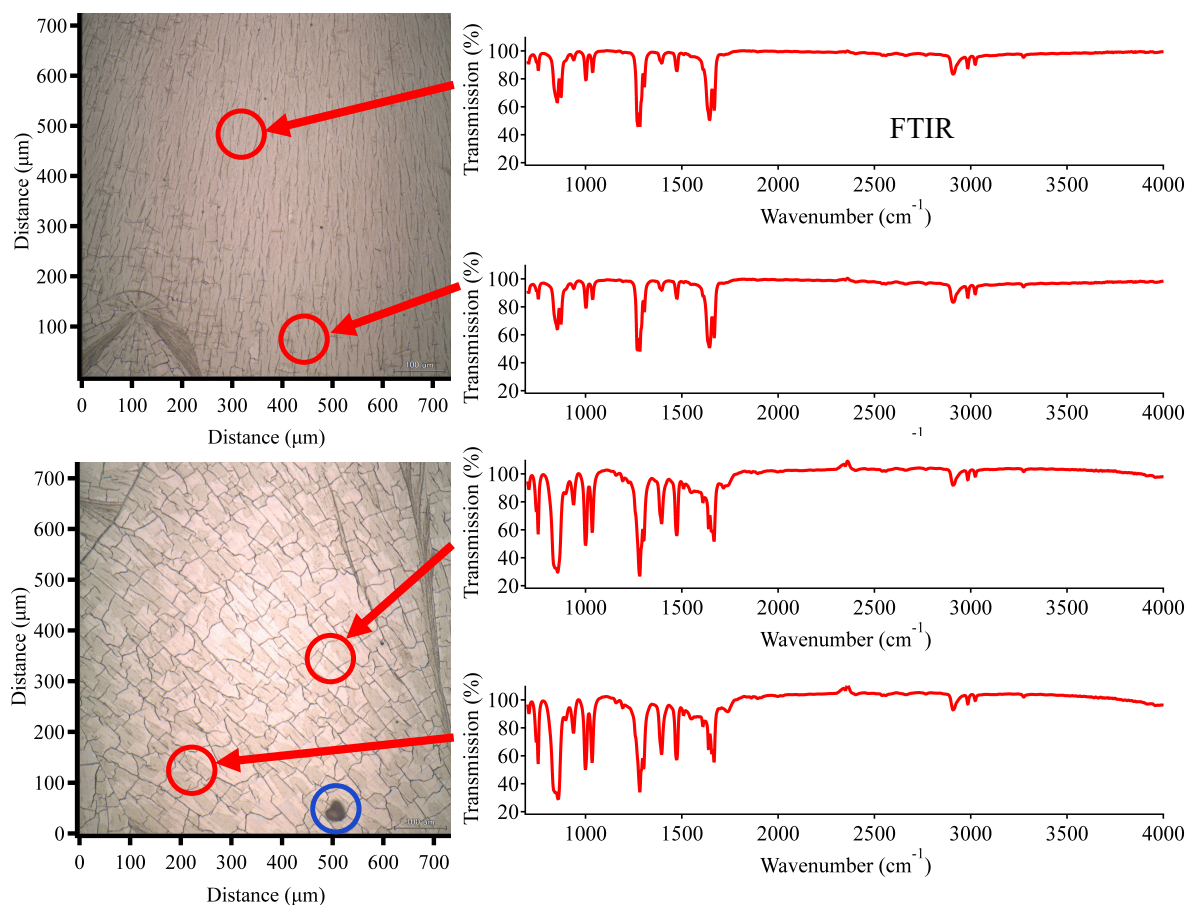
Figure 32 (left) Microscope images of two PETN substrates with varying crystal structures. Observable are thin "needle-like" platelets as seen in the red circles top image, "brick-like" platelets, and microcrystal as in the red and blue circles respectively in the bottom image. (right) FTIR microscope traces of various crystals on the substrates. There are minimal differences in shape, only in absorption strength, in the FTIR traces between the positions on each substrate, even though the microstructures look different. Highlighted regions enclosed by the red and blue circles are a similar size as the shock diameter.
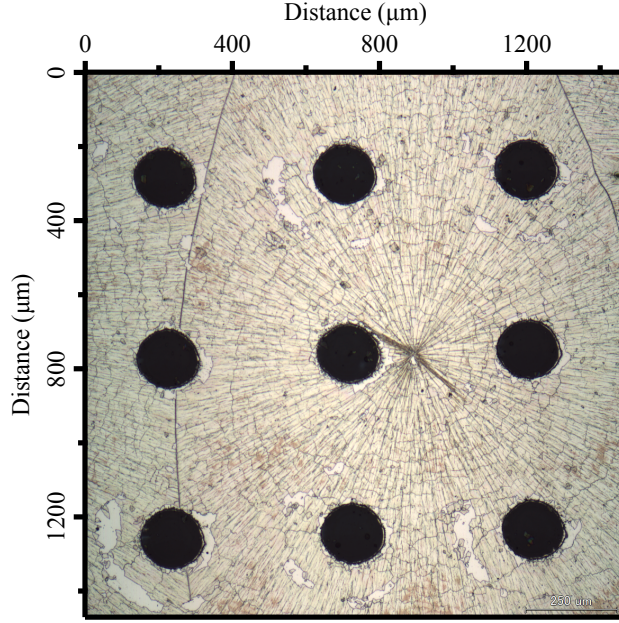
Figure 33 Post-mortem microscope image of an area subjected to shocks. Areas shocked show significant microscale features which were averaged over.

4.3 Results

4.3.1 Shock state determination

Particle and shock velocities were measured in PETN using impedance matching and low-angle (LA) UDE. High angle UDE was not performed on these samples as the sample roughness and microstructure increased scattering and degraded high angle imaging compared to homogenous materials. LA-UDE and ultrafast spectral interferometry (USI) fitting methods, which are similar in many regards,[56, 83] were attempted; however; both fitting methods were largely unsuccessful due to sample roughness. When the LA-UDE and USI data fits were deficient, the shock pressure was estimated by impedance matching the free surface velocity of aluminum to an extrapolated linear fit (in the shock velocity-particle velocity plane) of the unreactive Hugoniot for single crystal PETN. The shock and particle velocities displayed in Fig. 34 are: single crystal data from Marsh, single crystal data from Dick, ultrafast measurements of shocked PETN from Park et al., UDE data at high pressure (35-40 GPa) from this study, and impedance matched values of the aluminum drive layer from our experiment to single crystal data from Marsh.[10, 17, 84] UDE and impedance matched values are available in tabular form in Table 1. Reported are data in four pressure ranges in these experiments: low (3-6 GPa), medium (30-35 GPa), high (35-40 GPa), and

extreme (50-55 GPa). These pressure regimes were selected to correspond to anticipated chemical reaction regions where there should be no reaction at low pressure, some reaction at medium and high pressure, and faster, stronger, reaction at extreme pressure. Example LA UDE data fits in the high pressure region are shown in Fig. 35, which correspond to a shock pressure of ~34 GPa. Impedance matched pressures were found to be at most ~18% higher than those measured through UDE and USI. This error is likely due to the linear extrapolation of the Hugoniot assumed. USI fitted results were <5% different from UDE results when both were used.
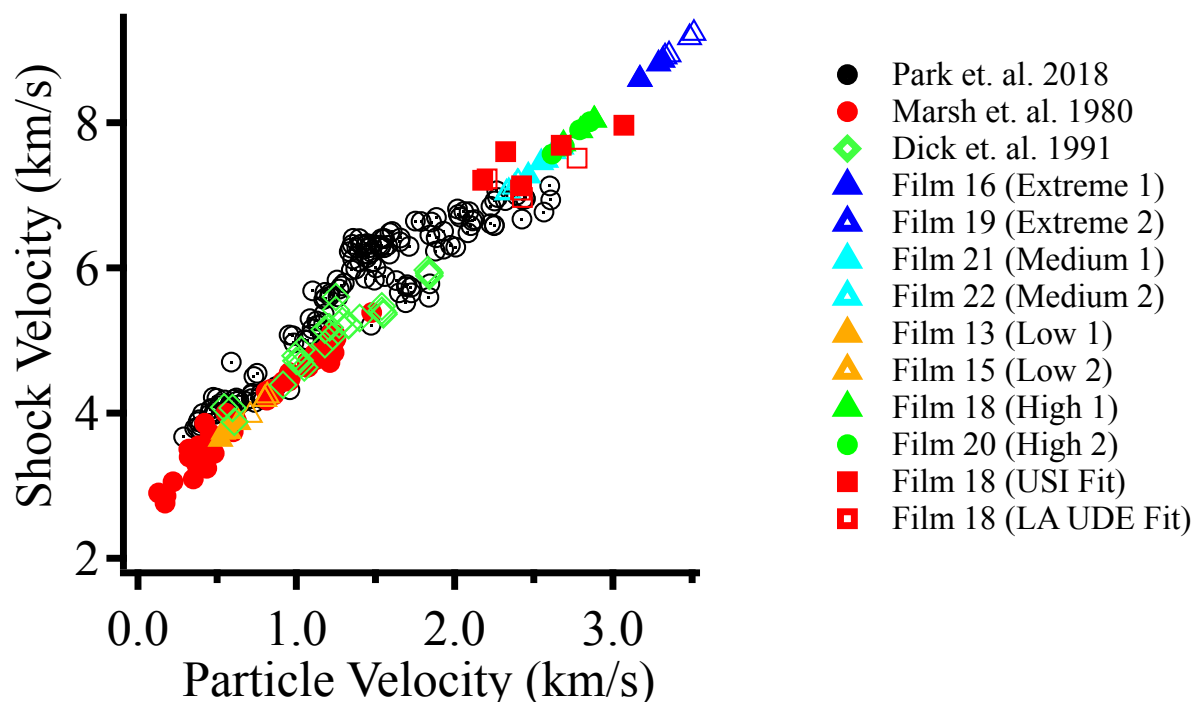
Figure 34 Shock and particle velocities from these experiments compared to previously published data. Values measured in these experiments were impedance matched to a linear extrapolation of single crystal data from Marsh.[10]
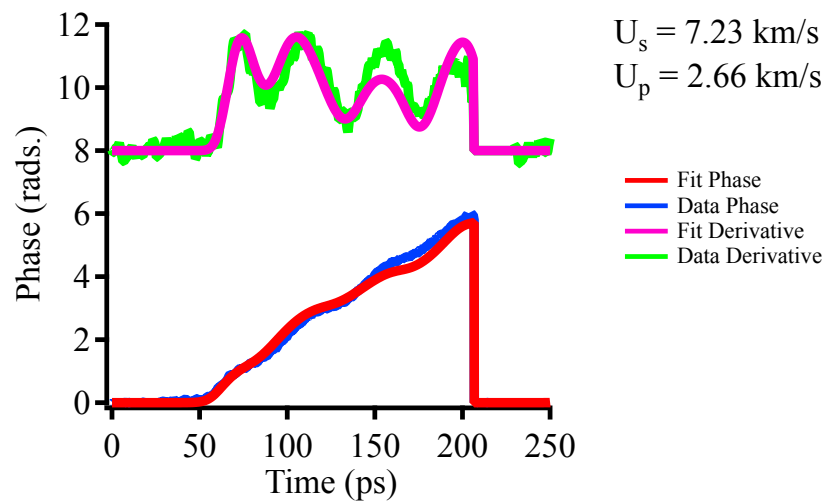
Figure 35 Low angle UDE fits to both the phase and derivative in the high pressure region (35-40 GPa). Using the crystal density of PETN this shock and particle velocity corresponded to 34 GPa. Impedance matched values for this substrate were ~40 GPa.

Table 1 UDE impedance matched points for the substrates in this study, u_{fs}: free surface velocity of the aluminum layer, u_p: impedance matched particle velocity of aluminum u_{fs} into PETN, u_s: impedance matched shock velocity of aluminum u_{fs} into PETN, P: pressure as calculated by $P = \rho u_s u_p$, where ρ is the density of PETN which was assumed to be crystal density of 1.77 g/cm^3.

Film Identifier	u_{fs} (km/s)	u_p (km/s)	u_s (km/s)	P (GPa)
Film 16 (Extreme 1)	5.552	3.288	8.810	51.3
	5.336	3.171	8.598	48.3
	5.627	3.315	8.860	52.0
	5.458	3.169	8.598	48.2
Film 19 (Extreme 2)	5.675	3.354	8.935	53.0
	5.632	3.329	8.907	52.5
	5.968	3.511	9.231	57.4
	5.916	3.484	9.172	56.6
Film 21 (Medium 1)	4.375	2.627	7.602	35.3
	4.266	2.578	7.483	34.1
	4.422	2.675	7.665	36.3
	4.051	2.465	7.268	31.7
	4.193	2.547	7.451	33.6
Film 22 (Medium 2)	3.874	2.328	7.034	29.0
	4.004	2.378	7.114	29.9
	3.944	2.397	7.177	30.5
	3.819	2.342	7.053	29.2
	3.93	2.403	7.171	30.5
Film 13 (Low 1)	0.812	0.566	3.754	3.8
	0.884	0.574	3.749	3.8
	0.927	0.635	3.87	4.3
	0.806	0.539	3.738	3.6
	0.912	0.521	3.640	3.4
Film 15 (Low 1)	1.189	0.801	4.189	5.9
	1.097	0.709	3.97	5.0
	1.181	0.800	4.189	5.9
	1.203	0.816	4.238	6.1
Film 18 (High 1)	4.696	2.795	7.891	39.0
	4.841	2.883	8.035	41.0
	4.916	2.881	8.041	41.0
	4.682	2.687	7.710	36.7
Film 20 (High 2)	4.754	2.855	8.014	40.5
	4.629	2.693	7.676	36.6
	4.455	2.615	7.567	35.0
	4.691	2.789	7.902	39.0

4.3.2 Visible (VIS) transient absorption spectroscopy

Visible transient absorption spectroscopy measurements were taken at 25 ps time steps from -50 ps to 250 ps time delay relative to the shock arrival at the aluminum/PETN interface for each pressure range. The resulting VIS absorbance spectra can be seen in Fig. 36. While the shock transits the film in 110 ps (extreme pressure) to 250 ps (low pressure), later time delays were also measured to observe effects that occur during shock release of the sample to help separate any reversible pressure-induced changes from chemistry effects. Examples of shock and release effects can be viewed in Chapter 5 in Figs. 46 and 47 for trinitrotoluene. There were no significant visible absorption changes observed in the low pressure case; the small (<3%) changes were most likely due to roughening of the aluminum layer.[56] For the medium, high, and extreme pressure cases, an increasing absorption feature grew during the shock and did not recover upon release. The high and extreme pressure spectra had slightly higher absorbances in blue wavelength regions.
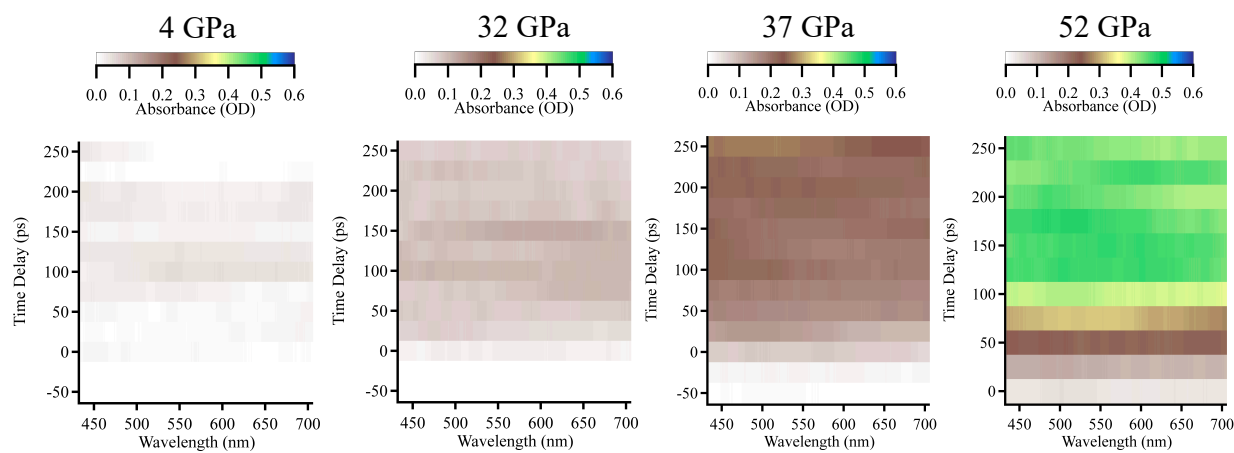
Figure 36 VIS absorption images for the pressure ranges measured in the experiment. VIS absorptions scale as a function of pressure with absorption of 3% at 4 GPa and 60% absorption at 52 GPa.

4.3.3 Mid-infrared (MIR) transient absorption spectroscopy

The low frequency range MIR shocked spectra, lineouts at three specific time delays, and specific bond behavior under the low, medium, and extreme pressure regions are presented in Figs. 37-39. This frequency range covers several bonds of interest in PETN: the symmetric NO_2 stretch (ν_s-NO_2) at 1280 cm^{-1}, CH_2 wag and rock at 1400 and 1450 cm^{-1} respectively, and the anti-symmetric NO_2 stretch (ν_a–NO_2) at 1650 cm^{-1}.[49, 85] Decreasing transmission is equivalent to

increased absorption, which is the parameter used in descriptions for subsequent figures and discussion, like those seen in Fig. 37. To observe spectral changes as a function of pressure, three lineouts were selected from the plots in Fig. 37 at time delays of 0, 100, and 200 ps to show transmission of the MIR in static PETN, during the shock wave, and during release of the material; these are shown in Fig. 38. The CO_2 artifact is observable at 2350 cm^{-1}. Due to the presence of ambient CO_2 in the laboratory air there is always a residual in the normalization process. It is difficult to differentiate if CO_2 is being generated from chemical reactions in these experiments, or if absorptions change based on ambient concentration changes from experiment to experiment. Since the MIR vibrations of PETN showed pressure-induced frequency shifts of less than 30 cm^{-1}, a vertical lineout in the time dimension was used to compare the behavior of the NO_2 bonds of shocked PETN as shown in Fig. 39. The pressure shifted behavior in these experiments is small compared to static high pressure experiments where pressure shifts were measured to be 2 cm^{-1}/GPa for the ν_s-NO_2 and 0.9-3.18 cm^{-1}/GPa for ν_a-NO_2;[45-47, 50] however, this phenomenon is commonly observed with the increased temperature in a dynamic experiment.[65, 67, 86-88] Additionally for the reactive cases, the amount of shocked PETN compared to ambient and product/intermediate materials results in very small contributions to the total infrared absorption spectrum.[89] There were minimal pressure induced frequency shifts, of at most 40 cm^{-1}, of the nitro-stretches over 250 ps. Similar comparisons of shocked spectra are shown in Fig. 40 for the high frequency region.
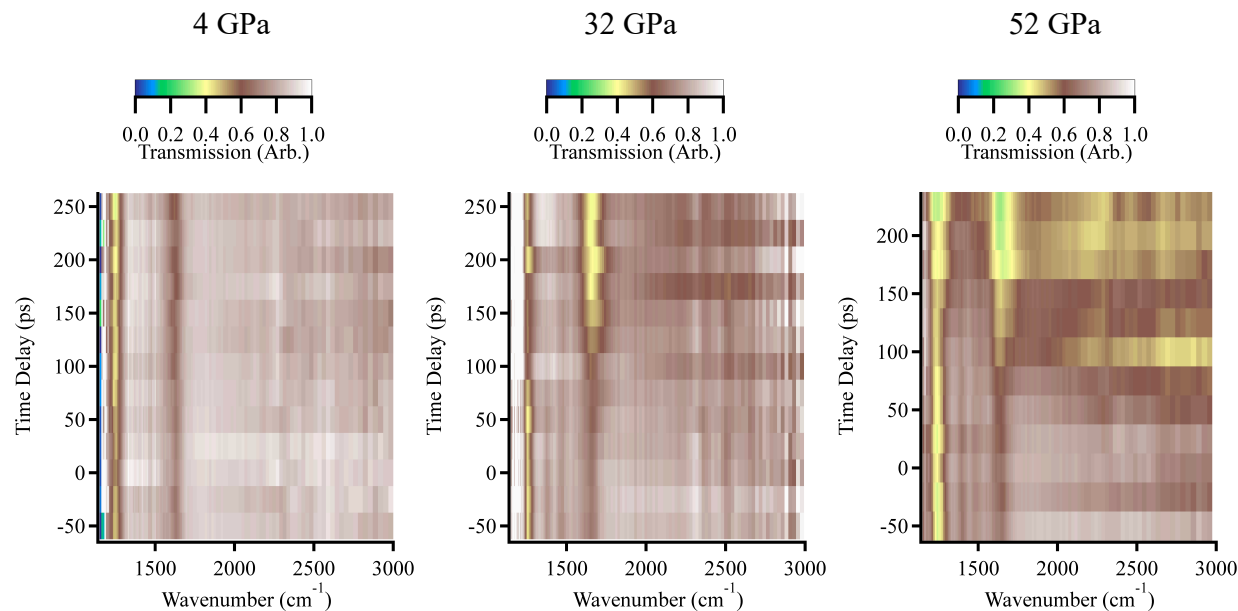
Figure 37 Shocked transmission spectra of PETN for three pressure ranges: low, medium, and extreme. Transmission changes do not appear to happen at 4 GPa. A decreased transmission, or increased absorbance, feature appears and grows in the 32 GPa case for the ν_a-NO_2 and not the ν_s-NO_2. This increased absorbance is enhanced in the 52 GPa case.
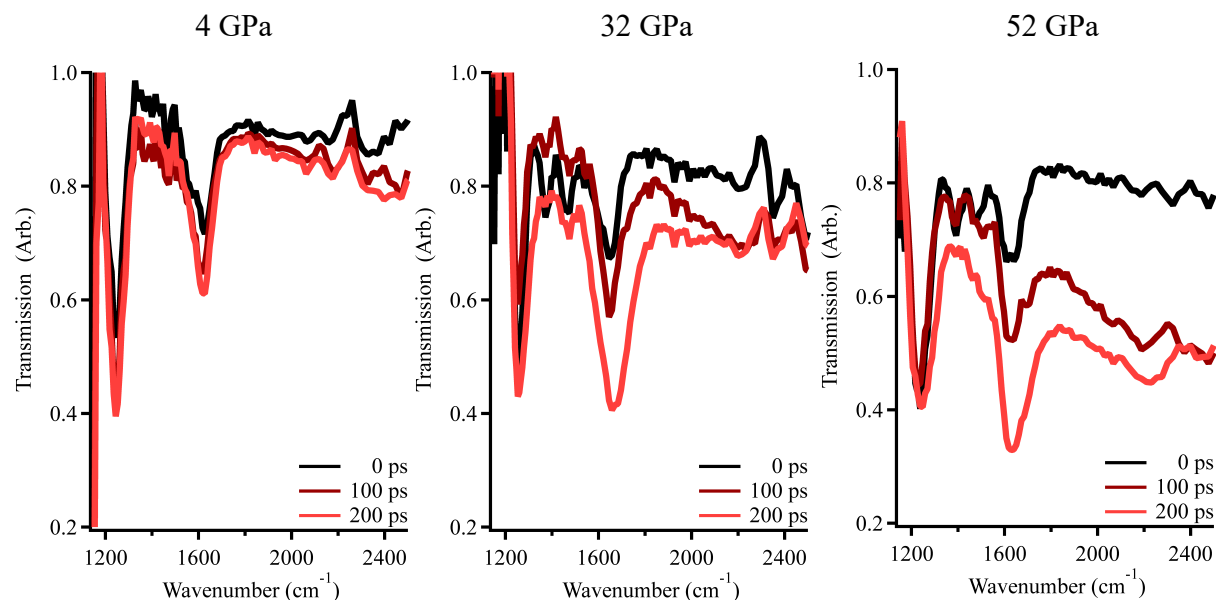
Figure 38 Lineouts corresponding to three specific time delay regions: prior to the shock entering the sample 0, 100, and 200 ps later. Similar to Fig. 37 there is minimal change at low pressure, significant changes at medium pressure, and enhanced changes at extreme pressure. ν_s-NO_2 and ν_a-NO_2 show similar trends at low pressure, but altered behavior at reactive pressures. There is a feature that grows on the red-edge of the CO_2 stretch at reactive pressures.
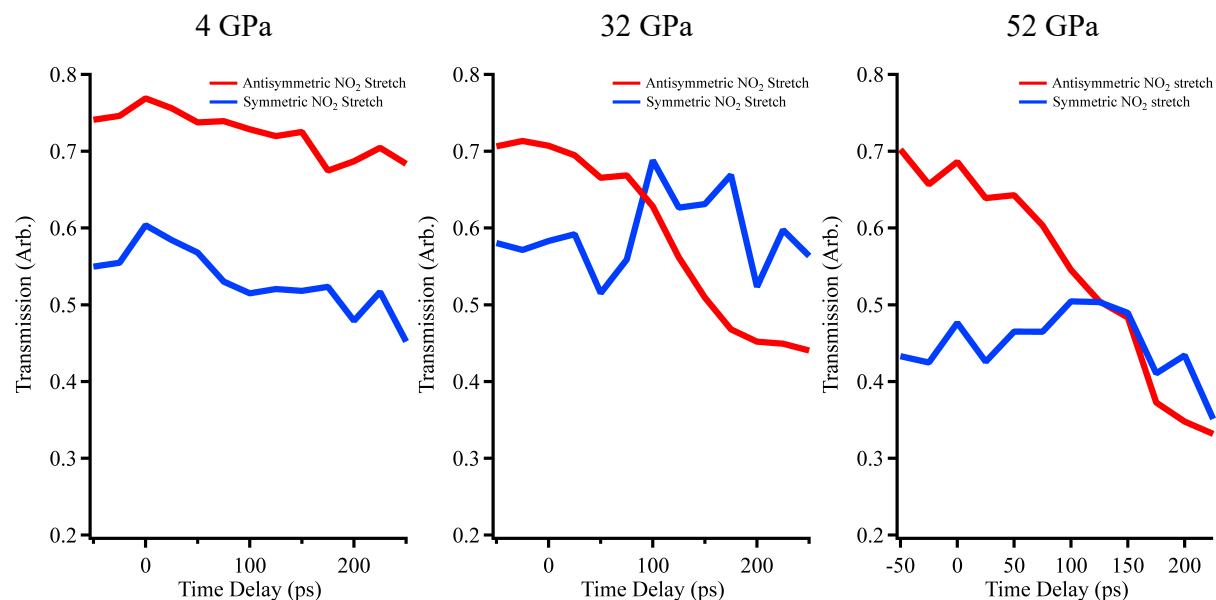
Figure 39 Comparison of the behavior of the ν_s-NO_2 and ν_a-NO_2 at three pressures. At low pressures the two bonds change in the same direction. At reactive pressures (medium and greater) there is an almost opposite behavior between the two bonds. Reactions show some delay at medium pressure and are almost prompt at extreme pressure.
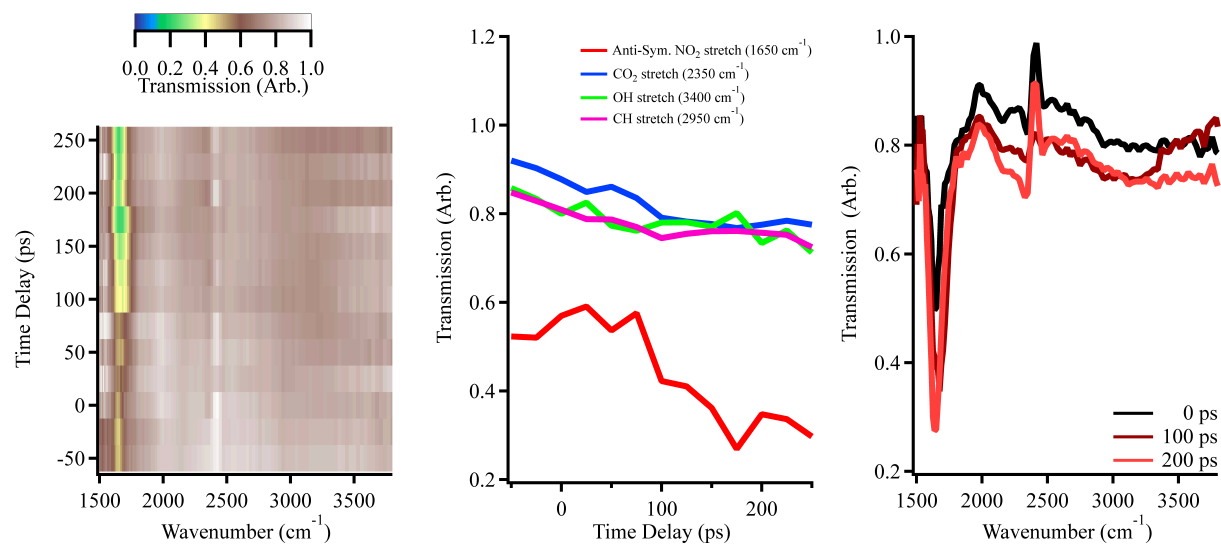
Figure 40 Shocked transmission spectra (left), specific bond lineouts (center), and three selected time delay lineouts for the high pressure (~37 GPa) high frequency region case. The high frequency region allowed access to observe the CH-, NH-, and OH- stretches. No strongly absorbing intermediates were observed for the OH, NH, and CH region. A shoulder did appear near the CO_2 stretch similar to low frequency reactive regimes.

95

4.4   Discussion

4.4.1   Shock state determination: UDE, USI, and impedance matching

Sample roughness accounted for most of the difficulty in measuring shock and particle velocities in these experiments. Shocks averaged over multiple crystals with multiple microstructures, like those shown in Fig. 33. Similar difficulties associated with UDE measurements on thin crystalline films of RDX and PETN were encountered previously in this lab, requiring the impedance matching technique to determine the shock state.[70] UDE data were able to be fit for the high pressure case, which yielded at most 18% lower pressures than the impedance matched points. Again, this difference is most likely due to the linear extrapolation of the assumed unreactive Hugionot for PETN where measured points do not exist. Since samples were not perfectly matched there was a spread in measured pressures within each pressure regime even with impedance matching. This fact did not adversely affect the VIS and MIR absorption spectroscopies as spectroscopic results looked nearly identical as observed changes were consistent between experiments and substrates even though the impedance matched pressure values were different by up to 10% between substrates. It is posited that pressures calculated from impedance matching of an extrapolated single crystal PETN Hugoniot are higher than UDE measurements, but are a reasonable state determination for these spectroscopic measurements. For UDE points measured in the high pressure region, the shock velocities were higher for each particle velocity than those measured by Park et al. for similar time and length scales, possibly attributable to differences in sample morphology. PETN films used in these experiments consisted of randomly oriented microcrystals with sizes ranging from <25 μm to 100 μm. The films used by Park et al. were more uniform with nano-scale crystal packing and a known crystal orientation.[84] Spin-cast PETN films had a random orientation of larger crystals with micrometer-scale features. Orientation effects for the reactivity of PETN are known to result in almost a factor of 3 difference in shock sensitivity.[16,17] For a randomly oriented distribution of crystals there could be a mix of more and less sensitive crystals, so that measurements would be an average of those properties for PETN films like those used in these experiments.

4.4.2 VIS transient absorption spectroscopy

Often we observed in the VIS spectra the characteristic transmission oscillations typical of thin film interference effects. An example of this effect can be seen in Fig. 41 for an extreme pressure case at a time delay of 100 ps into the shock. These effects are smoothed over in the averaged data reported above, since the films were not uniform across the substrate so that multiple thicknesses are probed at a single time delay. Averaging over multiple sample locations removed this coherent interference effect, and the averaged result agrees well with previous research.[16, 17, 28, 41, 43] At the 3-6 GPa low pressure, the VIS spectra showed no significant absorption (approximately 3%) across the entire wavelength range, indicating no sample changes beyond roughening of the aluminum drive layer. At the 30-35 GPa medium pressure, the VIS absorption results showed a broad absorbance similar to that observed by Dreger et al., but at significantly earlier times due to the much higher single shock pressures in our experiments.[16, 17, 43] It has been shown before for reactive liquids and solids that a stronger shock on ps time scales is required to obtain Hugoniot and VIS absorption results similar to longer time scale experiments.[62-64, 69, 70] High and extreme pressure VIS results displayed an increased absorbance over the medium pressure case, indicating faster reactions. Absorbances for all three "reactive" cases show absorbances that do not decrease (and perhaps even increase) in optical density after the shock has transited the sample and the release wave begins, typically at 110-140 ps time delay for reactive cases. We attributed these changes in absorbance to chemistry induced in the sample, as has been observed in several other materials using this method.[64, 70]
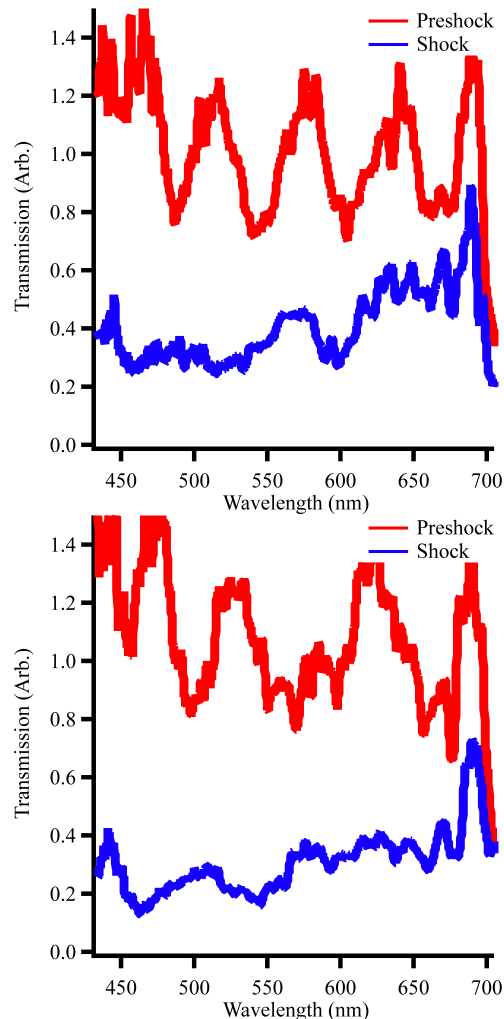
Figure 41 VIS images from extreme pressures. The oscillatory behavior is due to thin film interference effects from the ~1 μm film of PETN. These shots were approximately 2 mm apart on the sample and notably show different oscillation frequency prior to, and during the shock.

4.4.3   MIR transient absorption spectroscopy

Data at each time delay were averaged over 25 shots and four experiments with two experiments collected on one substrate. This averaging over multiple thicknesses (800-1300 nm) for the time delays probed was responsible for averaging out any thin film interference effects. In the low frequency MIR region, at low pressures there was at most a 10% change in the spectrum as the PETN was shocked and released (see Figs 37 and 38). The ν_s-NO$_2$ and ν_a-NO$_2$ bands (1280 and 1650 cm^{-1} respectively) showed similar trends to each other with a slight decrease in

transmission. Notably, the transmission outside of the resonance peaks decreased by a similar quantity to the two nitro stretches, indicating the data can be explained by increasing sample surface roughness reflectivity decrease or increasing sample light scattering with time after the shock. The shocked material experienced a small temperature increase due to shock compression, which produced a small amount of broadening and shifting of the vibrational bands. It has been shown in several static high pressure experiments that NO_2 stretches demonstrate weak shifting and broadening for low pressures of 2 and 0.9-3 cm^{-1}/GPa for the ν_s-NO_2 and ν_a-NO_2 respectively, but also changes in absorption magnitude similar to these experiments.[38, 45-47, 50, 51] Due to the infrared spectral resolution capabilities of the prism spectrometer and the INO detector used in these experiments, resolving shifts of ~10 cm^{-1} was not feasible.

In the case of medium pressures, there were observable changes in the spectral features as the sample was shocked into a reactive regime. The spectral regions at the ν_s-NO_2 and ν_a-NO_2 modes showed nearly opposite MIR absorption behavior with time delay starting at about 75 ps, as the ν_s-NO_2 peak shows a slightly decreasing absorption, while the spectral region at the ν_a-NO_2 peak features a strongly increasing absorption. These spectral changes did not recover after the release from the PETN/air surface, which was consistent with the VIS results, i.e., irreversible chemical changes were induced in the sample. The difference in behavior of the NO_2 stretches is consistent with the occurrence of a chemical reaction. The CH_2 wag and stretch peaks at 1400 and 1450 cm^{-1} also appear to be decreasing in intensity; however, given the signal to noise of those peaks it is difficult to draw any conclusions about whether the origin of those changes is from chemistry or sample pressure induced variations or a combination of the two. Also noteworthy in this MIR frequency range is the CO_2 stretch region (2350 cm^{-1}), like that seen in Fig. 38. It is difficult to make any determination of absolute CO_2 changes in these experiments as CO_2 was present in the laboratory atmosphere making absolute normalization difficult. There was, however, a notable increased absorption on the red edge of the CO_2 stretch from ~2100-2250 cm^{-1}. This change could be from shifting, broadening, and/or generation of CO_2 from the experiment, but the lack of new absorption at 3600 cm^{-1} strongly suggests this is not the case.[90, 91] Rather, this change is most likely due to formation of an intermediate consistent with N_2O[91, 92] or C≡O absorption spectra.[91, 93]

To substantiate that the observed changes in the MIR and VIS spectra presented above were from chemistry and not other mechanisms like frequency dependent thin film interference or

vibrational hot bands,[52, 65, 67, 72, 86, 88] we increased the shock drive laser energy to provoke strong chemical changes. Pressures achieved from impedance matching in the extreme pressure case ranged from 50-55 GPa, and the spectral data are shown in Figs. 37 and 38. Larger and faster changes were observed in the MIR spectra for this pressure range compared to the medium pressure. Similar trends were observed in the MIR for the ν_s-NO_2 and ν_a-NO_2 band regions, where the ν_s-NO_2 showed either a slight decrease in absorption or minimal change with time delay, while the ν_a-NO_2 showed a strongly absorbing feature that started almost immediately (25-50 ps). This ν_a-NO_2 band region behavior did not recover after release, and actually increased in absorption. This result was again complementary to the VIS spectroscopy results where large absorption changes were observed promptly following the introduction of the shock and increased even after shock release. At frequencies higher than the NO_2 stretch, a relatively broad absorptive feature was observed over the entire spectral range even in a range where CHNO bonds have no strong absorptions. The change in the spectral range greater than the NO_2 stretch could be attributable to strong scattering changes in the MIR. Another notable feature was the increased absorption on the red-edge of the CO_2 stretch, similar but stronger than was observed in the medium pressure case.

For the high pressure experiments performed using the high frequency MIR region, the ν_a-NO_2 band region showed a similar trend to the low frequency, extreme pressure MIR range discussed above, with increased absorption growth with time, even after release. The data also showed an increased absorption near the red-edge of the CO_2 stretch. The VIS absorbance measurements again also indicated that there was irreversible shock induced absorption changes in the sample. This high frequency MIR region simultaneously monitored the ν_a-NO_2 stretch as well as the single hydrogenic bond stretch regions (CH-, NH-, and OH-) in every shot. Absorption due to the CH-bonds of PETN in the dynamic single shot MIR spectrometer could only be observed at the ~1% level, even at time delays prior to entrance of the shock. Most intermediate pathways should produce absorptive features in the CH-, NH-, and OH-stretch region; however, the MIR data does not show this. No observable increased absorbance feature was measured in this region (2800-3500 cm^{-1}) when viewing multiple lineouts in various regions in Fig 40 or Fig. 42. The lack of significant absorptions from CH-, NH-, or OH-stretches suggests that these bonds are <u>not</u> formed in the first steps of the shock induced chemistry for PETN.
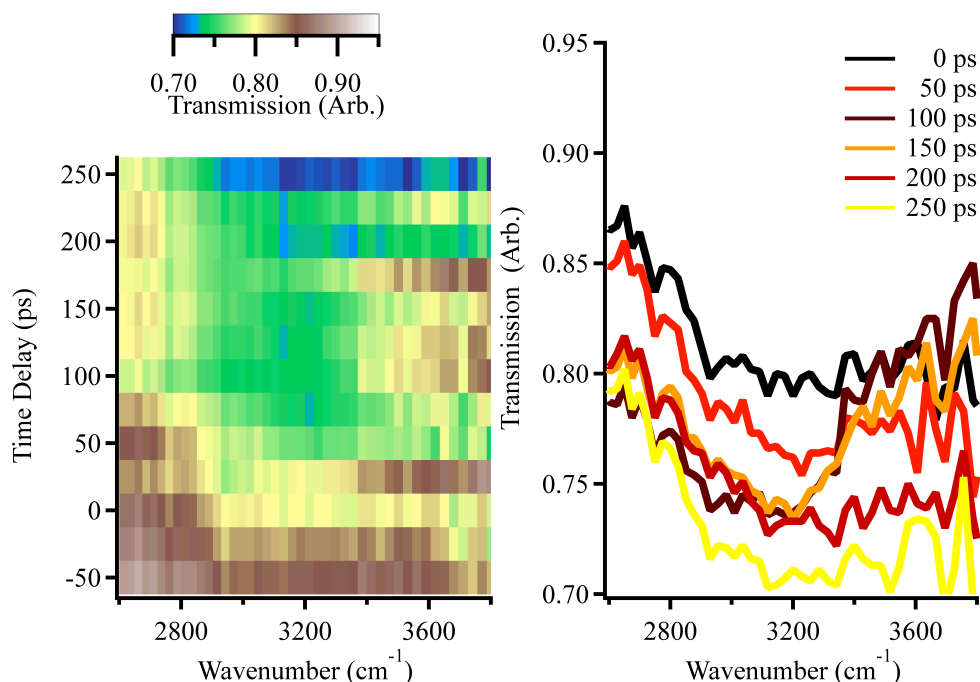
Figure 42 Left, Transmission spectra of shocked PETN. Right, time delayed lineouts for the high frequency region that is focused on CH-, NH-, and OH- stretch region. Some absorption is observed near 3200 cm^{-1}; however, it only a few percent above the total broad scattering changes of the spectrum. No new peaks were observed in this data.

To recapitulate several of the spectral features measured in these experiments, 1.) There were irreversible VIS and MIR absorptions induced in PETN at pressures that are considered reactive with increased absorptions at higher pressures, 2.) the ν_s-NO$_2$ absorption remained constant but the ν_a-NO$_2$ absorption spectral region grew substantially, 3.) no significant absorptions were measured in the high frequency region where CH-, NH-, and OH-stretches are typically observed, and 4.) a broad absorptive feature was present at 2100-2250 cm^{-1} that grew with time for all reactive experiments. Considering the lack of absorptions in the high frequency region for PETN there is no evidence to suggest there is generation of HONO, HONO$_2$, or CH$_2$O species.[33, 35, 44] Static measurements of HE that contain NH bonds and NO$_2$ stretches show these two bonds exhibit similar absorption strength in the MIR.[94, 95] OH- and NH- stretches exhibit similar absorption strengths as well.[96-100] N$_2$O was considered as a possible intermediate because of its absorption band in the 2200 cm^{-1} region; however, it also has similar strength absorption at 1284 cm^{-1} which was not observed.[91, 101] We also observe nearly opposite NO$_2$ stretch region absorption behavior with the ν_s-NO$_2$ showing slight increases in transmission and ν_a-NO$_2$ showing

strongly enhanced absorption. Additionally, with the lack of CH_2O absorption region near 1700-1800 cm^{-1}, these results do not support previous observations and mechanisms that suggest NO_2 is the primary intermediate formed in the shock induced chemistry of PETN.[33, 35, 38-41, 43, 49, 53, 54, 102] If NO_2 were the primary intermediate, the MIR spectra of the two NO_2 stretches would presumably exhibit equal changes, as the absorptions of the two stretches of NO_2 in various environments are nearly equivalent.[91, 103-106] This was not observed experimentally. For similar reasons we do not think the signature of NO_3 radical is consistent with our observations.[107-111] The C-C bond cleavage mechanism based on previous experiments[40] is not inconsistent with these observations. An interpretation of the 2200 cm^{-1} peak is that it is a signature of C≡O formation.[91, 93] Similarly, another interpretation of the ν_a-NO_2 behavior is the formation of methyl nitrite which exhibits a very strong ν_a-NO_2, while having a weaker ν_s-NO_2.[112] One mechanism consistent with the MIR data is shown in Fig. 43. Two PETN (A and B) molecules collide and an oxygen atom is removed from an NO_3 group on PETN A and supplants a C-C bond in the central PETN B structure, removing a CH_2ONO_2 group. This reaction generates a molecule similar to methyl nitrite CH_2O-N=O on one arm of PETN A. The double and single bonded oxygen structure on the NO_2 group matches the ν_s-NO_2 and ν_a-NO_2 behavior that is observed in the shocked MIR spectra.[113] The CH_2ONO_2 radical retains ν_s-NO_2 and ν_a-NO_2 mode behavior, which supports why those peaks are still well-defined in these measurements. Methyl nitrite has a larger absorption at 1650 than at 1280 cm^{-1}, consistent with the largest spectral change observed. Multiple other C-C bonds of PETN B may then break, forming higher order bonds with the central carbon atom and oxygen of PETN B until C≡O is formed. The red-edge of the CO_2 band shows a broad moderate strength absorbance feature similar to C≡O absorption spectra.[93] Although not completely substantiated, methyl nitrite and carbon monoxide formation are possible explanations for the shocked MIR spectral features measured in these experiments. A review of possible pathways and consistency with the MIR absorption results measured in experiments are presented in Table 2.

Table 2 Possible intermediate pathways for shocked PETN and consistency with MIR results measured in these experiments.

Intermediate Pathway	References	Inconsistent with MIR results*
NO scission	36	~
NO2 scission	33-35, 38-41, 54, 55	~
NO3 scission	35, 37, 40, 42, 43, 55	~
HNO3 formation	44	X
HONO elimination	33, 44	X
C-C bond cleavage	35, 40	O
H-ion formation	35	X
O-radical formation	35	O

*-X = true, O = false, ~ = not entirely possible to eliminate
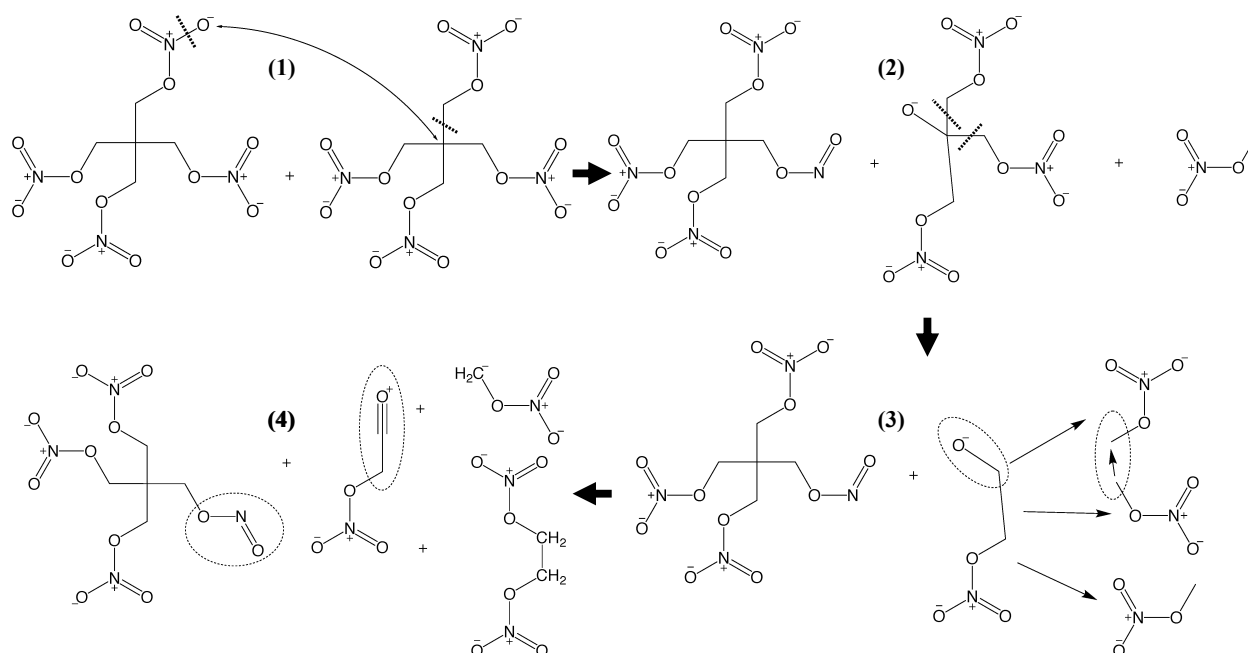
Figure 43 Image of possible chemical pathway. (1) An oxygen is removed from PETN A and replaces one of the C-C bonds in PETN B. (2) The central C-C bonds of PETN B begin to break off. (3) The donated oxygen to PETN B forms higher order bonds with the central carbon (circled) and two of the nearly methyl nitrate groups bond to form stable intermediates. (4) The final mechanism that explains some of the infrared measurements made in these experiments. C≡O forms which has a broad absorption from 2200-2350 cm^{-1} and methyl nitrite forms which has a strong ν_a-NO2 and a weak ν_s-NO2.

4.5 Conclusions

Measurements of shock induced chemistry of PETN were made using ultrafast VIS and MIR absorption spectroscopy. The proposed mechanism of NO_2 scission having a primary role in PETN shock initiation chemistry is inconsistent with the time dependent spectral data measured in these experiments. There is a small decreased absorption in the ν_s-NO_2 absorption and large increase in absorption at the ν_a-NO_2 band regions, which does not coincide with NO_2 absorption spectra. Additionally, there were no apparent absorptions in the CH-, NH-, or OH- stretch regions, meaning that molecules with these vibrational modes are not yet formed, or were formed and quickly underwent subsequent reactions without building to significant concentrations. The observed MIR spectra are consistent with mechanisms that form methyl (or alkyl) nitrite and carbon monoxide as important intermediates in PETN shock chemistry, presumably formed via bimolecular scission of the C-C bond.

4.6 References

1. Zakar, E. Technology challenges in solid energetic materials for micro propulsion applications; ARMY RESEARCH LAB ADELPHI MD: 2009.
2. Deal, W., Measurement of Chapman-Jouguet pressure for explosives. The Journal of Chemical Physics 1957, 27 (3), 796-800.
3. Fowles, G.; Duvall, G.; Asay, J.; Bellamy, P.; Feistmann, F.; Grady, D.; Michaels, T.; Mitchell, R., Gas gun for impact studies. Review of Scientific Instruments 1970, 41 (7), 984-996.
4. Gibbs, T.; Popolato, A., Los Alamos scientific laboratory explosive property data. University of California Press, Berkeley.[279t]: 1980.
5. Glass, I.; Chan, S.; Brode, H., Strong planar shock waves generated by explosively-driven spherical implosions. AIAA Journal 1974, 12 (3), 367-374.
6. Gustavsen, R. L.; Sheffield, S. A.; Alcon, R. R., Detonation wave profiles in HMX based explosives. AIP Conference Proceedings 1998, 429 (1), 739-742.

7.   Gustavsen, R. L.; Sheffield, S. A.; Alcon, R. R.; Forbes, J. W.; Tarver, C. M.; Garcia, F., Embedded Electromagnetic Gauge Measurements and Modeling of Shock Initiation in the TATB Based Explosives LX-17 and PBX 9502. AIP Conference Proceedings 2002, 620 (1), 1019-1022.

8.   Halleck, P.; Wackerle, J., Dynamic elastic-plastic properties of single-crystal pentaerythritol tetranitrate. Journal of Applied Physics 1976, 47 (3), 976-982.

9.   Jones, A. H.; Isbell, W.; Maiden, C., Measurement of the very-high-pressure properties of materials using a light-gas gun. Journal of Applied Physics 1966, 37 (9), 3493-3499.

10.   Marsh, S. P., LASL shock Hugoniot data. Univ of California Press: 1980; Vol. 5.

11.   Campbell, A.; Davis, W.; Ramsay, J.; Travis, J., Shock initiation of solid explosives. The Physics of Fluids 1961, 4 (4), 511-521.

12.   Sheffield, S. A.; Gustavsen, R. L.; Alcon, R. R., Hugoniot and initiation measurements on TNAZ explosive. AIP Conference Proceedings 1996, 370 (1), 879-882.

13.   Sheffield, S. A.; Engelke, R.; Alcon, R. R.; Gustavsen, R. L.; Robins, D.; Stahl, D. B.; Stacy, H. L.; Whitehead, M., Particle velocity measurements of the reaction zone in nitromethane. In 12th International Detonation Symposium, San Diego, CA, 2002; pp 159-166.

14.   Walsh, J. M.; Christian, R. H., Equation of State of Metals from Shock Wave Measurements. Physical Review 1955, 97 (6), 1544-1556.

15.   Winey, J.; Duvall, G.; Knudson, M.; Gupta, Y., Equation of state and temperature measurements for shocked nitromethane. The Journal of Chemical Physics 2000, 113 (17), 7492-7501.

16.   Dick, J., Anomalous shock initiation of detonation in pentaerythritol tetranitrate crystals. Journal of applied physics 1997, 81 (2), 601-612.

17.   Dick, J.; Mulford, R.; Spencer, W.; Pettit, D.; Garcia, E.; Shaw, D., Shock response of pentaerythritol tetranitrate single crystals. Journal of applied physics 1991, 70 (7), 3572-3587.

18.   Dodson, B. W.; Graham, R. A., Shock-induced organic chemistry. AIP Conference Proceedings 1982, 78 (1), 42-51.

19. Hill, J.; Moore, D.; Schmidt, S.; Storm, C., Infrared, Raman, and coherent anti-Stokes Raman spectroscopy of the hydrogen/deuterium isotopomers of nitromethane. The Journal of Physical Chemistry 1991, 95 (8), 3037-3044.

20. Moore, D.; Schmidt, S.; Shaner, J.; Shampine, D.; Holt, W., Coherent anti-Stokes Raman scattering in benzene and nitromethane shock-compressed to 11 GPa. In Shock Waves in Condensed Matter, Springer: 1986; pp 207-211.

21. Schmidt, S.; Moore, D.; Shaner, J.; Shampine, D.; Holt, W., Coherent anti-stokes Raman scattering in benzene and nitromethane shock-compressed to 10 GPa. Physica B+ C 1986, 139, 587-589.

22. Schmidt, S. C.; Moore, D. S., Vibrational spectroscopy of high-temperature, dense molecular fluids by coherent anti-Stokes Raman scattering. Accounts of Chemical Research 1992, 25 (9), 427-432.

23. Wackerle, J.; Johnson, J.; Halleck, P. Shock initiation of high-density PETN; Los Alamos Scientific Lab., N. Mex.(USA): 1976.

24. Boade, R., Compression of porous copper by shock waves. Journal of Applied Physics 1968, 39 (12), 5693-5702.

25. Dick, R., Shock compression data for liquids. III. Substituted methane compounds, ethylene glycol, glycerol, and ammonia. The Journal of Chemical Physics 1981, 74 (7), 4053.

26. Gilman, J. J., Chemical reactions at detonation fronts in solids. Philosophical Magazine B 1995, 71 (6), 1057-1068.

27. Graham, R., Measurement of wave profiles in shock-loaded solids. In High-Pressure Science and Technology, Springer: 1979; pp 1886-1901.

28. Gruzdkov, Y. A.; Gupta, Y. M.; Dick, J. J., Time-resolved absorption spectroscopy in shocked PETN single crystals. AIP Conference Proceedings 2000, 505 (1), 929-932.

29. Hardesty, D., An investigation of the shock initiation of liquid nitromethane. Combustion and Flame 1976, 27, 229-251.

30. Rice, M.; McQueen, R. G.; Walsh, J., Compression of solids by strong shock waves. In Solid State Physics, Elsevier: 1958; Vol. 6, pp 1-63.

31. Pangilinan, G.; Gupta, Y., Time-resolved Raman measurements in nitromethane shocked to 140 kbar. The Journal of Physical Chemistry 1994, 98 (17), 4522-4529.

32.   Kunz, A. B., AnAb Initio Investigation of Crystalline PETN. MRS Online Proceedings Library Archive 1995, 418.

33.   Landerville, A. C.; Oleynik, I. I.; White, C. T., Reactive Molecular Dynamics of Hypervelocity Collisions of PETN Molecules. The Journal of Physical Chemistry A 2009, 113 (44), 12094-12104.

34.   Wu, C. J.; Manaa, M. R.; Fried, L. E., Tight binding molecular dynamic simulation of PETN decomposition at an extreme condition. MRS Online Proceedings Library Archive 2006, 987.

35.   Wu, C. J.; Ree, F. H.; Yoo, C. S., A quantum mechanical molecular dynamics study of binary collisions of pentaerythritol tetranitrate (PETN): Its correlation to shock sensitivity. Propellants, Explosives, Pyrotechnics: An International Journal Dealing with Scientific and Technological Aspects of Energetic Materials 2004, 29 (5), 296-303.

36.   Yu, Z.; Bernstein, E. R., Decomposition of pentaerythritol tetranitrate [C (CH2ONO2) 4] following electronic excitation. The Journal of chemical physics 2011, 135 (15), 154305.

37.   Zhurova, E. A.; Stash, A. I.; Tsirelson, V. G.; Zhurov, V. V.; Bartashevich, E. V.; Potemkin, V. A.; Pinkerton, A. A., Atoms-in-molecules study of intra-and intermolecular bonding in the pentaerythritol tetranitrate crystal. Journal of the American Chemical Society 2006, 128 (45), 14728-14734.

38.   Gruzdkov, Y. A.; Gupta, Y. M., Vibrational properties and structure of pentaerythritol tetranitrate. The Journal of Physical Chemistry A 2001, 105 (25), 6197-6202.

39.   Hemmi, N.; Dreger, Z.; Gruzdkov, Y.; Winey, J.; Gupta, Y., Raman spectra of shock compressed pentaerythritol tetranitrate single crystals: anisotropic response. The Journal of Physical Chemistry B 2006, 110 (42), 20948-20953.

40.   Ng, W.; Field, J.; Hauser, H., Thermal, fracture, and laser-induced decomposition of pentaerythritol tetranitrate. Journal of applied physics 1986, 59 (12), 3945-3952.

41.   Gruzdkov, Y. A.; Gupta, Y. M., Shock wave initiation of pentaerythritol tetranitrate single crystals: Mechanism of anisotropic sensitivity. The Journal of Physical Chemistry A 2000, 104 (47), 11169-11176.

42.   Davis, L. L.; Brower, K. R., Reactions of organic compounds in explosive-driven shock waves. The Journal of Physical Chemistry 1996, 100 (48), 18775-18783.

43. Dreger, Z. A.; Gruzdkov, Y. A.; Gupta, Y. M.; Dick, J. J., Shock wave induced decomposition chemistry of pentaerythritol tetranitrate single crystals: time-resolved emission spectroscopy. The Journal of Physical Chemistry B 2002, 106 (2), 247-256.

44. Naud, D. L.; Brower, K. R., Pressure effects on the thermal decomposition of nitramines, nitrosamines, and nitrate esters. The Journal of Organic Chemistry 1992, 57 (12), 3303-3308.

45. Ciezak, J. A.; Byrd, E. F.; Rice, B. M. Exploring the high-pressure behavior of PETN: A combined quantum mechanical and experimental study; Army Research Lab Aberdeen Proving Ground MD: 2006.

46. Ciezak, J. A.; Jenkins, T. A. New outlook on the high-pressure behavior of pentaerythritol tetranitrate; Army Research Lab Aberdeen Proving Ground MD Weapons and Materials Research …: 2007.

47. Ciezak, J. A.; Jenkins, T. A. The Low-Temperature Vibrational Behavior of Pentaerythritol Tetranitrate; ARMY RESEARCH LAB ABERDEEN PROVING GROUND MD WEAPONS AND MATERIALS RESEARCH …: 2008.

48. Dreger, Z. A.; Gupta, Y. M., High pressure–high temperature polymorphism and decomposition of pentaerythritol tetranitrate (PETN). The Journal of Physical Chemistry A 2013, 117 (25), 5306-5313.

49. Gruzdkov, Y. A.; Dreger, Z. A.; Gupta, Y. M., Experimental and theoretical study of pentaerythritol tetranitrate conformers. The Journal of Physical Chemistry A 2004, 108 (29), 6216-6221.

50. Lipinska-Kalita, K. E.; Pravica, M. G.; Nicol, M., Raman Scattering Studies of the High-Pressure Stability of Pentaerythritol Tetranitrate, C(CH2ONO2)4. The Journal of Physical Chemistry B 2005, 109 (41), 19223-19227.

51. Pravica, M.; Lipinska-Kalita, K.; Quine, Z.; Romano, E.; Shen, Y.; Nicol, M. F.; Pravica, W. J., Studies of phase transitions in PETN at high pressures. Journal of Physics and Chemistry of Solids 2006, 67 (9-10), 2159-2163.

52. Tailleur, M.; Cherville, J., Etude des conditions d'initiation de la pentrite (PETN) par spectrométrie raman ultra-rapide. Propellants, Explosives, Pyrotechnics 1982, 7 (1), 22-27.

53. Gruzdkov, Y.; Gupta, Y.; Dick, J. In Time-resolved absorption spectroscopy in shocked PETN single crystals, AIP Conference Proceedings, AIP: 2000; pp 929-932.

54.   Budzien, J.; Thompson, A. P.; Zybin, S. V., Reactive Molecular Dynamics Simulations of Shock Through a Single Crystal of Pentaerythritol Tetranitrate. The Journal of Physical Chemistry B 2009, 113 (40), 13142-13151.

55.   Shan, T.-R.; Wixom, R. R.; Mattsson, A. E.; Thompson, A. P., Atomistic Simulation of Orientation Dependence in Shock-Induced Initiation of Pentaerythritol Tetranitrate. The Journal of Physical Chemistry B 2013, 117 (3), 928-936.

56.   Powell, M. S.; Bowlan, P. R.; Son, S. F.; Bolme, C. A.; Brown, K. E.; Moore, D. S.; McGrane, S. D., A benchtop shock physics laboratory: Ultrafast laser driven shock spectroscopy and interferometry methods. Review of Scientific Instruments 2019, 90 (6), 063001.

57.   Bolme, C.; Funk, D., Ultrafast dynamic ellipsometry measurements of early time laser ablation of titanium thin films. Applied Physics A 2008, 92 (4), 761.

58.   Bolme, C.; McGrane, S.; Moore, D.; Funk, D., Single shot measurements of laser driven shock waves using ultrafast dynamic ellipsometry. Journal of Applied Physics 2007, 102 (3), 033513.

59.   Bolme, C.; McGrane, S.; Moore, D.; Whitley, V.; Funk, D., Single shot Hugoniot of cyclohexane using a spatially resolved laser driven shock wave. Applied Physics Letters 2008, 93 (19), 191903.

60.   Bolme, C. A. Ultrafast dynamic ellipsometry of laser driven shock waves. Massachusetts Institute of Technology, 2008.

61.   Bowlan, P.; Powell, M.; Perriot, R.; Martinez, E.; Kober, E. M.; Cawkwell, M. J.; McGrane, S., Probing ultrafast shock-induced chemistry in liquids using broad-band mid-infrared absorption spectroscopy. The Journal of chemical physics 2019, 150 (20), 204503.

62.   Brown, K. E.; Bolme, C. A.; McGrane, S. D.; Moore, D. S., Ultrafast shock-induced chemistry in carbon disulfide probed with dynamic ellipsometry and transient absorption spectroscopy. Journal of Applied Physics 2015, 117 (8), 085903.

63.   Brown, K. E.; McGrane, S. D.; Bolme, C. A.; Moore, D. S., Ultrafast chemical reactions in shocked nitromethane probed with dynamic ellipsometry and transient absorption spectroscopy. The Journal of Physical Chemistry A 2014, 118 (14), 2559-2567.

64. Dang, N.; Bolme, C.; Moore, D.; McGrane, S., Shock induced chemistry in liquids studied with ultrafast dynamic ellipsometry and visible transient absorption spectroscopy. The Journal of Physical Chemistry A 2012, 116 (42), 10301-10309.

65. Funk, D.; Moore, D.; McGrane, S.; Gahagan, K.; Reho, J.; Buelow, S.; Nicholson, J.; Fisher, G.; Rabie, R., Ultrafast studies of shock waves using interferometric methods and transient infrared absorption spectroscopy. Thin Solid Films 2004, 453, 542-549.

66. McGrane, S.; Bowlan, P.; Powell, M.; Brown, K.; Bolme, C., Broadband mid-infrared measurements for shock-induced chemistry. AIP Conference Proceedings 2018, 1979 (1), 130004.

67. McGrane, S.; Moore, D.; Funk, D., Shock induced reaction observed via ultrafast infrared absorption in poly (vinyl nitrate) films. The Journal of Physical Chemistry A 2004, 108 (43), 9342-9347.

68. McGrane, S.; Moore, D.; Funk, D. In Measurement of shocked thin polymer film Hugoniot properties with ultrafast dynamic ellipsometry, AIP Conference Proceedings, AIP: 2004; pp 1181-1186.

69. McGrane, S.; Moore, D. S.; Whitley, V. H.; Bolme, C. A.; Eakins, D. E. In Molecular shock response of Explosives: Electronic absorption spectroscopy, AIP Conference Proceedings, AIP: 2009; pp 1301-1304.

70. Mcgrane, S. D.; Dang, N. C.; Whitley, V. H.; Bolome, C. A.; Moore, D. Transient absorption spectroscopy of laser shocked explosives; Los Alamos National Lab.(LANL), Los Alamos, NM (United States): 2010.

71. McGrane, S. D.; Moore, D. S.; Funk, D. J. In Ultrafast spectroscopy and interferometry of laser-shocked thin films: practical considerations, High-Power Laser Ablation V, International Society for Optics and Photonics: 2004; pp 165-170.

72. Moore, D., Influence of hot bands on vibrational spectra of shock compressed materials. The Journal of Physical Chemistry A 2001, 105 (19), 4660-4663.

73. Moore, D. S.; McGrane, S. D.; Funk, D. J., Ultrashort laser shock dynamics. In Shock Wave Science and Technology Reference Library, Springer: 2007; pp 47-104.

74.   Schulze, P. A.; Dang, N. C.; Bolme, C. A.; Brown, K. E.; McGrane, S. D.; Moore, D. S., Shock Hugoniot equations of state for binary ideal (toluene/fluorobenzene) and nonideal (ethanol/water) liquid mixtures. The Journal of Physical Chemistry A 2013, 117 (29), 6158-6163.

75.   Schulze, P. A.; Ivanov, T. W.; Bolme, C. A.; Brown, K. E.; McGrane, S. D.; Moore, D. S., Shock Hugoniot equations of state for binary water-alcohol liquid mixtures. Journal of Applied Physics 2014, 115 (2), 023512.

76.   Whitley, V.; McGrane, S.; Eakins, D.; Bolme, C.; Moore, D.; Bingert, J., The elastic-plastic response of aluminum films to ultrafast laser-generated shocks. Journal of Applied Physics 2011, 109 (1), 013505.

77.   Zuanetti, B.; McGrane, S. D.; Bolme, C. A.; Prakash, V., Measurement of elastic precursor decay in pre-heated aluminum films under ultra-fast laser generated shocks. Journal of Applied Physics 2018, 123 (19), 195104.

78.   Fuji, T.; Nomura, Y., Generation of phase-stable sub-cycle mid-infrared pulses from filamentation in nitrogen. Applied Sciences 2013, 3 (1), 122-138.

79.   Fuji, T.; Suzuki, T., Generation of sub-two-cycle mid-infrared pulses by four-wave mixing through filamentation in air. Optics letters 2007, 32 (22), 3330-3332.

80.   Nomura, Y.; Wang, Y.-T.; Kozai, T.; Shirai, H.; Yabushita, A.; Luo, C.-W.; Nakanishi, S.; Fuji, T., Single-shot detection of mid-infrared spectra by chirped-pulse upconversion with four-wave difference frequency generation in gases. Optics express 2013, 21 (15), 18249-18254.

81.   Sandoval, J.; Quinlin, W. PETN homologs; Mason and Hanger-Silas Mason Co., Inc., Amarillo, TX (United States): 1972.

82.   Cady, H. H.; Larson, A., Pentaerythritol tetranitrate II: its crystal structure and transformation to PETN I; an algorithm for refinement of crystal structures with poor data. Acta Crystallographica Section B: Structural Crystallography and Crystal Chemistry 1975, 31 (7), 1864-1869.

83.   Armstrong, M.; Crowhurst, J.; Bastea, S.; Zaug, J. Observation of off-Hugoniot shocked states with ultrafast time resolution; Lawrence Livermore National Lab.(LLNL), Livermore, CA (United States): 2010.

84.   Park, S. D.; Armstrong, M. R.; Kohl, I. T.; Zaug, J. M.; Knepper, R.; Tappan, A. S.; Bastea, S.; Kay, J. J., Ultrafast Shock-Induced Reactions in Pentaerythritol Tetranitrate Thin Films. The Journal of Physical Chemistry A 2018, 122 (41), 8101-8106.

85.   Lewis, I. R.; Daniel, N. W.; Griffiths, P. R., Interpretation of Raman Spectra of Nitro-Containing Explosive Materials. Part I: Group Frequency and Structural Class Membership. Applied Spectroscopy 1997, 51 (12), 1854-1867.

86.   Moore, D.; McGrane, S.; Funk, D., Infrared complex refractive index measurements and simulated reflection mode infrared absorption spectroscopy of shock-compressed polymer thin films. Applied spectroscopy 2004, 58 (5), 491-498.

87.   Moore, D.; McGrane, S.; Funk, D. In Ultrafast spectroscopic investigation of shock compressed energetic polymer films, AIP Conference Proceedings, AIP: 2004; pp 1285-1288.

88.   Moore, D. S.; McGrane, S. D., Comparative infrared and Raman spectroscopy of energetic polymers. Journal of molecular structure 2003, 661, 561-566.

89.   Moore, D. S.; Bolme, C. A.; Brown, K.; Greenfield, M. T.; McGrane, S. D. In A comparison of infrared, Raman, and coherent Raman spectroscopies in studies of shock-induced chemistry, Shock Conference of Condensed Matter, Portland, OR, AIP: Portland, OR, 2019.

90.   Edwards, D. K., Absorption by Infrared Bands of Carbon Dioxide Gas at Elevated Pressures and Temperatures*. J. Opt. Soc. Am. 1960, 50 (6), 617-626.

91.   Pierson, R. H.; Fletcher, A. N.; Gantz, E. S. C., Catalog of infrared spectra for qualitative analysis of gases. Analytical Chemistry 1956, 28 (8), 1218-1239.

92.   Andrews, L.; Johnson, G. L., Infrared spectra of the $CO_2\cdots$ HF and $N_2O\cdots$ HF complexes in solid argon at 12 K. The Journal of Chemical Physics 1982, 76 (6), 2875-2880.

93.   Ewing, G. E.; Pimentel, G. C., Infrared spectrum of solid carbon monoxide. The Journal of Chemical Physics 1961, 35 (3), 925-930.

94.   Bishop, M. M.; Chellappa, R. S.; Pravica, M.; Coe, J.; Liu, Z.; Dattlebaum, D.; Vohra, Y.; Velisavljevic, N., 1, 1-diamino-2, 2-dinitroethylene under High Pressure-Temperature. The Journal of chemical physics 2012, 137 (17), 174304.

95.   Makashir, P.; Kurian, E., Spectroscopic and thermal studies on the decomposition of l, 3, 5-triamino-2, 4, 6-trinitrobenzene (TATB). Journal of thermal analysis 1996, 46 (1), 225-236.

96. Silverstein, R. M.; Bassler, G. C.; Morrill, T. C., Spectrometric identification of organic compounds. 1981.

97. Rao, C.; Venkataraghavan, R., Correlations of Infrared Group Frequencies and Band Intensities in Organic Molecules with Substituent Constants: A Statistical Evaluation. Canadian Journal of Chemistry 1961, 39 (9), 1757-1764.

98. Brown, T. L., Infrared intensities and molecular structure. Chemical Reviews 1958, 58 (3), 581-608.

99. Bernstein, H., The average XH stretching frequency as a measure of XH bond properties. Spectrochimica Acta 1962, 18 (2), 161-170.

100. Kjaergaard, H. G.; Daub, C. D.; Henry, B. R., The role of electron correlation on calculated XH-stretching vibrational band intensities. Molecular Physics 1997, 90 (2), 201-213.

101. Moore, D. S., Private Communication, Paper in Preparation. 2019.

102. Trott, W. M.; Renlund, A. M., Single-pulse Raman scattering studies of heterogeneous explosive materials. Applied optics 1985, 24 (10), 1520-1525.

103. Milligan, D. E.; Jacox, M. E.; Guillory, W. A., Infrared Spectrum of the NO2− Ion Isolated in an Argon Matrix. The Journal of Chemical Physics 1970, 52 (8), 3864-3868.

104. St. Louis, R. V.; Crawford Jr, B., Infrared Spectrum of Matrix-Isolated NO2. The Journal of Chemical Physics 1965, 42 (3), 857-864.

105. Hadjiivanov, K.; Bushev, V.; Kantcheva, M.; Klissurski, D., Infrared spectroscopy study of the species arising during nitrogen dioxide adsorption on titania (anatase). Langmuir 1994, 10 (2), 464-471.

106. Fateley, W. G.; Bent, H. A.; Crawford Jr, B., Infrared spectra of the frozen oxides of nitrogen. The Journal of Chemical Physics 1959, 31 (1), 204-217.

107. Kawaguchi, K.; Ishiwata, T.; Hirota, E.; Tanaka, I., Infrared spectroscopy of the NO3 radical. Chemical Physics 1998, 231 (2), 193-198.

108. Goebbert, D. J.; Garand, E.; Wende, T.; Bergmann, R.; Meijer, G.; Asmis, K. R.; Neumark, D. M., Infrared spectroscopy of the microhydrated nitrate ions NO3−(H2O) 1− 6. The Journal of Physical Chemistry A 2009, 113 (26), 7584-7592.

109. Pathak, A.; Mukherjee, T.; Maity, D., Microhydration of NO3-: A theoretical study on structure, stability and IR spectra. The Journal of Physical Chemistry A 2008, 112 (15), 3399-3408.

110. Klug, D.; Whalley, E., Nitrite and nitrate ions as infrared pressure gauges for diamond anvils. Review of scientific instruments 1983, 54 (9), 1205-1208.

111. Tsuboi, M.; Hisatsune, I., Infrared Spectrum of Matrix-Isolated Nitrate Ion. The Journal of Chemical Physics 1972, 57 (5), 2087-2093.

112. Klaboe, P.; Jones, D.; Lippincott, E., The infrared spectra and the rotational isomerism of methyl and ethyl nitrite. Spectrochimica Acta Part A: Molecular Spectroscopy 1967, 23 (12), 2957-2971.

113. Rook, F. L., Preparation, vapor pressure, and infrared spectrum of methyl nitrite. Journal of Chemical & Engineering Data 1982, 27 (1), 72-73.

5. INSIGHT INTO THE CHEMISTRY OF TNT DURING SHOCK COMPRESSION THROUGH ULTRAFAST MID-INFRARED ABSORPTION SPECTROSCOPY

5.1   Introduction

Trinitrotoluene (TNT) is a relatively insensitive high explosive (HE) that was developed in the late 1800's. Uses of TNT can range from defense applications to underwater mining operations. The usage of TNT is currently being phased out, but the process has been slow due to several favorable traits that TNT possesses. Due to the large disparity between its melting and decomposition point,[1] TNT is one of the few HE capable of being melt casted into cavities. This feature is very useful when combined with higher performing HE like RDX. Detonation velocity and pressure are adequate, especially considering the decreased sensitivity to initiation of TNT when compared to other higher performing HE.[1, 2] For as long as TNT has been in use, the decomposition chemistry is still subject to debate[3-21] including its detonation chemistry.[4, 5, 9, 14, 22-31]

Emulation of the detonation state can be achieved using shock waves.[32] Multiple mechanisms have been suggested on TNT detonation and decomposition chemistry pathways between simulations[11, 22, 25-27, 30, 31, 33] and experiments.[4-7, 9, 10, 13-21, 23, 24] Homolysis of the C-N bonds at the nitro group has been a common suggestion.[4-6, 13, 14, 22, 26, 27, 29, 31, 33] Oxidation of the methyl group has been another possible path followed during decomposition.[4-6, 12, 15, 16, 18-20, 28] Bimolecular species of TNT could be formed through Diels-Alder reactions prior to formation of simpler species.[23, 25, 30, 33] Cyclization via the methyl and nitro group,[5, 10] nitrite rotation,[5] or C-H α attack[5, 22, 24, 28] mechanisms are other possible explanations of TNT decomposition chemistry. These are all suggested first step reaction mechanisms, which then can branch through several other chemical steps on the way to products. Understanding the chemistry that occurs during detonation of HE would allow for tailoring the performance and safety for future HE based on mechanisms present in current HE materials like TNT. Combined with experimental results, models could provide predictive capabilities of detonation performance and safety characteristics of possible HE molecules prior to any synthesis work.

The goal of this work is to measure the bond specific shock chemistry of TNT to gain insight into the first chemical steps that occur during detonation. Measurements of the bond specific

chemistry will be performed using the benchtop ultrafast laser system at Los Alamos National Laboratory which is capable of generating and characterizing shock waves in materials, while simultaneously probing electronic and vibrational absorption spectroscopic changes.[34] Interpretations of changes observed in the vibrational and visible absorptions will be presented with comparisons to previous chemical mechanisms. These results will be used to guide the physics and chemistry present in current models to refine the predictive capabilities similar to PETN results in Chapter 4.

5.2   Experimental methods

The laser shock apparatus described in previous publications[34-38] was used for the spectroscopic measurements on shock compressed TNT. Shock drive, interferometry, and spectroscopy beams were generated simultaneously from a single pulse out of a Ti:sapphire chirped pulse amplification (CPA) system. Techniques that are available to these experiments have been described in great detail elsewhere[34], but a short review will be provided here for clarity.

A portion of the 150 ps duration chirped pulse (~6 mJ) was used to both generate the shock in a material as well as characterize the wave mechanics through interferometry. Fitting of the interferometry data to a series of shock physics and optics equations yields information on the pressure, and shock and particle velocities induced in the sample. Ultrafast dynamic ellipsometry (UDE)[35, 36] was performed. The remainder of the ~6 mJ pulse was compressed in the laser to 35 fs and was used to generate the broadband visible (VIS) and mid-infrared (MIR) absorption spectroscopy probes. The generated VIS radiation spanned 450-700 nm. Two MIR ranges could be generated on a single shot basis depending on the compression of the CPA: 1150-3000 cm^{-1} and 1450-4000 cm^{-1}. The former range is useful for viewing the symmetric and antisymmetric nitro stretches (ν_s-NO_2 and ν_a-NO_2 respectively) and the hydrogenic stretches present in TNT[39] as well as atmospheric CO_2, while the latter range is useful for viewing all portions of the hydrogenic stretch region namely CH-, NH-, and OH-stretches (2800-3000, 3000-3200, 3200-3500 cm^{-1} respectively) for CHNO containing species. The VIS and MIR were simultaneously collected during the experiments; however, the interferometric data (UDE) were collected prior to spectroscopic measurements. VIS and MIR were collected at 25 ps time steps from -50 ps to 250 ps relative to shock entry into the TNT layer. Temporally this range coincides to spectroscopic measurements collected prior to the shock, during the shock, and during rarefaction of the TNT.

The shock pressure was assumed to be constant for the temporal duration of the chirped pulse (150 ps). 25 shots were averaged for each time step. The 25-shot averaged response for all time delays was defined as an experiment. These experiments were performed four times per substrate and were averaged. Three pressure ranges were selected ~16, ~33, and ~40 GPa which correspond to unreactive, partially reactive, and reactive chemistry regimes.

Samples were similar to previous thin film crystal experiments.[34, 40] Layers consisted of a tamper material of 500 μm of sapphire, with 1 μm of aluminum vapor deposited onto the tamper, and 1 μm of TNT deposited onto the aluminum drive layer. The thickness of aluminum and TNT was chosen to be commensurate with the shock duration of the experiment. TNT was recrystallized in solution to remove potential contaminants from the manufacturing process. The recrystallized TNT was then dissolved in acetone to ~16% by mass. This solution was spin cast onto substrates using 250 μL of solution. Notable spin casting parameters included speed, acceleration, and spin duration which were 1500 rpm, 500 rpm/s, and 25 seconds, respectively. Resulting films of TNT were nominally 1 μm in thickness (typically in the range 0.8-1.2 μm). Film thickness was measured using a white light interferometer. Prior to experiments, some TNT was removed from the substrate at a small spot. The resulting bare aluminum layer was used as an impedance matching surface to the unreactive Hugoniot of TNT in the case that UDE fitting was inadequate. Unfortunately, multiple metastable phases, polymorphs, and crystal structures can be present in TNT at room temperature and pressure.[41] It is uncertain exactly what TNT polymorph or crystal orientation was present in the TNT on the substrates used in these experiments. An image of the TNT microstructure is shown in Fig. 44. The microstructure imaged was similar between substrates.
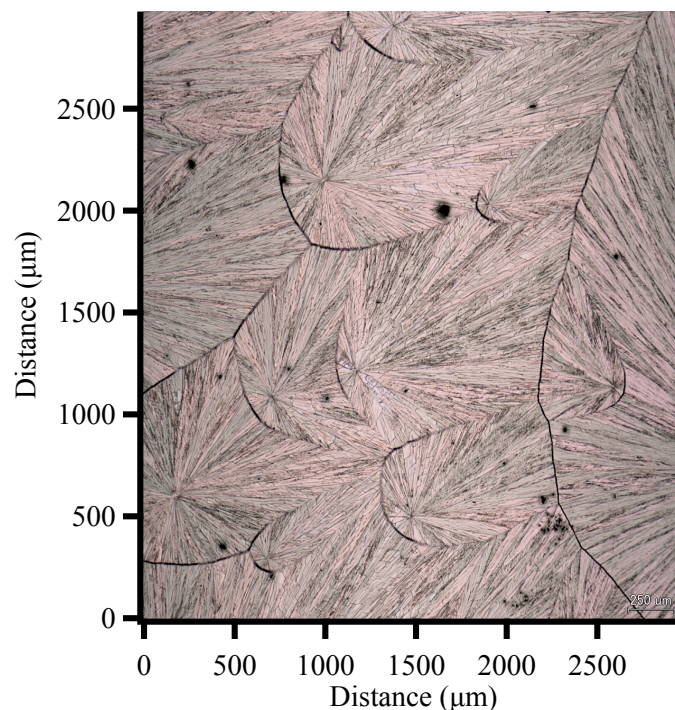
Figure 44 Image of TNT using white light confocal microscopy. Microstructure was consistent between substrates.

5.3   Results

5.3.1   Determination of the shock state

The shock state was determined through impedance matching. Impedance matching provided a rapid method for determining the pressure induced in the sample by matching the release isentrope of the aluminum drive layer to a linearly extrapolated fit to the unreactive Hugoniot for cream cast TNT.[2] This technique has been shown to give results that are at most 18% higher in pressure than through direct measurements in Chapter 4. Three pressure regions labeled low, medium, and high were measured for TNT and are shown in Fig. 45. Low pressure corresponded to pressures that ranged 16-17 GPa, medium pressures were 30-34 GPa, and high pressure were 38-40 GPa. Films 1, 2, and 6 were films that were probed when the MIR frequency was in the 1150-3000 cm^{-1} range, while Films 4 and 5 were probed with the 1450-4000 cm^{-1} MIR range. Film numbers do no correspond to when experiments were performed. In the event that there is an unreactive Hugoniot measured in the future, Table 3 has the particle velocity of the

118

aluminum drive layer, impedance matched shock and particle velocities for TNT, and the tabulated pressure induced in the sample.
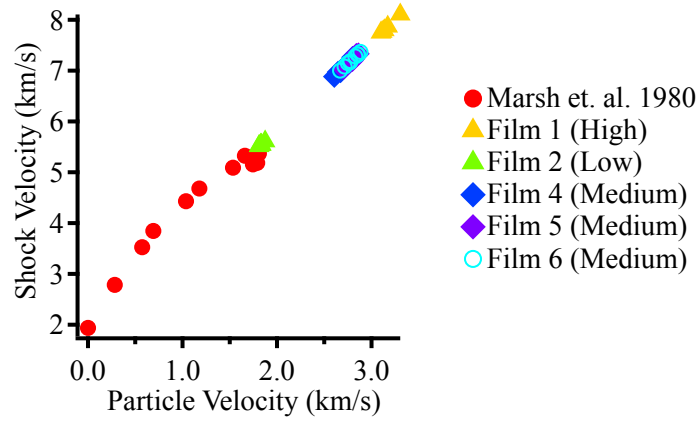
Figure 45 State determination for shock compressed TNT measured in these experiments. Marsh data started to show reactions at ~15 GPa, where low pressure is reported for this data. Due to the vastly shorter times scales (ps vs. µs) in these experiments there was no reaction observed at low pressures.

Table 3 UDE impedance matched points for the substrates in this study, u_{fs}: free surface velocity of the aluminum layer, u_p: impedance matched particle velocity of aluminum u_{fs} into TNT, u_s: impedance matched shock velocity of aluminum u_{fs} into TNT, P: pressure as calculated by $P = \rho u_s u_p$, where ρ is the density of TNT which was assumed to be cream cast density of 1.624 g/cm^3

Film Identifier	u_{fs} (km/s)	u_p (km/s)	u_s (km/s)	P (GPa)
Film 1 (High)	4.95	3.10	7.75	38.9
	5.01	3.14	7.80	39.6
	5.31	3.30	8.11	43.4
	4.97	3.11	7.76	39.1
	5.07	3.17	7.87	40.4
Film 2 (Low)	2.75	1.83	5.55	16.4
	2.75	1.83	5.54	16.4
	2.72	1.81	5.52	16.2
	2.83	1.87	5.61	17.0
	2.77	1.83	5.55	16.5
	2.72	1.81	5.52	16.2
Film 6 (Medium)	4.27	2.72	7.08	31.1
	4.18	2.67	7.00	30.2
	4.38	2.78	7.19	32.3
	4.51	2.85	7.32	33.8
	4.56	2.88	7.37	34.4
	4.47	2.83	7.28	33.4
	4.33	2.75	7.15	31.8
	4.36	2.77	7.16	32.2

Table 3 continued

	4.51	2.86	7.32	33.9
Film 4 (Medium)	4.25	2.70	7.06	30.9
	4.19	2.67	6.98	30.2
	4.15	2.65	6.97	29.9
	4.21	2.68	7.01	30.4
	4.43	2.80	7.26	32.9
	4.11	2.61	6.88	29.1
Film 5 (Medium)	4.50	2.84	7.32	33.7
	4.43	2.81	7.24	32.9
	4.25	2.70	7.04	30.8
	4.53	2.86	7.33	34.0
	4.48	2.81	7.24	33.0
	4.43	2.79	7.21	32.6
	4.45	2.80	7.20	32.6
	4.45	2.80	7.20	32.6

5.3.2 Visible (VIS) transient absorption spectroscopy

VIS transient absorption spectra were collected for time delays ranging from -50 to 250 ps for all pressure ranges. The shock transited the film in approximately 180 ps to 120 ps for the low to high pressure range respectively. This temporal range was selected to view changes that occur before, during, and after the shock has transited the film. Rarefaction of the sample occurs when the shock has fully transited the film and pressure is being released into air in front of the sample. Absorption was probed during rarefaction to determine the reversibility of the absorptions provoked upon release of pressure. Changes in VIS absorptions for the low frequency MIR region can be viewed in Fig. 46. No observable changes were noted at pressures of 16 GPa. Changes were at most ~5% across the spectral range for this pressure. When TNT was shocked to higher pressures there was a strong blue centered absorption in the VIS that grew during the shock. Recovery was observed for the 33 GPa case; however, it was not for 40 GPa. VIS measurements were measured for the high frequency MIR region at 30 GPa and are shown Fig. 47. 30 GPa results are comparable to 33 GPa with similar absorption features.
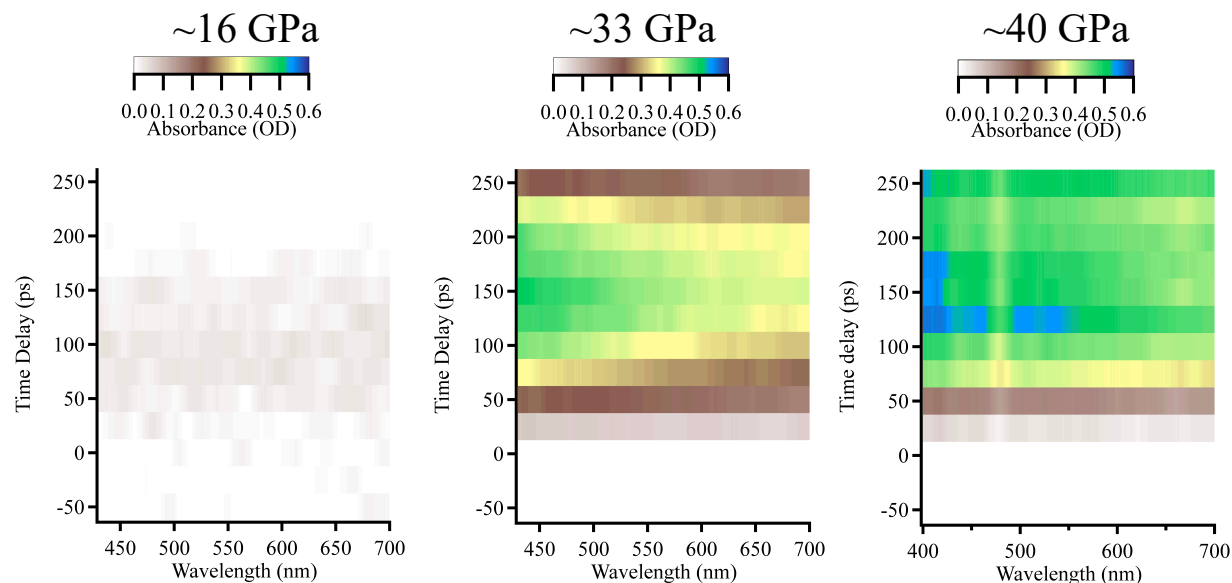
Figure 46 Comparison of VIS absorptions for low, medium, and high pressure cases. VIS absorptions suggest no reaction, some reaction with reversibility, and full reaction at low, medium, and high pressures respectively. The feature at 475 nm in the high pressure case was an artifact present in the static spectrum.
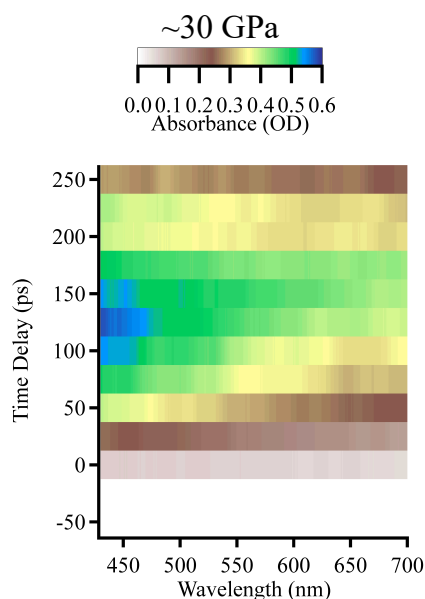
Figure 47 Additional VIS absorption spectra for the MIR high frequency region experiments. Similar results were measured for 30 GPa compared to 33 GPa with absorption growing in the shock and recovering during rarefaction.

5.3.3 Mid-infrared (MIR) transient absorption spectroscopy

Low frequency region MIR transmission spectra for 16, 33, and 40 GPa cases can be seen in Fig 48. Transmission changes that show decreased transmission of the spectra observed are due to increased absorption in the sample. In this frequency range the ν_s-NO_2 and ν_a-NO_2 at 1350 and 1540 cm^{-1} respectively[39] can be probed simultaneously. Multiple CH- stretches are present at 2900-3000 cm^{-1}, but the absorptions are very weak for these bonds compared to the NO_2 stretches.[39] In fact, the CH stretch modes were not observed statically in these experiments. A carbon dioxide (CO_2) artifact is present in this range at 2350 cm^{-1}, due to the presence of CO_2 in the atmosphere, which results in imperfect normalization of the transmission peak, leaving a residual feature. Without removing the CO_2 from the laboratory air, it is not entirely possible to suggest what changes may have occurred near this frequency (+/-50 cm^{-1}). High frequency MIR behavior for shock compressed TNT at medium pressure was also probed, and can be viewed in Fig. 49.

Figure 48 Comparison of the shocked transmission behavior for TNT at 16, 33, and 40 GPa. At 16 GPa no changes were observed. At 33 GPa, the NO_2 stretches broadened by ~50 cm^{-1}, and an absorption feature grew in the hydrogenic stretch region. Partial recovery was observed at 250 ps delay. At 40 GPa a broad absorption feature was observed over most of the spectral range. There was less absorption at >2700 cm^{-1} compared to 33 GPa. At 40 GPa, the ν_a-NO_2 transmission decreased from 40% to 25%, a decrease that is not duplicated at the ν_s-NO_2 mode. This could be due to strong scattering of the shocked sample. Sample thickness variations were also present as seen by the increased absorption in static measurements at negative time delays in the 33 and 40 GPa cases for vibrational groups of TNT.
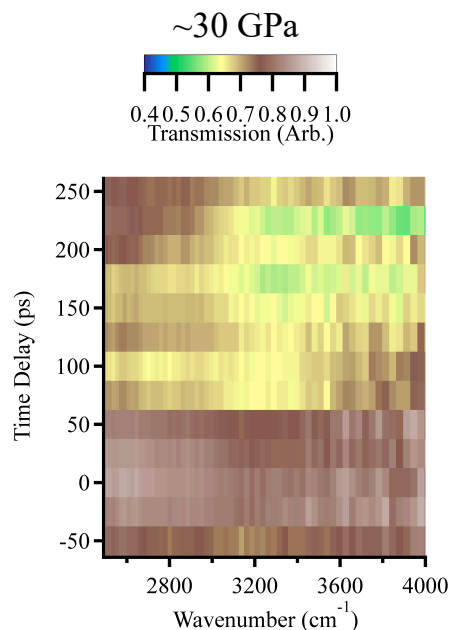
Figure 49 Transmission spectra in the high frequency MIR region for ~30 GPa. The spectra showed a broad absorption feature across most of the hydrogenic stretch region with minimal recovery of behavior except at 250 ps.

5.4   Discussion

5.4.1   Shock state from impedance matching

UDE measurements were not straightforward to perform for the films used in these experiments. As seen in Fig. 44, the microstructure scattered the sample illumination beam for both low angle and high angle UDE measurements. These localized highly textured features caused significant phase wrapping issues in the UDE analysis and fitting process. Local regions of uniform crystals on the TNT films could yield analyzable results; however, these portions were not present on most substrates. Although knowledge of the exact pressure would be useful, it was not the intended goal of these measurements. Fig 46 and 47 show the VIS absorption results for pressures of ~33 and ~30 GPa respectively. Even though the induced pressure was ~10% different between the two substrates, the VIS absorption changes and recovery were very similar. Similar conclusions can be made when viewing the MIR absorption changes in Fig 48 and 49. For these reasons the impedance matching technique was used to compute the shock pressure induced in samples. All of the shocked states measured in these experiments were greater than those measured by Marsh.[2] The shock pressure induced in samples for ultrafast experiments needs to be stronger

to observe similar reactions reported from shock induced chemistry reactions observed in gas gun experiments.[42] Unfortunately, no Hugoniot data for the shock and particle velocities measured in these experiments could be found. Provided in Table 3 are all of the measured drive velocities achieved for the low, medium, and high pressure cases for future reference. Alternatively, other sample production methods that result in less surface roughness would potentially allow UDE measurements to be performed.

5.4.2   VIS transient absorption spectroscopy

For the low frequency MIR region, at 16 GPa, there was ~5% total VIS absorption changes observed. These changes can be attributed to light scattering from the drive layer surface.[36, 37] When TNT was shocked to 33 GPa there was a strong, blue absorbing feature that grew during the shock; however, the transmission recovered during the rarefaction event from the front surface of TNT. Notably, full recovery of the VIS absorption was not observed even at the latest time delay measured (250 ps). Partial chemistry could have been induced when comparing MIR spectral features. Additionally, there may be scattering from particle motion, possibly ejecta, at the TNT front surface causing some irreversible change. For high pressures there was an enhanced absorption feature similar to that observed in the 33 GPa experiments (blue focused and broad) that did not recover upon rarefaction from the front surface. The feature at 475 nm for 40 GPa is not a real absorption feature as it was present prior to the shock entering the sample. It is believed to be a product of normalization used to convert transmission spectra into absorption. Since VIS absorptions did not recover at these higher shock pressures, some irreversible change was induced in TNT. The surface roughness of the TNT films prevented any thin film interference effects in the VIS absorptions. Such thin film interference effects were problematic when interpreting the optical density of the VIS absorption changes in PETN in Chapter 4. For high pressures the blue centered absorbing feature is most likely due to absorption from intermediate species, a claim which is corroborated by the MIR absorption results.

VIS transient absorption was also measured during the experiments performed for the high frequency MIR region. At 30 GPa, there was a blue centered broad VIS absorption that recovered upon release. These results were nearly identical to the 33 GPa case, except the VIS absorptions observed were slightly stronger. The increased absorption does not correspond with the pressure measured. A possible explanation for these results is that the microstructure was coarser for the 30

GPa substrate than for the 33 GPa substrate. Increased roughness of the sample would lead to features that look like increased absorption due to scattering of the VIS beam from the TNT surface. This feature would normalize out for a series if the scattering were similar between sample positions, but this was not the case. More data would aid in understanding the changes stimulated in this region. Even with this oddity, similar conclusions for the 30 GPa and the 33 GPa cases can be that VIS absorptions were induced, but almost entirely reversed upon release of the pressure.

5.4.3   MIR transient absorption spectroscopy

For the low frequency MIR region, results at 16 GPa for TNT were similar to the VIS results as there were no significant changes observed. Broadening and shifting of the NO_2 stretches was not perceived in this pressure range. Static high pressure experiments have suggested that the ν_s-NO_2 should have shifted by ~2.5 cm^{-1}/GPa.[43] The lack of broadening and shifting behavior in the shocked MIR absorption experiment has been observed before, also can be seen in Chapter 4.[34, 40, 44]

MIR results at 33 GPa contrasted VIS results. In the VIS region, the absorptions increased during the shock and recovered during rarefaction. In the MIR region, the absorptions grew during the shock as well as during most of the rarefaction. Partial recovery of the MIR spectra was observed at the latest time delay of 250 ps. The ν_s-NO_2 and ν_a-NO_2 mode vibrations showed only broadening of 50 cm^{-1} of the peaks, with no increased absorptions. A broad feature from 2700-3000 cm^{-1} increased in absorption as more material was shocked and continued increasing during rarefaction. There was some absorption on the blue side of the CO_2 stretch, but this feature was most likely an extension of the absorption feature from the hydrogenic stretch region. These MIR absorption results at 33 GPa suggest there was partial chemistry induced in the sample particularly near the hydrogenic stretches, while VIS absorptions suggest simple shock compression of the sample followed by recovery. High pressure experiments were performed to resolve this inconsistency.

In order to distinguish shock chemistry from other effects like thin film interference in the MIR or vibrational hot bands,[45-47] TNT was shocked using the maximum energy of the shock drive beam. Shocking TNT films to 40 GPa showed different results than those observed at 33 GPa. Both the ν_s-NO_2 and ν_a-NO_2 mode vibrations showed broadening of 50-100 cm^{-1}. Additionally,

the ν_a-NO_2 showed a slightly (~37.5%) increased absorption that did not recover upon release of the pressure induced. This could be attributable to the large scattering as there was an ~60% absorbing feature was observed from 1550-2600 cm^{-1} and did not recover during rarefaction of the sample. The 1700-2600 cm^{-1} region does not have several absorptions for CHNO containing species. Additionally, an absorption feature grew in the hydrogenic stretch region, but was less strong compared to either hydrogenic stretch feature present at 33 GPa or the feature that spanned the most of the MIR range (1550-2600 cm^{-1}) for this pressure. MIR and VIS absorptions suggest similar results in that there was an irreversible change induced in TNT that had a broad MIR absorption signature and was stable or grew in strength when the pressure was released. This change is most likely attributable to chemical reactions; however, there was strong scattering present. More data would resolve and aid in interpretation of the spectral features observed in the VIS and MIR absorption measurements.

The MIR frequency region was shifted to 1450-4000 cm^{-1} to focus on the hydrogenic stretch region (>2800 cm^{-1}) as results at 33 GPa suggested there was a strong 60% absorbing feature, like that in Fig. 49. TNT when shocked to 30 GPa had a similar hydrogenic stretch absorption feature to 33 GPa. Centered at 3300 cm^{-1}, a broadly absorbing feature was observed to grow during the shock and for most of the rarefaction, except at the latest time delay. Again, the result for MIR absorption changes are almost opposite to VIS absorption changes at this pressure. A possible explanation is that a small concentration of a strongly absorbing intermediate, like an OH-stretch, is generated.[48-51] It is planned to increase the pressure to >40 GPa for the high frequency MIR region to better interpret the hydrogenic stretch region absorption changes as seen in Fig 48.

Recapitulating several of the features observed in these experiments on TNT 1.) a nearly completely reversible VIS absorption was induced at ~30 GPa pressures; however, MIR absorptions did not show such strong recovery with a strong absorption >2,800 cm^{-1}, 2.) TNT shocked to >40 GPa showed strong, blue centered VIS absorptions with strong broadband MIR absorptions from 1550-2600 cm^{-1}, 3.) NO_2 stretches mostly broadened, not strongly increased absorption on these peaks like those in PETN, and 4.) shifting and broadening in the MIR bonds were not present at low shock pressures of ~17 GPa. There is not enough evidence to suggest the exact cause for each change, but a few conclusions can be made from these observations. First, TNT may have partially reacted at ~30 GPa generating an intermediate with a strong hydrogenic stretch. Even at low concentrations, NH- and OH- stretches have strong MIR absorptions.[48-51]

Since the CH-stretches were not observed at early times prior to the shock at -50 ps in these experiments, it would be assumed that this feature could not be due to CH-stretch absorptions. Partial reaction at this pressure is suggested as VIS absorptions demonstrate shock and release changes, whereas MIR changes do not seem to recover in transmission. Second, since NO_2 stretches do not show strong decreased or increased (<-50% and >50%) absorption they must still mostly be present. Only at the highest pressure does the ν_a-NO_2 show an increased absorption (~37.5%), while the ν_s-NO_2 had no apparent change in absorption. This feature for the ν_a-NO_2 does not continue to grow in strength, but rather starts broadening. Third, there was an irreversible change induced in TNT at high pressure due to the lack of VIS absorption recovery like those seen with any medium pressure. Fourth, there was a strong absorption or strong scattering feature over the most of the MIR spectral range for the high pressure case. Not many strongly absorbing bonds are present in this region for combinations of CHNO containing species;[52] however, carbon monoxide and carbon dioxide do have absorptions at 2,200-2,400 cm^{-1} which could partially explain the changes in this region.[52, 53] Mechanisms that have been suggested in previous work that are consistent the current work are shown in Table 4. More data is required to eliminate more inconsistent mechanisms and better interpret the results measured in these experiments.

Table 4 Possible intermediate pathways for shocked TNT and consistency with MIR spectra results

Intermediate Pathway	References	Inconsistent with MIR results?*
C-N homolysis	4-6,13,14,22,26,27,29,31,33	O
CH$_3$ oxidation	4-6,12,15,16,18-20,28	O
Diels-Alder Reaction	23,25,30,33	?
Cyclization reaction	5,10	X
C-H α attack	5,22,24,28	X
NO$_2$ rotation	5	X

*-X = true, O = false, ? = difficult to suggest

5.5   Conclusions

Some preliminary results of the shock chemistry of TNT were measured using ultrafast MIR and VIS absorption. Contrary to diamond anvil cell experiments, TNT showed minimal observable shifting and broadening (few wavenumbers) under shock compression to pressures of ~16 GPa. There was partial chemistry observed when TNT was shocked to ~30 GPa with a strongly

absorbing hydrogenic stretch feature when observing the MIR spectral changes. NO_2 stretches were found to only broaden at this pressure suggesting these bonds are still present in some form. VIS absorption changes showed strong absorption during the shock, but almost full recovery during the rarefaction. More definitive signs of chemistry were observed when TNT was shocked to ~40 GPa. VIS changes were strong and irreversible even at late times during pressure release. MIR changes were also strongly absorbing and irreversible. The MIR changes induced at the higher pressure were not enhanced features present in the medium pressure case suggesting the changes were from a different mechanism. To better understand the chemistry that occurred for shock compressed and strongly reactive TNT, experiments should be repeated at the high pressure while measuring spectra in the high MIR frequency range to observe any signatures of hydrogenic stretch formation. Additionally, measuring UDE would give insight into the wave mechanics induced in the sample. UDE would provide direct measurements of the u_p, u_s, and P as well as deviations from the Hugoniot providing further evidence of chemistry.[37]

5.6   References

1.   Gibbs, T.; Popolato, A., LASL Explosives. *Property Data* **1980**.

2.   Marsh, S. P., *LASL shock Hugoniot data*. Univ of California Press: 1980; Vol. 5.

3.   Bowden, P.; Chellappa, R.; Dattelbaum, D.; Manner, V.; Mack, N.; Liu, Z. In *The high-pressure phase stability of 2, 4, 6-trinitrotoluene (TNT)*, Journal of Physics: Conference Series, IOP Publishing: 2014; p 052006.

4.   Brill, T.; James, K., Thermal decomposition of energetic materials. 62. Reconciliation of the kinetics and mechanisms of TNT on the time scale from microseconds to hours. *The Journal of Physical Chemistry* **1993,** *97* (34), 8759-8763.

5.   Brill, T. B.; James, K. J., Kinetics and mechanisms of thermal decomposition of nitroaromatic explosives. *Chemical reviews* **1993,** *93* (8), 2667-2692.

6.   Bulusu, S.; Axenrod, T., Electron impact fragmentation mechanisms of 2, 4, 6-trinitrotoluene derived from metastable transitions and isotopic labeling. *Organic Mass Spectrometry* **1979,** *14* (11), 585-592.

7.   Dacons, J. C.; Adolph, H. G.; Kamlet, M. J., Novel observations concerning the thermal decomposition of 2, 4, 6-trinitrotoluene. *The Journal of Physical Chemistry* **1970,** *74* (16), 3035-3040.

8. Dattelbaum, D. M.; Chellappa, R. S.; Bowden, P. R.; Coe, J. D.; Margevicius, M. A., Chemical stability of molten 2, 4, 6-trinitrotoluene at high pressure. *Applied Physics Letters* **2014,** *104* (2), 021911.

9. Dodson, B.; Graham, R. In *Shock-induced organic chemistry*, AIP Conference Proceedings, American Institute of Physics: 1982; pp 42-51.

10. Dubikhin, V.; Matveev, V.; Nazin, G., Thermal decomposition of 2, 4, 6-trinitrotoluene in melt and solutions. *Russian chemical bulletin* **1995,** *44* (2), 258-263.

11. Guidry, R. M.; Davis, L. P., Thermochemical decomposition of explosives. I. TNT kinetic parameters determined from ESR investigations. *Thermochimica Acta* **1979,** *32* (1-2), 1-18.

12. Jenkins, T. F.; Murrmann, R. P.; Leggett, D. C., Mass spectra of isomers of trinitrotoluene. *Journal of Chemical and Engineering Data* **1973,** *18* (4), 438-439.

13. Makashir, P.; Kurian, E., Spectroscopic and thermal studies on 2, 4, 6-trinitro toluene (TNT). *Journal of thermal analysis and calorimetry* **1999,** *55* (1), 173-185.

14. Monat, J.; Gump, J. In *Decomposition products of RDX and TNT after resonant laser excitation*, AIP Conference Proceedings, American Institute of Physics: 2009; pp 1309-1312.

15. Robert Carper, W.; Cameron Dorey, R.; Tomer, K. B.; Crow, F. W., Mass spectral fragmentation pathways in 2, 4, 6-trinitrotoluene derived from a MS/MS unimolecular and collisionally activated dissociation study. *Organic mass spectrometry* **1984,** *19* (12), 623-626.

16. Rogers, R. N., Combined pyrolysis and thin-layer chromatography. Study of decomposition mechanisms. *Analytical Chemistry* **1967,** *39* (7), 730-733.

17. Shackelford, S.; Beckmann, J.; Wilkes, J., Deuterium isotope effects in the thermochemical decomposition of liquid 2, 4, 6-trinitrotoluene: application to mechanistic studies using isothermal differential scanning calorimetry analysis. *The Journal of Organic Chemistry* **1977,** *42* (26), 4201-4206.

18. Swanson, J. T.; Davis, L. P.; Dorey, R. C.; Carper, W. R., An EPR study of the thermal decomposition of molten 2, 4, 6-trinitrotoluene and its isotopic analogs. *Magnetic Resonance in Chemistry* **1986,** *24* (9), 762-767.

19.   Yinon, J., Mass spectral fragmentation pathways in 2, 4, 6-trinitroaromatic compounds. A tandem mass spectrometric collision induced dissociation study. *Organic mass spectrometry* **1987,** *22* (8), 501-505.

20.   Zitrin, S.; Yinon, J., Chemical ionization mass spectra of 2, 4, 6-trinitroaromatic compounds. *Organic Mass Spectrometry* **1976,** *11* (4), 388-393.

21.   Murray, J. S.; Lane, P.; Politzer, P.; Bolduc, P. R., A relationship between impact sensitivity and the electrostatic potentials at the midpoints of C   NO2 bonds in nitroaromatics. *Chemical physics letters* **1990,** *168* (2), 135-139.

22.   Cohen, R.; Zeiri, Y.; Wurzberg, E.; Kosloff, R., Mechanism of thermal unimolecular decomposition of TNT (2, 4, 6-trinitrotoluene): a DFT study. *The Journal of Physical Chemistry A* **2007,** *111* (43), 11074-11083.

23.   Engelke, R.; Blais, N. C.; Sheffield, S. A.; Sander, R. K., Production of a chemically-bound dimer of 2, 4, 6-TNT by transient high pressure. *The Journal of Physical Chemistry A* **2001,** *105* (28), 6955-6964.

24.   Kamlet, M.; Adolph, H., The relationship of impact sensitivity with structure of organic high explosives. II. Polynitroaromatic explosives. *Propellants, Explosives, Pyrotechnics* **1979,** *4* (2), 30-34.

25.   Liu, H.; He, Y.; Li, J.; Zhou, Z.; Ma, Z.; Liu, S.; Dong, X., ReaxFF molecular dynamics simulations of shock induced reaction initiation in TNT. *AIP Advances* **2019,** *9* (1), 015202.

26.   Owens, F., Relationship between impact induced reactivity of trinitroaromatic molecules and their molecular structure. *Journal of Molecular Structure: THEOCHEM* **1985,** *121*, 213-220.

27.   Owens, F., Calculation of energy barriers for bond rupture in some energetic molecules. *Journal of Molecular Structure: THEOCHEM* **1996,** *370* (1), 11-16.

28.   Owens, F.; Sharma, J., X-ray photoelectron spectroscopy and paramagnetic resonance evidence for shock-induced intramolecular bond breaking in some energetic solids. *Journal of Applied Physics* **1980,** *51* (3), 1494-1497.

29.   Owens, F. J.; Jayasuriya, K.; Abrahmsen, L.; Politzer, P., Computational analysis of some properties associated with the nitro groups in polynitroaromatic molecules. *Chemical physics letters* **1985,** *116* (5), 434-438.

30. Quenneville, J.; Germann, T. C., A quantum chemistry study of Diels–Alder dimerizations in benzene and anthracene. *The Journal of chemical physics* **2009**, *131* (2), 024313.

31. Rice, B. M.; Sahu, S.; Owens, F. J., Density functional calculations of bond dissociation energies for NO2 scission in some nitroaromatic molecules. *Journal of Molecular Structure: THEOCHEM* **2002**, *583* (1-3), 69-72.

32. Fowles, G.; Duvall, G.; Asay, J.; Bellamy, P.; Feistmann, F.; Grady, D.; Michaels, T.; Mitchell, R., Gas gun for impact studies. *Review of Scientific Instruments* **1970**, *41* (7), 984-996.

33. Rom, N.; Hirshberg, B.; Zeiri, Y.; Furman, D.; Zybin, S. V.; Goddard III, W. A.; Kosloff, R., First-principles-based reaction kinetics for decomposition of hot, dense liquid TNT from ReaxFF multiscale reactive dynamics simulations. *The Journal of Physical Chemistry C* **2013,** *117* (41), 21043-21054.

34. Powell, M. S.; Bowlan, P. R.; Son, S. F.; Bolme, C. A.; Brown, K. E.; Moore, D. S.; McGrane, S. D., A benchtop shock physics laboratory: Ultrafast laser driven shock spectroscopy and interferometry methods. *Review of Scientific Instruments* **2019,** *90* (6), 063001.

35. Bolme, C. A. Ultrafast dynamic ellipsometry of laser driven shock waves. Massachusetts Institute of Technology, 2008.

36. Brown, K. E.; McGrane, S. D.; Bolme, C. A.; Moore, D. S., Ultrafast Chemical Reactions in Shocked Nitromethane Probed with Dynamic Ellipsometry and Transient Absorption Spectroscopy. *Journal of Physical Chemistry A* **2014,** *118* (14), 2559-2567.

37. Dang, N. C.; Bolme, C. A.; Moore, D. S.; McGrane, S. D., Shock Induced Chemistry In Liquids Studied With Ultrafast Dynamic Ellipsometry And Visible Transient Absorption Spectroscopy. *Journal of Physical Chemistry A* **2012,** *116* (42), 10301-10309.

38. Whitley, V. H.; McGrane, S. D.; Eakins, D. E.; Bolme, C. A.; Moore, D. S.; Bingert, J. F., The elastic-plastic response of aluminum films to ultrafast laser-generated shocks. *Journal of Applied Physics* **2011,** *109* (1).

39. Nash, C.; Nelson, T.; Stewart, J.; Carper, W. *Molecular structure and vibrational analysis of 2, 4, 6-trinitrotoluene and 2, 4, 6-trinitrotoluene-a-d3*; FRANK J SEILER RESEARCH LAB UNITED STATES AIR FORCE ACADEMY CO: 1989.

40. Powell, M.; Bowlan, P.; Son, S.; McGrane, S., Ultrafast Mid-Infrared Spectroscopy on Shocked Thin Film Explosive Crystals. In *16th International Detonation Symposium*, Office of Naval Research: Cambridge, MD, 2018; pp 790-796.

41. Ravindran, T.; Rajan, R.; Venkatesan, V., Review of Phase Transformations in Energetic Materials as a Function of Pressure and Temperature. *The Journal of Physical Chemistry C* **2019,** *123* (48), 29067-29085.

42. McGrane, S. D.; Brown, K. E.; Bolme, C. A.; Moore, D. S., Interaction between measurement time and observed Hugoniot cusp due to chemical reactions. *AIP Conference Proceedings* **2017,** *1793* (1), 030033.

43. Goryainova, S. V.; Volodinb, V. A.; Danilenkod, A. M., Raman spectroscopic study of 2, 4, 6–trinitrotoluene at high pressure. **2011**.

44. Bowlan, P.; Powell, M.; Perriot, R.; Martinez, E.; Kober, E. M.; Cawkwell, M. J.; McGrane, S., Probing ultrafast shock-induced chemistry in liquids using broad-band mid-infrared absorption spectroscopy. *The Journal of chemical physics* **2019,** *150* (20), 204503.

45. McGrane, S.; Moore, D.; Funk, D., Shock induced reaction observed via ultrafast infrared absorption in poly (vinyl nitrate) films. *The Journal of Physical Chemistry A* **2004,** *108* (43), 9342-9347.

46. Moore, D., Influence of hot bands on vibrational spectra of shock compressed materials. *The Journal of Physical Chemistry A* **2001,** *105* (19), 4660-4663.

47. Moore, D.; McGrane, S.; Funk, D., Infrared complex refractive index measurements and simulated reflection mode infrared absorption spectroscopy of shock-compressed polymer thin films. *Applied spectroscopy* **2004,** *58* (5), 491-498.

48. Brown, T. L., Infrared intensities and molecular structure. *Chemical Reviews* **1958,** *58* (3), 581-608.

49. Kjaergaard, H. G.; Daub, C. D.; Henry, B. R., The role of electron correlation on calculated XH-stretching vibrational band intensities. *Molecular Physics* **1997,** *90* (2), 201-213.

50. Rao, C.; Venkataraghavan, R., Correlations of Infrared Group Frequencies and Band Intensities in Organic Molecules with Substituent Constants: A Statistical Evaluation. *Canadian Journal of Chemistry* **1961,** *39* (9), 1757-1764.

51. Silverstein, R. M.; Bassler, G. C.; Morrill, T. C., Spectrometric identification of organic compounds. **1981**.

52.   Pierson, R. H.; Fletcher, A. N.; Gantz, E. S. C., Catalog of infrared spectra for qualitative analysis of gases. *Analytical Chemistry* **1956,** *28* (8), 1218-1239.

53.   Ewing, G. E.; Pimentel, G. C., Infrared spectrum of solid carbon monoxide. *The Journal of Chemical Physics* **1961,** *35* (3), 925-930.

6.   CONCLUSIONS FROM ULTRAFAST SHOCK SPECTROSCOPIES

6.1   Conclusions

It has been demonstrated in this document how to turn a benchtop ultrafast chirped pulse amplification (CPA) system into shock physics and chemistry laboratory. Wave mechanics that are comparable to gas gun experiments can achieved with CPA systems,[1, 2] except at significantly shorter time and length scales. Ultrafast dynamic ellipsometry (UDE), an interferometry technique, provided measurements on material and shock motion. This data, when fit by a series of shock physics and optics equations, ultimately yielded important state parameters including pressure, particle velocity, and shock velocity. Volumetric changes induced in shocked samples can be measured using this technique. These volume changing mechanisms can give some insight into chemistry that happens during shock compression;[3-12] however, inferring chemical mechanisms is difficult with these measurements alone. Spectroscopic measurements can provide more information on chemical reactions. Visible (VIS) transient absorption spectroscopy was the first method used to better interpret the volumetric changes. VIS absorption changes have been shown to coincide with deviations from the unreacted Hugoniot where volumetric changes occur.[8-10, 12] Absorption changes in the VIS are very sensitive to chemical changes[8-10, 12-15], but these measurements are not chemically specific to what bonds may have formed or changed. This lack of precise chemistry determination necessitated development and use of a technique capable of chemical specificity. Vibrational spectroscopy is specific to bonds and functional groups in the infrared.[16, 17] Even though most high explosives (HE) have similar bonds comprised of combinations of CHNO atoms, HE molecules can be uniquely identified in the infrared based on the frequency and strength of these modes.[18] Using an ultrafast MIR source, chemical specificity can be measured during fast events like a shock. Results from these measurements can be found in Chapters 2-5. These types of measurements were implemented to measure the shock chemistry of TNT and PETN. By changing the arrival time of the shock, MIR spectra were recorded as a time delay series probing for changes in bonds present in TNT and PETN, whilst probing for the formation of new bonds. Shocked chemistry results for both TNT and PETN were unexpected compared to previous literature for decomposition mechanisms. Several suggested chemical mechanisms could be eliminated for both materials, narrowing the chemical pathways possible for

detonation chemistry for HE. For PETN, it was suggested that a C-C bond breaking mechanism, with subsequent C≡O and methyl nitrite formation, was consistent with results measured using the ultrafast apparatus. TNT results suggested that a mechanism that yielded a strong hydrogenic stretch like OH- or NH-bond would be probable, although not completely substantiated. More data would be needed to validate that claim. Results from these experiments can be directly compared to models to provide guidance on assumptions of the physics and chemistry during detonation. Work is already in progress to meet this goal.

6.2   Future work

Although the primary goal of providing experimental measurements of chemistry and physics at comparable time and length scales to models was achieved in this research, several additional experiments could be appended. First, the list of materials tested in the experiments presented was not exhaustive. TNT and PETN were chosen for the simplicity of making films appropriate to the shock duration and necessary optical clarity. Other films could be utilized in these experiments if the HE thicknesses could be tailored to the correct size and if the films could be made to be optically clear. Researchers at Sandia National Laboratory have capabilities of making HE films with these characteristics.[19] Measurements on new HE would provide more materials for comparing experiments to models. Second, using either nano-lithography[20] or femtosecond laser machining to induce nanoscale to microscale features into HE films would enable the study of nanoscale features. MIR spectral changes induced during shock compression of these films would be compared to uniform crystalline films. These measurements would give results on any mechano-chemistry provoked effects to modeling efforts. Third, ring up pressure loading mechanisms[21] could be implemented with the CPA. Ring up shocks, comparable to ramp loading, provide a way of achieving high pressure with small temperature increases in compressed samples. Ring up shocks would allow for observing pressure induced chemistry effects as opposed to high pressure and temperature chemistry for models. Fourth, laser driven flyer plates could be used to look at longer duration shocks and chemistry.[22, 23] Laser driven flyer plates typically sustain shocks for tens of nanoseconds,[22, 23] which for shock velocities would require 10-100's of microns of material. HE like 1,3,5-Trinitro-1,3,5-triazinane (RDX) or 1,3,5,7-Tetranitro-1,3,5,7-tetrazoctane (HMX) that can be pressed into pellets could be used in this apparatus. Alternatively, crystals could be polished to sizes commensurate to the sustained shock. Longer duration shock

135

experiments would most likely require a different infrared absorption technique like attenuated total reflectance (ATR) Fourier transform infrared (FTIR) spectroscopy. Lastly, cocrystals could be used in these experiments. Co-crystallization provides a means of altering traits of current HE crystals by combing crystals at the molecular scale.[24] Spin casting could be used to get HE films to usable thicknesses for the ultrafast apparatus or polished crystals or pressed pellets could be used with a laser driven flyer plate apparatus. The suggestions presented here are not a comprehensive list of all possible experiments, but are sufficient for several research thrusts.

6.3 References

1. Fowles, G.; Duvall, G.; Asay, J.; Bellamy, P.; Feistmann, F.; Grady, D.; Michaels, T.; Mitchell, R., Gas gun for impact studies. *Review of Scientific Instruments* **1970,** *41* (7), 984-996.

2. Powell, M. S.; Bowlan, P. R.; Son, S. F.; Bolme, C. A.; Brown, K. E.; Moore, D. S.; McGrane, S. D., A benchtop shock physics laboratory: Ultrafast laser driven shock spectroscopy and interferometry methods. *Review of Scientific Instruments* **2019,** *90* (6), 063001.

3. Bolme, C.; Funk, D., Ultrafast dynamic ellipsometry measurements of early time laser ablation of titanium thin films. *Applied Physics A* **2008,** *92* (4), 761.

4. Bolme, C.; McGrane, S.; Moore, D.; Whitley, V.; Funk, D., Single shot Hugoniot of cyclohexane using a spatially resolved laser driven shock wave. *Applied Physics Letters* **2008,** *93* (19), 191903.

5. Bolme, C. A. Ultrafast dynamic ellipsometry of laser driven shock waves. Massachusetts Institute of Technology, 2008.

6. Bolme, C. A.; McGrane, S. D.; Moore, D. S.; Funk, D. J., Single shot measurements of laser driven shock waves using ultrafast dynamic ellipsometry. *Journal of Applied Physics* **2007,** *102* (3).

7. Bolme, C. A.; McGrane, S. D.; Moore, D. S.; Funk, D. J., Ultrafast dynamic ellipsometry of laser ablated silicon. In *High-Power Laser Ablation VII, Pts 1-2*, Phipps, C. R., Ed. 2008; Vol. 7005.

8.   Brown, K. E.; Bolme, C. A.; McGrane, S. D.; Moore, D. S., Ultrafast shock-induced chemistry in carbon disulfide probed with dynamic ellipsometry and transient absorption spectroscopy. *J. Appl. Phys.* **2015,** *118* (8), 85903.

9.   Brown, K. E.; McGrane, S. D.; Bolme, C. A.; Moore, D. S., Ultrafast Chemical Reactions in Shocked Nitromethane Probed with Dynamic Ellipsometry and Transient Absorption Spectroscopy. *Journal of Physical Chemistry A* **2014,** *118* (14), 2559-2567.

10.   Dang, N. C.; Bolme, C. A.; Moore, D. S.; McGrane, S. D., Shock Induced Chemistry In Liquids Studied With Ultrafast Dynamic Ellipsometry And Visible Transient Absorption Spectroscopy. *Journal of Physical Chemistry A* **2012,** *116* (42), 10301-10309.

11.   McGrane, S. D.; Brown, K. E.; Bolme, C. A.; Moore, D. S., Interaction between measurement time and observed Hugoniot cusp due to chemical reactions. *AIP Conference Proceedings* **2017,** *1793* (1), 030033.

12.   Schulze, P. A.; Dang, N. C.; Bolme, C. A.; Brown, K. E.; McGrane, S. D.; Moore, D. S., Shock Hugoniot Equations of State for Binary Ideal (Toluene/Fluorobenzene) and Nonideal (Ethanol/Water) Liquid Mixtures. *Journal of Physical Chemistry A* **2013,** *117* (29), 6158-6163.

13.   Dick, J., Anomalous shock initiation of detonation in pentaerythritol tetranitrate crystals. *Journal of applied physics* **1997,** *81* (2), 601-612.

14.   Dick, J.; Mulford, R.; Spencer, W.; Pettit, D.; Garcia, E.; Shaw, D., Shock response of pentaerythritol tetranitrate single crystals. *Journal of applied physics* **1991,** *70* (7), 3572-3587.

15.   Dreger, Z. A.; Gruzdkov, Y. A.; Gupta, Y. M.; Dick, J. J., Shock wave induced decomposition chemistry of pentaerythritol tetranitrate single crystals: time-resolved emission spectroscopy. *The Journal of Physical Chemistry B* **2002,** *106* (2), 247-256.

16.   Brown, T. L., Infrared intensities and molecular structure. *Chemical Reviews* **1958,** *58* (3), 581-608.

17.   Pierson, R. H.; Fletcher, A. N.; Gantz, E. S. C., Catalog of infrared spectra for qualitative analysis of gases. *Analytical Chemistry* **1956,** *28* (8), 1218-1239.

18.   Gibbs, T.; Popolato, A., Los Alamos scientific laboratory explosive property data. University of California Press, Berkeley.[279t]: 1980.

19. Knepper, R.; Tappan, A. S.; Wixom, R. R.; Rodriguez, M. A., Controlling the microstructure of vapor-deposited pentaerythritol tetranitrate films. *Journal of Materials Research* **2011,** *26* (13), 1605-1613.

20. Nafday, O. A.; Pitchimani, R.; Weeks, B. L.; Haaheim, J., Patterning high explosives at the nanoscale. *Propellants, Explosives, Pyrotechnics: An International Journal Dealing with Scientific and Technological Aspects of Energetic Materials* **2006,** *31* (5), 376-381.

21. Gruzdkov, Y. A.; Gupta, Y. M.; Dick, J. J., Time-resolved absorption spectroscopy in shocked PETN single crystals. *AIP Conference Proceedings* **2000,** *505* (1), 929-932.

22. Brown, K. E.; Shaw, W. L.; Zheng, X.; Dlott, D. D., Simplified laser-driven flyer plates for shock compression science. *Review of Scientific Instruments* **2012,** *83* (10), 103901.

23. Paisley, D.; Warnes, R.; Kopp, R., Laser-driven flat plate impacts to 100 GPa with sub-nanosecond pulse duration and resolution for material property studies. In *Shock Compression of Condensed Matter–1991*, Elsevier: 1992; pp 825-828.

24. Bolton, O.; Matzger, A. J., Improved stability and smart-material functionality realized in an energetic cocrystal. *Angewandte Chemie International Edition* **2011,** *50* (38), 8960-8963.

VITA

Michael S. Powell completed his B.S degree in aerospace engineering at West Virginia University (WVU) in the spring of 2014, graduating cum laude. He enrolled, initially, for a M.S.M.E under Dr. Steven Son at Purdue University starting immediately after graduation from WVU. After successfully defending his thesis in the Fall of 2016, he continued on for a Ph.D in mechanical engineering. He was requested to join the experimental side of the Predictive Chemistry and Physics at Extreme Conditions (PCP@Xtreme) in the Fall of 2016, requiring a transition to Los Alamos National Laboratory. He currently works for his research advisor and mentor Dr. Steven Son, for the PCP@Xtreme project headed by Dr. Alejandro Strachan, and is mentored by Dr. Shawn McGrane and Dr. David Moore for research in shock physics.

PUBLICATIONS

1. **Powell, M. S**.; Bowlan, P. R.; Son, S. F.; Bolme, C. A.; Brown, K. E.; Moore, D. S.; McGrane, S. D., A benchtop shock physics laboratory: Ultrafast laser driven shock spectroscopy and interferometry methods. *Review of Scientific Instruments* 2019**,** *90* (6), 063001.

2. **Powell, M. S**.; Sakano, M. N.; Cawkwell, M. J.; Bowlan, P. R.; Brown, K. E.; Bolme, C. A.; Moore, D. S.; Son, S. F.; Strachan, A.; McGrane, S. D., Insight into the Chemistry of PETN Under Shock Compression Through Ultrafast Broadband Mid-Infrared Absorption Spectroscopy. *Journal of Chemical Physics (in progress)* 2020

3. **Powell, M. S**.; Sakano, M. N.; Cawkwell, M. J.; Bowlan, P. R.; Brown, K. E.; Bolme, C. A.; Moore, D. S.; Son, S. F.; Strachan, A.; McGrane, S. D., Insight into the Chemistry of TNT Under Shock Compression Through Ultrafast Broadband Mid-Infrared Absorption Spectroscopy. *Journal of Chemical Physics (in progress)* 2020

4. **Powell, M. S.;** Bowlan, P.; Son, S.; McGrane, S., Ultrafast Mid-Infrared Spectroscopy on Shocked Thin Film Explosive Crystals. In *16th International Detonation Symposium*, Office of Naval Research: Cambridge, MD, 2018; pp 790-796.

5. **Powell, M. S**.; Gunduz, I. W.; Shang, W.; Chen, J.; Son, S. F.; Chen, Y.; Guildenbecher, D. R., Agglomerate sizing in aluminized propellants using digital inline holography and traditional diagnostics. Journal of Propulsion and Power 2018, 34 (4), 1002-1014.

6. Bowlan, P.; **Powell, M**.; Perriot, R.; Martinez, E.; Kober, E. M.; Cawkwell, M. J.; McGrane, S., Probing ultrafast shock-induced chemistry in liquids using broad-band mid-infrared absorption spectroscopy. *The Journal of chemical physics* 2019**,** *150* (20), 204503.

7. Martínez, E.; Perriot, R.; Kober, E. M.; Bowlan, P.; **Powell, M**.; McGrane, S.; Cawkwell, M. J., Parallel replica dynamics simulations of reactions in shock compressed liquid benzene. The Journal of Chemical Physics 2019, 150 (24), 244108.

8. Satija, A.; Ruesch, M. D.; **Powell, M. S**.; Son, S. F.; Lucht, R. P., Innovative scheme for high-repetition-rate imaging of CN radical. Optics letters 2018, 43 (3), 443-446.

9. McGrane, S.; Bowlan, P.; **Powell, M**.; Brown, K.; Bolme, C., Broadband mid-infrared measurements for shock-induced chemistry. AIP Conference Proceedings 2018, 1979 (1), 130004.